

Heavy-Duty Vehicle Chassis Dynamometer Testing for  
Emissions Inventory, Air Quality Modeling, Source  
Apportionment and Air Toxics Emissions Inventory

Project E-55/59

Phase 2 Final Report

July 12, 2005

SPONSORS:

COORDINATING RESEARCH COUNCIL, INC.  
CALIFORNIA AIR RESOURCES BOARD  
U.S. ENVIRONMENTAL PROTECTION AGENCY  
U.S. DEPARTMENT OF ENERGY Office of FreedomCAR & Vehicle  
Technologies  
through the NATIONAL RENEWABLE ENERGY LABORATORY  
SOUTH COAST AIR QUALITY MANAGEMENT DISTRICT  
ENGINE MANUFACTURERS ASSOCIATION

Heavy-Duty Vehicle Chassis Dynamometer Testing for  
Emissions Inventory, Air Quality Modeling, Source  
Apportionment and Air Toxics Emissions Inventory

Project E-55/59

Phase 2 Final Report

July 12, 2005

Submitted by:

West Virginia University Research Corporation  
886 Chestnut Ridge Road  
P. O. Box 6845  
Morgantown, WV 26506

Prepared by:

West Virginia University Research Corporation  
Nigel N. Clark & Mridul Gautam (Principal Investigators)  
W. Scott Wayne, Donald W. Lyons & Gregory Thompson  
(Co-Principal Investigators)  
Department of Mechanical & Aerospace Engineering  
West Virginia University  
Morgantown, WV 26505-6106

## Executive Summary

Project E-55/59 Phase 2 (E-55/59-2) had the objective of acquiring regulated and non-regulated emissions measurements from in-use trucks in southern California. The Phase 2 test fleet for regulated emissions consisted of ten Heavy Heavy-Duty Diesel Trucks (HHDDT) and nine Medium Heavy-Duty Trucks (MHDT), which included seven diesel-fueled MHDT and two gasoline-fueled MHDT, ranging in model year from 1982 to 2004. The Phase 2 data were valuable in adding two 2004 model year (exhaust gas recirculation-equipped) HHDDT to the E-55/59 program. Non-regulated species were measured from five (HHDDT) and one diesel-fueled Medium Heavy-Duty Truck (MHDT) (total of 6) in the Phase 2 test fleet. The HHDDT emissions were characterized using the West Virginia University Transportable Heavy-Duty Emissions Testing Laboratory (TransLab), with a test weight set at 56,000lb. The MHDT were tested at unladen (50% of gross vehicle weight rating (GVWR)) and laden (75% of GVWR) weights. The Urban Dynamometer Driving Schedule (UDDS) and five modes of the HHDDT Schedule were used for the HHDDT. The MHDT were all tested using a Lower Speed Transient Mode (MHDTL0), a Higher Speed Transient Mode (MHDTHI) and a Cruise Mode (MHDTCR) of a recently developed California Air Resources Board (CARB) MHDT Schedule, and three MHDT were tested using the High Speed HHDDT\_S mode of the HHDDT Schedule as well.

Table 1 provides a summary of data for the HHDDT fleet. Oxides of nitrogen (NO<sub>x</sub>) were high (32.1 g/mile) on the Transient Mode for a 1998 Model Year (MY) truck, but all other trucks had NO<sub>x</sub> emissions below 19 g/mile on that mode. Two of the HHDDT were 2004 MY trucks that had 2003 model year engines with exhaust gas recirculation (EGR). Although both of these trucks produced similar NO<sub>x</sub> emissions on the Transient Mode, one produced 35% greater NO<sub>x</sub> emissions than the other on the High Speed Cruise (HHDDT\_S) Mode. PM emissions for the HHDDT fleet were below 3.4 g/mile for the Transient Mode, except for one high emitter (E55CRC-45) discussed below. The two 2004 model year trucks emitted 0.42 and 0.26 g/mile PM on the Transient Mode, and 0.28 and 0.14 g/mile on the HHDDT\_S.

**Table 1: Highest, lowest and average emissions of NO<sub>x</sub> and PM for all HHDDT tested at 56,000lb.**

	Idle	HHDDT Creep	HHDDT Transient	HHDDT Cruise	HHDDT HHDDT_S	UDDS
	(g/min)	(g/mile)	(g/mile)	(g/mile)	(g/mile)	(g/mile)
<b>Highest NO<sub>x</sub></b>	3.27	163	32.06	26.27	22.24	24.03
<b>Average NO<sub>x</sub></b>	1.36	62.33	18.46	13.15	14.56	16.18
<b>Lowest NO<sub>x</sub></b>	0.82	28.88	13.68	7.67	8.05	11.98
<b>Highest PM</b>	0.71	67.77	17.14	1.12	1.56	3.04
<b>Average PM</b>	0.05	7.92	2.21	0.41	0.51	1.27
<b>Lowest PM</b>	0.00	0.47	0.26	0.06	0.09	0.13

One HHDDT (E55CRC-45: 1993 model year) produced very high PM emissions (16.59 g/mile on the Transient Mode) and was found to have a defective solenoid for the fuel

pump. This vehicle was repaired and re-tested, but the PM emissions rose substantially on the HHDDT\_S and fell only slightly on the Transient Mode. No further action was taken on this vehicle.

NO<sub>x</sub> emissions from diesel – fueled MHDT varied little from truck to truck. For example, for the Lower Speed Transient Mode, the range (for laden tests) was 13.5 to 20.5 g/mile. PM varied more from truck to truck. Table 2 presents NO<sub>x</sub> and PM data for the diesel MHDT fleet at the laden test weight. One diesel MHDT (E55CRC-57) was unable to follow a high speed target trace, and this was believed to be due to a faulty temperature sensor, that caused reduced power operation. Except for this truck, NO<sub>x</sub> was lower at unladen weight than laden weight on the MHDTL0. However, test weight did not cause a large change in NO<sub>x</sub>, and had virtually no effect on the Cruise Mode for diesel – fueled MHDT for all trucks of MY earlier than 1998. In contrast, test weight had a stronger influence on distance-specific PM for the diesel MHDT. Two gasoline MHDT were tested. The 2001 MY gasoline vehicle showed low NO<sub>x</sub> (7.42 and 3.81 g/mile on laden MHDTL0 and MHDTHI), but the older 1993 gasoline truck emitted NO<sub>x</sub> at levels similar to the diesel vehicles. PM was very low for both gasoline MHDT.

The regulated emissions data for HHDDT (56,000lb. test weight) Phase 2 were compared to the data from Phases 1 and 1.5 of the program. Carbon dioxide data agreed well between phases, suggesting that vehicle loading was consistent from phase to phase. Data for carbon monoxide, NO<sub>x</sub> and PM were compared between phases. There were too few trucks, distributed over a wide range of model years, to reach emissions conclusions based on data from a single phase. The value of using the combined emissions data from all phases to reach conclusions on age or model year effects was evident. For example, the Phase 2 fleet included only one truck in the 1991-1993 model year range, and its NO<sub>x</sub> emissions were substantially lower than the NO<sub>x</sub> emissions from the five trucks in the 1991-1993 model year range tested in prior phases.

**Table 2: Highest, lowest and average emissions of NO<sub>x</sub> and PM for all diesel-fueled MHDT tested at 75% GVWR.**

	MHDT AC5080	MHDTCR	MHDTHI	MHDTL0	UDDS
	(g/mile)	(g/mile)	(g/mile)	(g/mile)	(g/mile)
<b>Highest NO<sub>x</sub></b>	9.69	11.32	12.46	20.54	13.18
<b>Average NO<sub>x</sub></b>	8.33	9.35	10.84	16.46	11.03
<b>Lowest NO<sub>x</sub></b>	6.57	6.36	8.61	13.52	9.31
<b>Highest PM</b>	0.92	1.07	0.96	1.31	0.95
<b>Average PM</b>	0.44	0.49	0.53	0.77	0.52
<b>Lowest PM</b>	0.13	0.18	0.15	0.28	0.18

**Table 3: The effect of changing test weight on the diesel-fueled MHDТ, in terms of a simple average of emissions for that fleet.**

	<b>MHDТ AC5080</b>	<b>MHDТCR</b>	<b>MHDТHI</b>	<b>MHDТLO</b>	<b>UDDS</b>
	(g/mile)	(g/mile)	(g/mile)	(g/mile)	(g/mile)
<b>Average Laden NO<sub>x</sub></b>	8.33	9.35	10.84	16.46	11.03
<b>Average Unladen NO<sub>x</sub></b>	8.10	8.67	9.85	16.49	10.49
<b>Average Laden PM</b>	0.44	0.49	0.53	0.77	0.52
<b>Average Unladen PM</b>	0.33	0.34	0.34	0.48	0.34

PM data were acquired using both conventional filters and a Tapered Element Oscillating Microbalance (TEOM). The TEOM correlated well with the filters ( $R^2 = 0.9893$ ) and provided distance specific emissions that were 7% lower than the filter. Comparison of carbon dioxide emissions data with the data from prior program phases confirmed repeatability of vehicle loading from phase to phase.

Size distributions of PM were characterized from six trucks that were selected for non-regulated emissions measurement. These data were acquired using a Scanning Mobility Particle Sizer (SMPS), as well as a Differential Mobility Spectrometer (DMS500), which was a newly released instrument. A raw exhaust slipstream was diluted by a factor of thirty in a mini-dilution tunnel, and this dilute stream was sampled by the SMPS. The DMS used the main dilution tunnel of the WVU TransLab, which had a fixed flow and a varying dilution ratio. The SMPS detected a bimodal distribution with a nuclei mode for Idle operation of one 2004 MY truck (E55CRC-40), and the DMS 500 detected both the nuclei mode and accumulation mode during deceleration on this truck. The nuclei mode was not evident under load for E55CRC-40. The other 2004 MY truck had only one mode, with a very low particle count on Idle. A 1989 MY truck had a bimodal Idle distribution, but the remaining HHDDT were unimodal. Comprehensive data were acquired for steady operation using the SMPS on all trucks, and the DMS500 acquired transient distributions for four of the trucks.

Chemical speciation was performed on the six trucks, with exhaust from the TransLab tunnel fed to a residence time chamber of the Desert Research Institute (DRI). Data were acquired for methane and volatile organic compounds using a canister and a field gas chromatograph. Semi-volatile organic compounds were captured in PUF/XAD media and PM soluble fraction was captured on Teflon-Impregnated Glass Fiber Filters (TIGF) filters, and these were extracted and analyzed at the DRI laboratory. Carbonyls were captured using DNPH cartridges, and nitrosamines were captured in Thermosorb cartridges. Ions and Elemental/Organic carbon (EC/OC) split were determined from quartz filters. Results from the speciation data are legion, and examples include the fact that the EC/OC split differed substantially on Idle between the two 2004 MY trucks equipped with EGR, and that the ion and metal analyses varied widely between trucks. The total carbon emissions from cruise mode were found to be the highest, while the total PM mass emissions rates were the highest from the transient mode. All pre-1999 vehicles, which were subjected to speciation analysis, were found to emit higher levels of engine wear elements, such as iron, than the newer vehicles. Likewise, oil control, as

demonstrated by the lubricating oil-based ash components, was better in post-1999 vehicles.

## Table of Contents

Executive Summary .....	iii
Table of Contents .....	vii
List of Figures .....	ix
List of Tables .....	xiii
List of Appendices .....	xiv
Acronyms .....	xv
Introduction .....	1
Vehicle Procurement.....	1
Test Site and Laboratory .....	3
Test Cycles.....	3
Test Weights .....	4
Test Runs .....	5
Vehicle Inspection .....	10
HHDDT Data Gathered .....	11
PM Versus NO <sub>x</sub> Plots.....	13
MHDT Data Gathered.....	14
PM Versus NO <sub>x</sub> Plot.....	19
Continuous Data.....	20
Correlation of PM Filter and TEOM Data.....	22
Correlation of NO <sub>x</sub> Data from two Analyzers .....	23
MHDT Effect of Test Weight.....	24
Comparison with Data from Prior Phases.....	26
Chemical Speciation and PM Size Measurement .....	30
Description of Dilution Systems .....	30
WVU Constant Volume Sampling System (CVS) .....	30
Residence Time Dilution System.....	33
Mini Dilution System.....	34
Particle Sampling .....	39
Total Particulate Matter .....	39
Particle Sizing with the SMPS.....	39
Particle sizing with the DMS500.....	42
Unregulated Emissions (West Virginia University and Desert Research Institute)	
Measurement.....	43
West Virginia University .....	43
Desert Research Institute .....	44
Speciation Fleet and Approach .....	44
Speciation and Sizing Results.....	45
E55CRC-39.....	46
E55CRC-40.....	58
E55CRC-41.....	62
E55CRC-42.....	73
E55CRC-43.....	77
E55CRC-44.....	81

Conclusions.....	85
Acknowledgements.....	90
References.....	91

## List of Figures

Figure 1: PM emissions of E55CRC-53 were tested at two weights.....	4
Figure 2: NO <sub>x</sub> emissions of E55CRC-53 were tested at two weights.....	5
Figure 3: NO <sub>x</sub> emissions for the Transient (Trans3) Mode (56,000lb.).....	11
Figure 4: NO <sub>x</sub> emissions for the HHDDT_S Mode (56,000lb.).....	12
Figure 5: PM emissions for the Transient (Trans3) Mode (56,000 lb.).....	12
Figure 6: PM emissions for the HHDDT_S Mode (56,000lb.).....	13
Figure 7: PM versus NO <sub>x</sub> for the HHDDT Modes (excluding Idle) for all Phase 2 trucks at 56,000 lb. test weight. ....	14
Figure 8: NO <sub>x</sub> emissions for the Lower Speed Transient Mode (both laden and unladen). .....	15
Figure 9: Shows the inability of E55CRC-57 to meet the target trace. ....	15
Figure 10: NO <sub>x</sub> emissions for the Higher Speed Transient Mode (both laden and unladen).....	16
Figure 11: NO <sub>x</sub> emissions for the Cruise Mode (both laden and unladen). ....	16
Figure 12: NO <sub>x</sub> emissions for the HHDDT_S Mode (both laden and unladen). ....	17
Figure 13: PM emissions for the Lower Speed Transient Mode (both laden and unladen). .....	17
Figure 14: PM emissions for the Higher Speed Transient Mode (both laden and unladen). .....	18
Figure 15: PM emissions for the Cruise Mode (both laden and unladen). ....	18
Figure 16: PM emissions for the HHDDT_S Mode (both laden and unladen). ....	19
Figure 17: PM versus NO <sub>x</sub> for the MHDT Modes for Phase 2 trucks (laden).....	19
Figure 18: PM versus NO <sub>x</sub> for the MHDT Modes for Phase 2 trucks, except E55CRC-45 and E55CRC-45RR (unladen). ....	20
Figure 19: Example of a continuous NO <sub>x</sub> emissions plot in g/second for E55CRC-42 at 56,000 lb. following the Transient Mode schedule.....	20
Figure 20: Example of a continuous HC emissions plot in g/second for E55CRC-42 at 56,000 lb. following the Transient Mode schedule.....	21
Figure 21: Example of a continuous CO emissions plot in g/second for E55CRC-42 at 56,000 lb. following the Transient Mode schedule.....	21
Figure 22: Example of a continuous exhaust temperature reading for E55CRC-42 at 56,000 lb. following the Transient Mode schedule.....	22
Figure 23: Comparison of TEOM filter weight to 70mm filter weight. ....	23
Figure 24: Comparison of NO <sub>x</sub> readings from the two TransLab analyzers. ....	24
Figure 25: PM emissions for Cruise Mode (laden and unladen) .....	24
Figure 26: NO <sub>x</sub> emissions for Cruise Mode (laden and unladen).....	25
Figure 27: PM emissions for the Higher Speed Transient Mode (laden and unladen).....	25
Figure 28: NO <sub>x</sub> emissions for the Higher Speed Transient Mode (laden and unladen). ..	26
Figure 29: Variation of HHDDT carbon dioxide emissions by vehicle model year and by phase of the program for the UDDS at 56,000 lb. test weight.....	27
Figure 30: Variation of HHDDT carbon monoxide emissions by vehicle model year and by phase of the program for the UDDS at 56,000 lb. test weight.....	27

Figure 31: Summary of HHDDT average emissions on the UDDS (56,000 lb. test weight) for vehicles in the 1990-93 and 1994-97 age groups.....	28
Figure 32: Variation of HHDDT oxides of nitrogen emissions by vehicle model year and by phase of the program for the UDDS at 56,000 lb. test weight.....	28
Figure 33: Variation of HHDDT oxides of nitrogen emissions by vehicle model year and by phase of the program for the Transient Mode at 56,000 lb. test weight. ....	29
Figure 34: Variation of HHDDT oxides of nitrogen emissions by vehicle model year and by phase of the program for the Cruise Mode at 56,000 lb. test weight. ....	29
Figure 35: WVU Sampling Train Schematic.....	32
Figure 36: Schematic of the DRI Residence Time Dilution Tunnel [6]. In the present application the DRI system sampled from the main CVS dilution tunnel.....	34
Figure 37: Exhaust Coupler with Sampling Probe .....	35
Figure 38: West Virginia University-Mini Dilution System .....	36
Figure 39: Schematic Representation of the Damping System .....	38
Figure 40: Exhaust Pulsation Damper .....	38
Figure 41: Differential Mobility Analyzer.....	39
Figure 42: TSI Model 3936 SMPS System .....	41
Figure 43: Working principle of the DMS500[8].....	43
Figure 44: SMPS Particle Size Distribution for E55CRC-39 Operating on an Idle Mode	47
Figure 45: SMPS Particle Size Distribution for E55CRC-39 Operating on Various Steady Cycles.....	48
Figure 46: PM Mass Emissions for E55CRC-39.....	48
Figure 47: Ion Composite Results for E55CRC- 39 .....	50
Figure 48: Elemental Carbon and Organic Carbon PM Analysis for E55CRC-39 .....	50
Figure 49: DMS500 Total Number of Particles and Vehicle Speed vs. Time during the UDDS for E55CRC-39 tested at 56,000 lb.....	51
Figure 50: DMS500 Total Number of Particles and Engine Power vs. Time during the UDDS for E55CRC-39 tested at 56,000 lb.....	52
Figure 51: DMS500 60nm and 20nm Particle Number vs. Time during the UDDS for E55CRC-39 tested at 56,000 lb. ....	52
Figure 52: DMS500 60nm Particle Number vs. 20nm Particle Number during the UDDS for E55CRC-39 tested at 56,000 lb.....	53
Figure 53: DMS500 60nm Particle Number vs. Total Hub Power during the UDDS for E55CRC-39 tested at 56,000 lb. ....	53
Figure 54: DMS500 20nm Particle Number vs. Total Hub Power during the UDDS for E55CRC-39 tested at 56,000 lb. ....	54
Figure 55: DMS500 size distribution of particles during Idle (t = 230 s) of the UDDS for E55CRC-39 tested at 56,000 lb. ....	55
Figure 56: DMS500 size distribution of particles during acceleration (t = 530 s) of the UDDS for E55CRC-39 tested at 56,000 lb.....	55
Figure 57: DMS500 size distribution of particles during deceleration (t = 770 s) of the UDDS for E55CRC-39 tested at 56,000 lb.....	56
Figure 58: DMS500 size distribution of particles during HHDDT_S and Vehicle Speed vs. Time for E55CRC-39 tested at 56,000 lb.....	56
Figure 59: DMS500 size distribution of particles during Transient and Vehicle Speed vs. Time for E55CRC-39 tested at 56,000 lb. ....	57

Figure 60: DMS500 size distribution of particles during Cruise3 and Vehicle Speed vs. Time for E55CRC-39 tested at 56,000 lb. ....	58
Figure 61: SMPS Particle Size Distribution for E55CRC-40 Operating on an Idle Mode59	
Figure 62: SMPS Particle Size Distribution for E55CRC-40 Operating on Various Steady Cycles.....	60
Figure 63: PM Mass Emissions for E55CRC-40.....	61
Figure 64: Ion Composite Results for E55CRC-40.....	61
Figure 65: Elemental Carbon and Organic Carbon PM Analysis for E55CRC-40 .....	62
Figure 66: SMPS Particle Size Distribution for E55CRC-41 Operating on an Idle Mode63	
Figure 67: Elemental Carbon and Organic Carbon PM Analysis for E55CRC-41 .....	64
Figure 68: Total PM Mass Emissions Rate (g/hour) for E55CRC-41 .....	65
Figure 69: SMPS Particle Size Distribution for E55CRC-41 Operating on Cruise and Steady Cycles.....	65
Figure 70: SMPS Particle Size Distribution for E55CRC-41 Operating on Cruise and Steady Cycles (50% GVWR).....	66
Figure 71: Ion Composite Results for E55CRC-41 .....	66
Figure 72: SMPS Single Particle Trace (82 nm) for E55CRC-41 Operating on UDDS, Low Transient and High Transient Cycles (75%GVWR) .....	67
Figure 73: SMPS Single Particle Trace (24 nm) for E55CRC-41 Operating on Low Transient and High Transient Cycles (75% GVWR) .....	68
Figure 74: SMPS Single Particle Trace (88 nm) for E55CRC-41 Operating on Low Transient and High Transient Cycles (50% GVWR) .....	68
Figure 75: DMS500 Total Number of Particles and Vehicle Speed vs. Time during UDDS for E55CRC-41 tested at 56,000 lb.....	69
Figure 76: DMS500 60nm and 20nm Particle Number vs. Time for E55CRC-41 tested at 56,000 lb. ....	70
Figure 77: DMS500 Total Number of Particles and CO vs. Time for E55CRC-41 tested at 56,000 lb. ....	71
Figure 78: DMS500 60nm Particle Number vs. 20nm Particle Number for E55CRC-41 tested at 56,000 lb. ....	71
Figure 79: DMS500 20nm Particle Number vs. Total Hub Power for E55CRC-41 tested at 56,000 lb.....	72
Figure 80: DMS500 60nm Particle Number vs. Total Hub Power for E55CRC-41 tested at 56,000 lb.....	72
Figure 81: DMS500 size distribution of particles during acceleration and deceleration for E55CRC-41 tested at 56,000 lb. ....	73
Figure 82: SMPS Particle Size Distribution for E55CRC-42 Operating on an Idle Mode74	
Figure 83: SMPS Particle Size distribution for E55CRC-42 operating on various steady cycles.....	74
Figure 84: PM Mass Emissions for E55CRC-42.....	75
Figure 85: Ion Composite Results for E55CRC-42.....	76
Figure 86: Elemental Carbon and Organic Carbon PM Analysis for E55CRC-42 .....	76
Figure 87: DMS500 Total Number of Particles and Vehicle Speed vs. Time on Transient Mode for E55CRC-42 tested at 56,000 lb. ....	77
Figure 88: SMPS Particle Size Distribution for E55CRC-43 Operating on an Idle Mode78	

Figure 89: SMPS Particle Size Distribution for E55CRC-43 Operating on Various Steady Cycles.....	78
Figure 90: PM Mass Emissions for E55CRC-43 .....	79
Figure 91: Ion Composite Results for E55CRC-43 .....	80
Figure 92: Elemental Carbon and Organic Carbon PM Analysis for E55CRC-43 .....	80
Figure 93: DMS500 Total Number concentration of Particles and Vehicle Speed vs. Time for E55CRC-43 tested at 56,000 lb.....	81
Figure 94: SMPS Particle Size Distribution for E55CRC-44 Operating on an Idle Mode	82
Figure 95: SMPS Particle Size Distribution for E55CRC-44 Operating on Various Steady Cycles.....	82
Figure 96: PM Mass Emissions for E55CRC-44 .....	83
Figure 97: Ion Composite Results for E55CRC-44 .....	84
Figure 98: Elemental Carbon and Organic Carbon PM Analysis for E55CRC-44 .....	84
Figure 99: Elemental Carbon Emissions (Percentage of Total Carbon).....	87
Figure 100: Inorganic Ionic Species Emissions.....	88
Figure 101: Lubrication Oil Emissions.....	89
Figure 102: Engine Wear Emissions.....	90

## List of Tables

Table 1: Highest, lowest and average emissions of NO <sub>x</sub> and PM for all HHDDT tested at 56,000lb. ....	iii
Table 2: Highest, lowest and average emissions of NO <sub>x</sub> and PM for all diesel-fueled MHDT tested at 75% GVWR. ....	iv
Table 3: The effect of changing test weight on the diesel-fueled MHDT, in terms of a simple average of emissions for that fleet.....	v
Table 4: Vehicles planned for recruiting in the E-55/59-2 program.....	1
Table 5: Basic Information on the 20 trucks actually recruited in Phase 2. ....	2
Table 6: Sequence number, run number and vehicle information for each reportable test	6
Table 7: Sampling System Description and Media Type, used in conjunction with the CVS tunnel.....	31
Table 8: Test Vehicle Details.....	45

## **List of Appendices**

- Appendix A: Photograph and Description of Each Test Vehicle
- Appendix B: Description of the WVU Transportable Heavy Duty Vehicle Emissions Testing Laboratory (TransLab)
- Appendix C: Graphical Representation of Each Test Schedule
- Appendix D: WVU Short Reports for Each Test
- Appendix E: WVU Test Vehicle Information Sheets
- Appendix F: WVU Vehicle Inspection Reports
- Appendix G: WVU Tampering and Malmaintenance (T&M) Issues Sheets
- Appendix H: WVU Summary Data Tables
- Appendix I: Tunnel Flow Rates and Dilution Factor for ARB contractors
- Appendix J: SMPS and CPC Reduction Program
- Appendix K: DRI Chemical Speciation-Sample Collection and Analytical Procedures
- Appendix L: List of Target Chemical Species Analyzed
- Appendix M: Chemical Speciation Section

## Acronyms

ATOFMS	Aerosol Time-Of-Flight Mass Spectrometer
BNC	Bayonet Neill Concelman connector
cfm	cubic feet per minute
CFR	Code of Federal Regulations
CFV	Critical Flow Venturi
CMD	Count Median Diameter
CNC	Condensation Nucleus Counter
CO	Carbon Monoxide
CO <sub>2</sub>	Carbon Dioxide
CPC	Condensation Particle Counter
CVS	Constant Volume Sampler
DAS	Data Acquisition System
DDC	Detroit Diesel Company
DMA	Differential Mobility Analyzer
DMS500	Differential Mobility Spectrometer, Model 500
DNPH	2,4-Dinitrophenylhydrazine
DRI	Desert Research Institute
CRC	Coordinating Research Council, Inc.
EC	Elemental Carbon
ECU	Engine Control Unit
EGR	Exhaust Gas Recirculation
EPA	Environmental Protection Agency
g/ahp-hr	grams per axle horsepower-hour
g/cycle	grams per cycle
g/gallon	grams per gallon
g/mile	grams per mile
g/minute	grams per minute
GM	General Motors
GSD	Geometric Standard Deviation
GVW	Gross Vehicle Weight
GVWR	Gross Vehicle Weight Rating
HC	Hydrocarbon
HDDT	Heavy-Duty Diesel Trucks
HEPA	High Efficiency Particulate Air Filters
Hg	Mercury
HHDDT	Heavy Heavy-Duty Diesel Truck
HHDDT_S	Heavy Heavy-Duty Diesel Truck - High Speed Cruise Mode
hp	Horsepower
Hz	hertz
KW	Kilowatt
lpm	liters per minute
m	meters
MHDT	Medium Heavy-Duty Truck

MHDTCR	Medium Heavy-Duty Truck Cruise Mode
MHDTHI	Medium Heavy-Duty Truck Higher Speed Mode
MHDTLO	Medium Heavy-Duty Truck Lower Speed Mode
mph	miles per hour
MY	Model Year
ng	nano-gram
nm	nano-meter
µm	micrometer
NO <sub>x</sub>	Oxides of Nitrogen
OC	Organic Carbon
PAHs	Polycyclic Aromatic Hydrocarbons
PM	Particulate Matter
PSVOC	Particulate/Semi-Volatile Organic Compound
PUF	Polyurethane Foam
RPM	rotations per minute
Scfm	standard cubic feet per minute
SMPS	Scanning Mobility Particle Sizer
SOF	Soluble Organic Fraction
SVOC	Semi-Volatile Organic Compound
T&M	Tampering & Malmaintenance
TEOM	Tapered Element Oscillating Microbalance
TIGF	Teflon-Impregnated Glass Fiber
TPM	Total Particulate Matter
TransLab	WVU Transportable Heavy Duty Vehicle Emissions Testing Laboratory
TSI	TSI Incorporated
UDDS	Urban Dynamometer Driving Schedule
URG	URG Corporation
US	United States
VOC	Volatile Organic Compounds
WVU	West Virginia University
XAD	Manufacturers name for a class of polymeric resin beads

## Introduction

Project E-55/59 Phase 2 (E-55/59-2) had the objective of acquiring regulated emissions measurements from nineteen in-use trucks in southern California, and supporting a third-party characterization of non-regulated species from five HHDDT and one diesel - fueled MHDT trucks (total of 6) in the Phase 2 test fleet. Non-regulated exhaust characterization included speciation of both particulate matter (PM) and volatile organic compounds (VOC), and determination of particle size distribution. In addition, one vehicle (E55CRC-45) was found to have a defective solenoid for the fuel pump. This vehicle was repaired and re-tested. A twentieth vehicle was added to the study when difficulties were encountered in testing a 2002 model year truck (E55CRC-52) on the medium-duty chassis dynamometer.

## Vehicle Procurement

Twenty vehicles were procured. Table 4 shows the nineteen vehicles identified in the original test plan, and identified whether each vehicle was a MHDT or HHDDT, whether they were fueled by gasoline or diesel, and whether they were subject to further chemical analysis. In Table 4 the term model year was intended to refer to the model year of manufacture of the truck chassis. Some vehicles that were recruited had an engine year that was one year earlier than the chassis model year, but the chassis model year prevailed in these circumstances in satisfying Table 4 requirements.

**Table 4: Vehicles planned for recruiting in the E-55/59-2 program.**

Wt class/ Fuel type	Model Year	Qty	Chemical analysis qty <sup>1</sup>	Post-1998 4.0g/bhp- hr NO <sub>x</sub> <sup>2</sup>	2004 2.5g/bhp-hr NO <sub>x</sub> +NMHC
HHDDT	84-86	1	0	0	NA
HHDDT	87-90	2	1	0	NA
HHDDT	91-93	1	0	0	NA
HHDDT	94-97	2	1	0	NA
HHDDT	98	1	0	0	NA
HHDDT	99-02	1	1	0	NA
HHDDT	03+	2	2	1	NA
Diesel MHDT	80-83	1	0	0	NA
Diesel MHDT	87-90	1	0	0	NA
Diesel MHDT	91-93	1	0	0	NA
Diesel MHDT	94-97	1	0	0	NA
Diesel MHDT	98	1	1	0	NA
Diesel MHDT	99+	2	0	1	NA
Gasoline MHDT	84-86	1	0	NA	0
Gasoline MHDT	00+	1	0	NA	1
Totals		19	6	2	1

<sup>1</sup>For chemical analyses, engines shall represent the three major HD engine manufacturer (Caterpillar, Cummins, or DDC), and no more than two engines per manufacturer shall be procured in each weight class. <sup>2</sup>This vehicle must be from one of the three major HD engine manufacturer (Caterpillar, Cummins, or DDC)

The actual vehicles procured differed from the vehicle distribution in Table 4. The only older gasoline - fueled MHDT available for procurement was a 1983 chassis (E55CRC-54). The last vehicle tested (E55CRC-58) had an engine remanufactured by Detroit Diesel. Table 5 provides information on the actual vehicles recruited. Of these nineteen vehicles, two were gasoline – fueled MHDT, seven were diesel – fueled MHDT, and ten were HHDDT. The GVWR ranged from 19,700 pounds to 33,000 pounds for the MHDT vehicles. All of the HHDDT vehicles were “full size” over-the-road tractors, which would be regarded normally as having a gross combination weight rating of 80,000 pounds.

**Table 5: Basic Information on the 20 trucks actually recruited in Phase 2.**

E55CRC-(truck)	Cycle*	Vehicle model year	Vehicle Manufacturer	Engine Model Year	Engine Model	Engine Power (hp)	Engine Manufacturer
E55CRC-39	H	2004	Volvo	2003	ISX	530	Cummins
E55CRC-40	H	2004	Freightliner	2003	Series 60	500	Detroit
E55CRC-41	M	1998	Ford	1997	B5.9	210	Cummins
E55CRC-42	H	2000	Freightliner	1999	3406	435	Caterpillar
E55CRC-43	H	1995	Peterbilt	1994	Series 60	470	Detroit
E55CRC-44	H	1989	Volvo	1989	3406	300 (est.)	Caterpillar
E55CRC-45	H	1993	Volvo GM	1993	L10-280	280	Cummins
E55CRC-46	H	1989	Volvo GM	1989	3176	400 (est.)	Caterpillar
E55CRC-47	H	1986	Ford	1986	6V92	350	Detroit
E55CRC-48	H	1998	Freightliner	1998	N14 Plus	447	Cummins
E55CRC-49	H	1994	International	1993	3406	300 (est.)	Caterpillar
E55CRC-50	M	2001	International	2001	DT466 C-195	195	International
E55CRC-51	M	1994	International	1994	DT-408 A210F	210	International
E55CRC-52	M	2002	Isuzu	2002	4HE1-TCS	175	Isuzu
E55CRC-53	M	2001	GMC	2001	1GMXH08.15 12 Gas V8	270	GM
E55CRC-54	M	1983	Ford	1983	370-2V Gas V8	296	Ford
E55CRC-55	M	1992	Ford	1991	210	210	Ford
E55CRC-56	M	1988	Ford	1988	3208	215	Caterpillar
E55CRC-57	M	2000	Freightliner	1999	3126	330	Caterpillar
E55CRC-58	M	1982	Ford	1999	V8-8.2 4087- 7300 770	160 (est.)	Detroit

\*M=MHDT, H=HHDDT

The trucks were recruited by West Virginia University staff and included rental trucks, in-use trucks, and trucks that were traded in for re-sale. In Phase 2, vehicles were recruited from dealerships, truck rental companies, and used truck sales lots. The 2004 model year vehicles were new. The rental trucks were in regular use. It was not known whether the trucks for sale had been traded-in simply due to age, or for a specific mechanical reason. However, the trucks were inspected prior to testing to insure that no major mechanical problems were present. Once recruited, a WVU driver or commercial driver (when required) drove each vehicle to the WVU test site. The driver inspected the vehicle before moving the vehicle: no vehicles were rejected based on this preliminary inspection during Phase 2 research.

Each vehicle was photographed at the laboratory site. These photographs are gathered in Appendix A to this report.

## **Test Site and Laboratory**

The characterization of the emissions took place using a WVU TransLab. For the first several vehicles, the TransLab was located at Ralphs Grocery, 1500 Eastridge Ave., Riverside, CA. The latter part of the testing was completed at 1084 Columbia Ave., Riverside, CA. The TransLab had the same arrangement as the TransLab used in the Phase 1.5 E-55/59 CRC Study. The laboratory equipment, including the analyzer bench, PM system and dilution system used, was the same as described in the final report for Phase 1.5 of this E-55/59 study. Procedures with respect to PM filter processing, analyzer calibration and background correction were the same as described in the Phase 1 report and are well established by the WVU laboratory. For completeness of this report, a description of the WVU TransLab has been included in Appendix B.

The laboratory used a TEOM analyzer to quantify continuous PM mass. The TEOM sampled at a setpoint flow rate of 2.0 liters/minute from the primary (full scale) dilution tunnel. TEOM temperature was set at 40°C.

In the Phase 1.5 and Phase 2 research, exhaust temperature was measured in the section of exhaust pipe used to connect the tailpipe to the dilution tunnel, using a J-type thermocouple. Exhaust temperature was not measured in Phase 1 research. Prior to commencing phase 1 of the E-55/59 program, the WVU laboratory participated in a crosscheck with other chassis dynamometer laboratories in North America [1].

## **Test Cycles**

Each vehicle was tested using a suite of test schedules, which are shown graphically in Appendix C of this report. The Heavy-Duty Urban Dynamometer Driving Schedule (UDDS) was used for all classes of vehicles.

For the heavy heavy-duty vehicles, the HHDDT Schedule [2], consisting of four modes (Idle, Creep, Transient and Cruise), was also used. A fifth mode, HHDDT\_S, representing higher speed freeway operation, was developed and added to the HHDDT schedule in the test plan for Phase 1.5. For Phase 2, this mode was intended for use in testing all heavy heavy-duty vehicles. HHDDT\_S has a maximum speed of 67 mph and an average speed of 50 mph. In some cases, trucks may be governed at a sufficiently low road speed that the HHDDT\_S Mode could not be executed reasonably. In these cases, as judged by the WVU field engineer, no HHDDT\_S Mode was to be attempted. In this phase of testing, all vehicles scheduled for this schedule successfully completed it.

For those HHDDT's subject to chemical analysis, the Idle, Creep, Transient, Cruise and HHDDT\_S modes were each repeated.

For the MHDT not subject to speciation, the AC5080 and the MHDT Schedule were added to the UDDS. The MHDT schedule consists of three modes: MHDTLO, MHDTHI, and MHDTCR [3]. For three of these vehicles, the HHDDT\_S mode was

included in the MHDT schedule. For the one MHDT subjected to further chemical analysis, Idle (not included on the other MHDT vehicles), Lower Speed Transient, Higher Speed Transient, and Cruise Modes were each repeated to create paired data sets at the laden weight.

### Test Weights

All ten of the HHDDT tested in this study were deemed to have gross vehicle weights of 80,000 lb., in that they were all typical over-the-road tractors. For tractor-trailers, it is the combination weight that is of interest, rather than the tractor weight. The test weights were 56,000 pounds.

The nine MHDT were tested at both laden and unladen weights. Laden weight was set to be 75% of the gross vehicle weight rating (GVWR). The unladen weight was set at 50% of the GVWR.

Figure 1 shows an example of the increase in PM with respect to test weight. Figure 2 shows that, with the exception of the AC5080 driving schedule, NO<sub>x</sub> emissions increased with test weight as well for the MHDT E55CRC-53. These emissions differences vindicated the effort associated with testing at two weights.

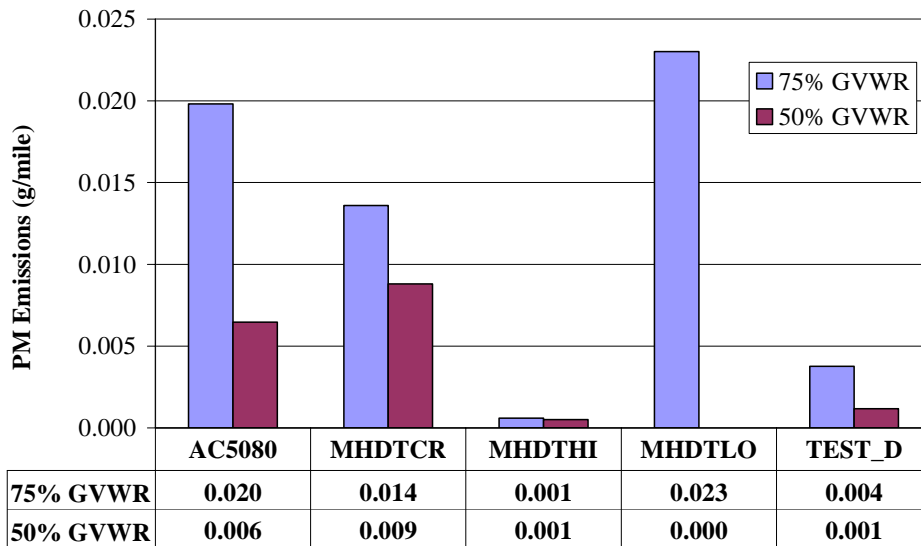


**Figure 1: PM emissions of E55CRC-53 were tested at two weights.**

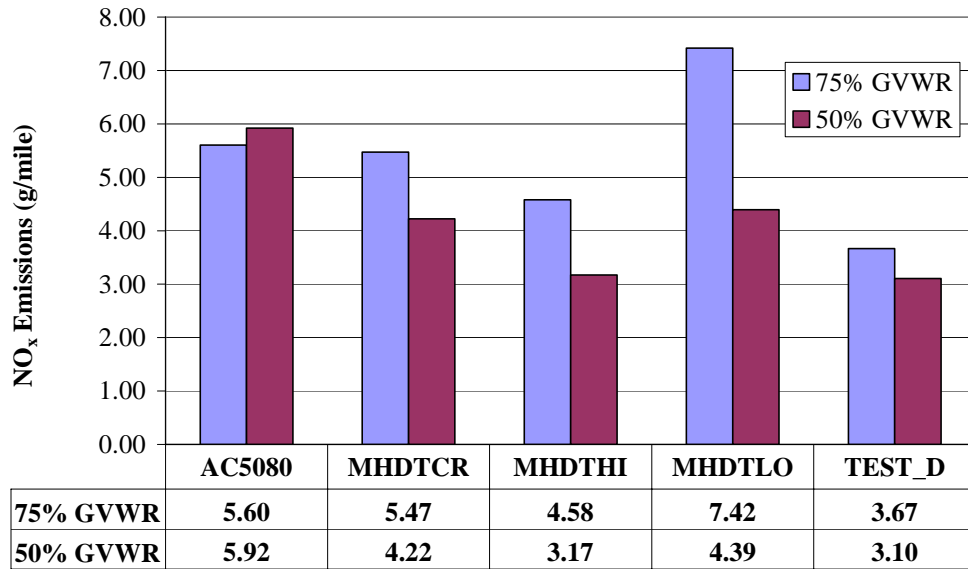


**Figure 2: NO<sub>x</sub> emissions of E55CRC-53 were tested at two weights.**

### Test Runs

In the interest of economy, a single test run was planned and executed for each combination of truck, weight and schedule or mode. A test run was repeated only if a fault was detected in executing the test.

Each execution of a cycle or mode was assigned a sequence number and a run number. Table 6 presents a listing of sequence and run numbers, with the corresponding name of the cycle, vehicle number and test weight. Some sequence and run numbers are omitted in Table 6 because they are associated with background tests or with rejected runs. In Table 6 the test modes or cycles are designated by the actual file names used. “Test D” corresponds to the UDDS, and Trans3 and Cruise3 refer to the “three point smoothed” versions of the Transient and Cruise Modes that are customarily used. Some modes were lengthened by being repeated to collect sufficient PM mass during the mode. Idle32 refers to a double length Idle (1,800 seconds instead of 900 seconds), and Creep34 refers to four repeats of a Creep run as a single mode. Table 6 corresponds to the sequence and run numbers in the short reports appearing in Appendix D.

**Table 6: Sequence number, run number and vehicle information for each reportable test**

Test Weight/ E55CRC- (truck)	Test ID	Test Run ID	Engine Manufacturer	Engine Model	Engine Model Year	Odometer Reading	Test Duration (in sec.)	Vehicle model year	Particulate Filter	Driving Schedule
56,000										
39	2858	1	Cummins	ISX	2003	45	667.9	2004	None	Trans3
39	2859	1	Cummins	ISX	2003	45	1039.9	2004	None	TEST_D
39	2863	1	Cummins	ISX	2003	45	2700	2004	None	Idle33
39	2863	2	Cummins	ISX	2003	45	2700	2004	None	Idle33
39	2863	3	Cummins	ISX	2003	45	1032	2004	None	Creep34
39	2863	7	Cummins	ISX	2003	45	688	2004	None	Trans3
39	2863	8	Cummins	ISX	2003	45	688	2004	None	Trans3
39	2863	9	Cummins	ISX	2003	45	2083	2004	None	Cruise3
39	2863	10	Cummins	ISX	2003	45	760	2004	None	HHDDT_S
39	2863	11	Cummins	ISX	2003	45	2083	2004	None	Cruise3
39	2863	12	Cummins	ISX	2003	45	760	2004	None	HHDDT_S
56,000										
40	2867	1	DDC	Series 60	2003	8916	1039.9	2004	None	TEST_D
40	2868	3	DDC	Series 60	2003	8916	1032	2004	None	Creep34
40	2872	1	DDC	Series 60	2003	8916	667.9	2004	None	Trans3
40	2872	2	DDC	Series 60	2003	8916	667.9	2004	None	Trans3
40	2872	3	DDC	Series 60	2003	8916	2062.9	2004	None	Cruise3
40	2872	4	DDC	Series 60	2003	8916	739.9	2004	None	HHDDT_S
40	2872	5	DDC	Series 60	2003	8916	2679.9	2004	None	Idle33
40	2872	6	DDC	Series 60	2003	8916	2679.9	2004	None	Idle33
40	2872	7	DDC	Series 60	2003	8916	2062.9	2004	None	Cruise3
40	2872	8	DDC	Series 60	2003	8916	739.9	2004	None	HHDDT_S
75% GVWR										
41	2877	1	Cummins	B5.9 210	1997	13029	194.8	1998		AC5080
41	2878	1	Cummins	B5.9 210	1997	13029	1039.9	1998		TEST_D
41	2879	1	Cummins	B5.9 210	1997	13029	2679.9	1998		Idle33
41	2879	2	Cummins	B5.9 210	1997	13029	2679.9	1998		Idle33
41	2879	4	Cummins	B5.9 210	1997	13029	349.9	1998		MHDTLO
41	2879	5	Cummins	B5.9 210	1997	13029	1169.9	1998		MHDTHI
41	2879	6	Cummins	B5.9 210	1997	13029	349.9	1998		MHDTLO
41	2879	7	Cummins	B5.9 210	1997	13029	1169.9	1998		MHDTHI
41	2879	8	Cummins	B5.9 210	1997	13029	1889.9	1998		MHDTCR
41	2879	9	Cummins	B5.9 210	1997	13029	1889.9	1998		MHDTCR
50% GVWR										
41	2883	1	Cummins	B5.9 210	1997	13029	188.6	1998		AC5080
41	2883	2	Cummins	B5.9 210	1997	13029	1039.9	1998		TEST_D
41	2883	3	Cummins	B5.9 210	1997	13029	349.9	1998		MHDTLO
41	2883	4	Cummins	B5.9 210	1997	13029	1169.9	1998		MHDTHI
41	2883	5	Cummins	B5.9 210	1997	13029	1889.9	1998		MHDTCR
56,000										
42	2886	1	Caterpillar	3406	1999	576998	2679.9	2000	None	Idle33
42	2886	2	Caterpillar	3406	1999	576998	2679.9	2000	None	Idle33
42	2890	1	Caterpillar	3406	1999	576998	1039.9	2000	None	TEST_D
42	2891	1	Caterpillar	3406	1999	576998	1011.9	2000	None	Creep34
42	2892	1	Caterpillar	3406	1999	576998	688	2000	None	Trans3
42	2892	2	Caterpillar	3406	1999	576998	667.9	2000	None	Trans3

42	2892	3	Caterpillar	3406	1999	576998	2062.9	2000	None	Cruise3
42	2892	4	Caterpillar	3406	1999	576998	739.9	2000	None	HHDDT_S
42	2892	5	Caterpillar	3406	1999	576998	2062.9	2000	None	Cruise3
42	2892	6	Caterpillar	3406	1999	576998	739.9	2000	None	HHDDT_S
56,000										
43	2896	1	DDC	Series 60	1994	899582	1039.9	1995	None	TEST_D
43	2897	1	DDC	Series 60	1994	899582	1011.9	1995	None	Creep34
43	2898	1	DDC	Series 60	1994	899582	688	1995	None	Trans3
43	2907	1	DDC	Series 60	1994	899582	667.9	1995	None	Trans3
43	2907	2	DDC	Series 60	1994	899582	2679.9	1995	None	Idle33
43	2907	3	DDC	Series 60	1994	899582	2679.9	1995	None	Idle33
43	2909	1	DDC	Series 60	1994	899582	2062.9	1995	None	Cruise3
43	2909	2	DDC	Series 60	1994	899582	739.9	1995	None	HHDDT_S
43	2909	3	DDC	Series 60	1994	899582	2062.9	1995	None	Cruise3
43	2909	4	DDC	Series 60	1994	899582	739.9	1995	None	HHDDT_S
56,000										
44	2913	1	Caterpillar	3406	1989	811202	2679.9	1989	None	Idle33
44	2913	2	Caterpillar	3406	1989	811202	2679.9	1989	None	Idle33
44	2913	3	Caterpillar	3406	1989	811202	1011.9	1989	None	Creep34
44	2920	1	Caterpillar	3406	1989	811202	667.9	1989	None	Trans3
44	2920	2	Caterpillar	3406	1989	811202	667.9	1989	None	Trans3
44	2920	3	Caterpillar	3406	1989	811202	1039.9	1989	None	TEST_D
44	2920	5	Caterpillar	3406	1989	811202	2062.9	1989	None	Cruise3
44	2920	6	Caterpillar	3406	1989	811202	739.9	1989	None	HHDDT_S
44	2920	7	Caterpillar	3406	1989	811202	2062.9	1989	None	Cruise3
44	2920	8	Caterpillar	3406	1989	811202	739.9	1989	None	HHDDT_S
56,000										
45	2985	1	Cummins	L10-280	1993	685168	1039.9	1993	None	TEST_D
45	2986	2	Cummins	L10-280	1993	685168	1032	1993	None	Creep34
45	2986	3	Cummins	L10-280	1993	685168	688	1993	None	Trans3
45	2986	5	Cummins	L10-280	1993	685168	760	1993	None	HHDDT_S
45	2986	6	Cummins	L10-280	1993	685168	1779.9	1993	None	Idle32
45	2986	7	Cummins	L10-280	1993	685168	2062.9	1993	None	Cruise3
45RR	200081		Cummins	L10-280	1993	685168	1039.9	1993	None	TEST_D
45RR	200091		Cummins	L10-280	1993	685168	1800	1993	None	Idle32
45RR	200092		Cummins	L10-280	1993	685168	1032	1993	None	Creep34
45RR	200093		Cummins	L10-280	1993	685168	688	1993	None	Trans3
45RR	200096		Cummins	L10-280	1993	685168	2062.9	1993	None	Cruise3
45RR	200097		Cummins	L10-280	1993	685168	739.9	1993	None	HHDDT_S
56,000										
46	2971	1	Caterpillar	3176	1993	935582	1039.9	1989	None	TEST_D
46	2972	1	Caterpillar	3176	1993	935582	1779.9	1989	None	Idle32
46	2972	2	Caterpillar	3176	1993	935582	1011.9	1989	None	Creep34
46	2972	4	Caterpillar	3176	1993	935582	2062.9	1989	None	Cruise3
46	2972	5	Caterpillar	3176	1993	935582	739.9	1989	None	HHDDT_S
46	2972	6	Caterpillar	3176	1993	935582	667.9	1989	None	Trans3
56,000										
47	2975	1	DDC	6V92	1986	760810	1039.9	1986	None	TEST_D
47	2976	1	DDC	6V92	1986	760810	1800	1986	None	Idle32
47	2976	2	DDC	6V92	1986	760810	1032	1986	None	Creep34
47	2976	3	DDC	6V92	1986	760810	688	1986	None	Trans3
47	2976	5	DDC	6V92	1986	760810	760	1986	None	HHDDT_S
47	2976	6	DDC	6V92	1986	760810	2083	1986	None	Cruise3

56,000										
48	2980	1	Cummins	N14 Plus	1998	753792	1039.9	1998	None	TEST_D
48	2981	1	Cummins	N14 Plus	1998	753792	1800	1998	None	Idle32
48	2981	2	Cummins	N14 Plus	1998	753792	1032	1998	None	Creep34
48	2981	3	Cummins	N14 Plus	1998	753792	688	1998	None	Trans3
48	2981	4	Cummins	N14 Plus	1998	753792	2083	1998	None	Cruise3
48	2981	5	Cummins	N14 Plus	1998	753792	760	1998	None	HHDDT_S
56,000										
49	20014	1	Caterpillar	3406	1993	650557	1039.9	1994	None	TEST_D
49	20015	1	Caterpillar	3406	1993	650557	1800	1994	None	Idle32
49	20015	2	Caterpillar	3406	1993	650557	1032	1994	None	Creep34
49	20015	3	Caterpillar	3406	1993	650557	688	1994	None	Trans3
49	20015	4	Caterpillar	3406	1993	650557	2083	1994	None	Cruise3
49	20015	5	Caterpillar	3406	1993	650557	760	1994	None	HHDDT_S
75% GVWR										
50	20145	1	International	DT466 C-195	2001	73077	196.3	2001	None	AC5080
50	20146	1	International	DT466 C-195	2001	73077	1060	2001	None	TEST_D
50	20146	2	International	DT466 C-195	2001	73077	1060	2001	None	MHDTLO
50	20146	3	International	DT466 C-195	2001	73077	1190	2001	None	MHDTHI
50	20146	4	International	DT466 C-195	2001	73077	1910	2001	None	MHDTCR
50	20146	5	International	DT466 C-195	2001	73077	760	2001	None	HHDDT_S
50% GVWR										
50	20150	1	International	DT466 C-195	2001	73132	188.7	2001	None	AC5080
50	20151	1	International	DT466 C-195	2001	73134	1060	2001	None	TEST_D
50	20151	2	International	DT466 C-195	2001	73134	370	2001	None	MHDTLO
50	20151	4	International	DT466 C-195	2001	73134	1190	2001	None	MHDTHI
50	20151	5	International	DT466 C-195	2001	73134	1910	2001	None	MHDTCR
50	20151	6	International	DT466 C-195	2001	73134	739.9	2001	None	HHDDT_S
75% GVWR										
51	20128	1	International	DT-408 A210F	1994	126477	206.5	1994	None	AC5080
51	20129	1	International	DT-408 A210F	1994	126477	1060	1994	None	TEST_D
51	20129	2	International	DT-408 A210F	1994	126477	370	1994	None	MHDTLO
51	20129	3	International	DT-408 A210F	1994	126477	1190	1994	None	MHDTHI
51	20129	4	International	DT-408 A210F	1994	126477	1910	1994	None	MHDTCR
50% GVWR										
51	20140	1	International	DT-408 A210F	1994	126477	1060	1994	None	TEST_D
51	20140	3	International	DT-408 A210F	1994	126477	1190	1994	None	MHDTHI
51	20140	5	International	DT-408 A210F	1994	126477	1910	1994	None	MHDTCR
51	20140	6	International	DT-408 A210F	1994	126477	370	1994	None	MHDTLO
51	20141	1	International	DT-408 A210F	1994	126566	199	1994	None	AC5080
75% GVWR										
53	20183	1	GM	1GMXH08.1512	2001	57282	199	2001	None	AC5080
53	20184	1	GM	1GMXH08.1512	2001	57284	1060	2001	None	TEST_D
53	20184	2	GM	1GMXH08.1512	2001	57284	370	2001	None	MHDTLO
53	20184	3	GM	1GMXH08.1512	2001	57284	1190	2001	None	MHDTHI
53	20184	4	GM	1GMXH08.1512	2001	57284	1889.9	2001	None	MHDTCR
50% GVWR										
53	20180	1	GM	1GMXH08.1512	2001	57221	199.1	2001	None	AC5080
53	20181	1	GM	1GMXH08.1512	2001	57224	1060	2001	None	TEST_D
53	20181	2	GM	1GMXH08.1512	2001	57224	370	2001	None	MHDTLO
53	20181	3	GM	1GMXH08.1512	2001	57224	1190	2001	None	MHDTHI
53	20181	5	GM	1GMXH08.1512	2001	57224	1889.9	2001	None	MHDTCR
75% GVWR										

54	20192	1	Ford	370-2V	1993	81668	209.9	1983	None	AC5080
54	20193	1	Ford	370-2V	1993	81668	1060	1983	None	TEST_D
54	20193	2	Ford	370-2V	1993	81668	370	1983	None	MHDTLO
54	20193	3	Ford	370-2V	1993	81668	1190	1983	None	MHDTHI
54	20193	4	Ford	370-2V	1993	81668	1889.9	1983	None	MHDTCR
50%										
54	20195	1	Ford	370-2V	1993	81668	206.1	1983	None	AC5080
54	20196	1	Ford	370-2V	1993	81711	1060	1983	None	TEST_D
54	20196	2	Ford	370-2V	1993	81711	370	1983	None	MHDTLO
54	20196	3	Ford	370-2V	1993	81711	1190	1983	None	MHDTHI
54	20202	1	Ford	370-2V	1993	81773	1889.9	1983	None	MHDTCR
75%										
55	20206	1	Ford	210	1991	590761	215.2	1992	None	AC5080
55	20207	1	Ford	210	1991	590761	1060	1992	None	TEST_D
55	20207	2	Ford	210	1991	590761	370	1992	None	MHDTLO
55	20207	3	Ford	210	1991	590761	1190	1992	None	MHDTHI
55	20207	4	Ford	210	1991	590761	1910	1992	None	MHDTCR
55	20207	5	Ford	210	1991	590761	760	1992	None	HHDDT_S
50%										
55	20211	1	Ford	210	1991	590826	212	1992	None	AC5080
55	20212	1	Ford	210	1991	590828	1060	1992	None	TEST_D
55	20212	2	Ford	210	1991	590828	370	1992	None	MHDTLO
55	20212	3	Ford	210	1991	590828	1190	1992	None	MHDTHI
55	20212	4	Ford	210	1991	590828	1910	1992	None	MHDTCR
55	20212	5	Ford	210	1991	590828	760	1992	None	HHDDT_S
75%										
56	20216	1	Caterpillar	3208	1988	149556	215.2	1988	None	AC5080
56	20217	1	Caterpillar	3208	1988	149558	1060	1988	None	TEST_D
56	20217	2	Caterpillar	3208	1988	149558	370	1988	None	MHDTLO
56	20217	3	Caterpillar	3208	1988	149558	1190	1988	None	MHDTHI
56	20217	4	Caterpillar	3208	1988	149558	1910	1988	None	MHDTCR
50%										
56	20219	1	Caterpillar	3208	1988	149602	203.3	1988	None	AC5080
56	20220	1	Caterpillar	3208	1988	149604	1060	1988	None	TEST_D
56	20224	1	Caterpillar	3208	1988	149617	349.9	1988	None	MHDTLO
56	20224	2	Caterpillar	3208	1988	149617	1169.9	1988	None	MHDTHI
56	20224	3	Caterpillar	3208	1988	149617	1889.9	1988	None	MHDTCR
75%										
57	20229	1	Caterpillar	3126	1999	101604	206.1	2000	None	AC5080
57	20230	2	Caterpillar	3126	1999	101606	1060	2000	None	TEST_D
57	20230	3	Caterpillar	3126	1999	101606	370	2000	None	MHDTLO
57	20230	4	Caterpillar	3126	1999	101606	1190	2000	None	MHDTHI
57	20230	6	Caterpillar	3126	1999	101606	1889.9	2000	None	MHDTCR
57	20233	1	Caterpillar	3126	1999	101655	739.9	2000	None	HHDDT_S
50%										
57	20235	1	Caterpillar	3126	1999	101664	193.4	2000	None	AC5080
57	20236	1	Caterpillar	3126	1999	101666	1060	2000	None	TEST_D
57	20236	2	Caterpillar	3126	1999	101666	370	2000	None	MHDTLO
57	20236	3	Caterpillar	3126	1999	101666	1190	2000	None	MHDTHI
57	20236	4	Caterpillar	3126	1999	101666	1910	2000	None	MHDTCR
57	20240	1	Caterpillar	3126	1999	101714	739.9	2000	None	HHDDT_S
50%										
58	20245	1	DDC	V8-8.2 4087-7300 770	1999	68662	1039.9	1982		TEST_D

58	20245	2	DDC	V8-8.2 4087-7300 770	1999	68662	370	1982		MHDTLO
58	20245	3	DDC	V8-8.2 4087-7300 770	1999	68662	1190	1982		MHDTHI
58	20245	4	DDC	V8-8.2 4087-7300 770	1999	68662	1910	1982		MHDTCR
58	20246	1	DDC	V8-8.2 4087-7300 770	1999	68662	200.7	1982		AC5080
75%										
58	20250	1	DDC	V8-8.2 4087-7300 770	1999	68679	241.5	1982		AC5080
58	20251	1	DDC	V8-8.2 4087-7300 770	1999	68679	1060	1982		TEST_D
58	20251	2	DDC	V8-8.2 4087-7300 770	1999	68679	370	1982		MHDTLO
58	20251	3	DDC	V8-8.2 4087-7300 770	1999	68679	1190	1982		MHDTHI
58	20251	4	DDC	V8-8.2 4087-7300 770	1999	68679	1889.9	1982		MHDTCR

## Vehicle Inspection

Each truck, when received at the test site, was inspected for safety, tampering or malmaintenance and engine control unit (ECU) status. The safety inspection was conducted by the truck's test driver (who in most instances also drove the vehicle from its source). The vehicle was inspected for:

- Exhaust leaks
- Air leaks in the brake system
- Other visible brake problems (including frayed lines, damaged slack adjusters)
- Damaged drive tires
- Drivetrain damage (including worn universal joints)
- Loose fan bearing or worn engine drive belts
- Damaged vehicle controls

Vehicle information was collected on the WVU Test Vehicle Information Sheets and they are included in Appendix E. The vehicle safety inspection was verified by the completion of WVU Vehicle Inspection Report. These sheets appear in Appendix F.

Each vehicle was also visually inspected for Tampering and Malmaintenance (T&M). This inspection was the same as that developed and used in Phase 1 of this program. Items for inspection appeared in the WVU Tampering and Malmaintenance (T&M) Issues sheet for each vehicle. Copies of the WVU Tampering and Malmaintenance (T&M) Issues Sheets appear in Appendix G of this report.

The Phase 2 E-55/59 program test plan included a provision for repair and retest of one vehicle that was identified during the T&M inspection or determined otherwise to have abnormally high emissions. The sponsors were notified of a faulty solenoid on the fuel pump of E55CRC-45, and they elected to authorize repair and retest. Data collected after the repair were collected under the vehicle designation E55CRC-45RR.

The ECU of each vehicle in the program was interrogated when possible. The ECU data were sought to confirm engine model year, engine rated power, mileage and hours of use. Additional data on the truck configuration were also available in many cases. The field engineer transmitted the interrogation results to WVU-Morgantown. In some cases, it was not possible to read the engine ECU, and in some cases, problems were experienced with the system used to read the data.

## HHDDT Data Gathered

The cycle- or mode-averaged data, in units of g/mile (except for Idle, which is in time-specific units) are all presented in Appendix D in the form of “short reports.” Data in units of g/mile, g/cycle, g/minute, g/ahp-hr and g/gallon have been gathered into summary tables in Appendix H. The full database containing continuous data has been made available to E55CRC separately in electronic form.

Discussion of individual truck emissions within the body of this report has emphasized two species, NO<sub>x</sub> and PM, for two modes, Transient and HHDDT\_S, since NO<sub>x</sub> and PM data are assumed to be of greatest interest to the sponsors. The Transient Mode data were collected to represent urban vehicle activity, and the HHDDT\_S data were chosen to represent freeway activity. None of the vehicles in the HHDDT weight class was “speed limited” to the point where it was so unable to follow the schedule trace that it was not tested for the HHDDT\_S. Figure 3 presents the NO<sub>x</sub> emissions for all of the trucks on the Transient Mode of the HHDDT. The years appearing in Figure 3 correspond to years of engine certification. It is not surprising that the 1998 vehicle shows the highest NO<sub>x</sub> emissions, since it falls toward the end of the period where off-cycle timing strategies were employed. After 1998 timing excursions were limited by the Consent Decree between manufacturers and the federal government, and NO<sub>x</sub> values would be expected to fall on most test schedules. The emissions of NO<sub>x</sub> prior to 1998 all lie between 12 and 20 g/mile.

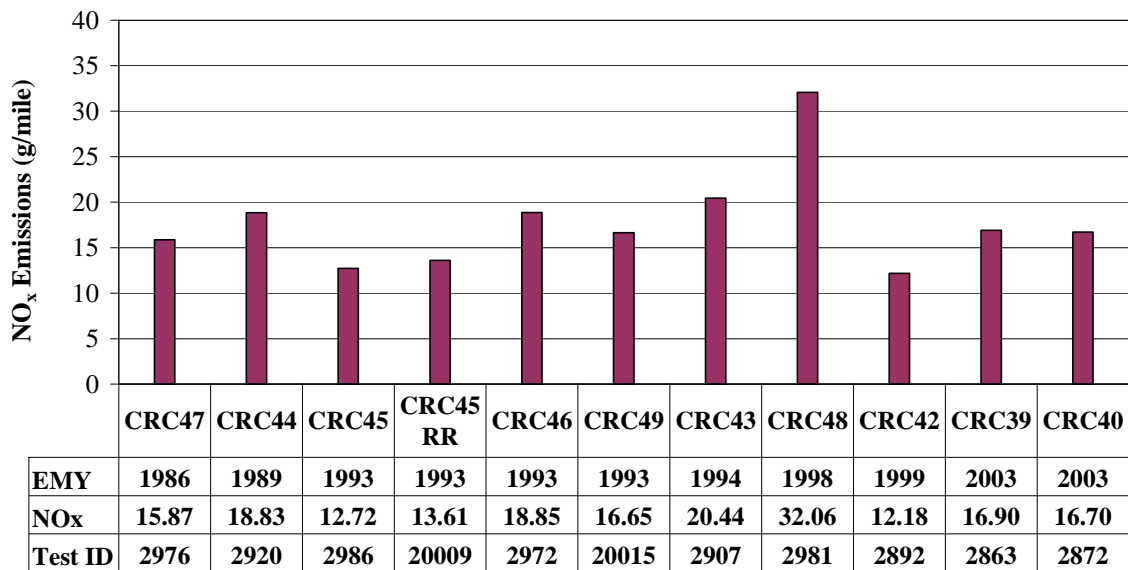


**Figure 3: NO<sub>x</sub> emissions for the Transient (Trans3) Mode (56,000lb.).**

Figure 4 shows NO<sub>x</sub> emissions for all HHDDT trucks operated through the HHDDT\_S mode at 56,000 lb. test weight. This mode has a high content of near-steady high-speed freeway operation. A 2003 year engine exhibited lowest NO<sub>x</sub>, at 8.05 g/mile. The 1994 and 1998 model year truck exhibited the highest NO<sub>x</sub> at approximately 22 g/mile. The

remaining vehicles produced NO<sub>x</sub> between 9 and 17 g/mile. Although the two 2003 vehicles emitted NO<sub>x</sub> at similar levels on the Transient Mode, one emitted NO<sub>x</sub> at a 26% loer level than the other on the HHDDT\_S.

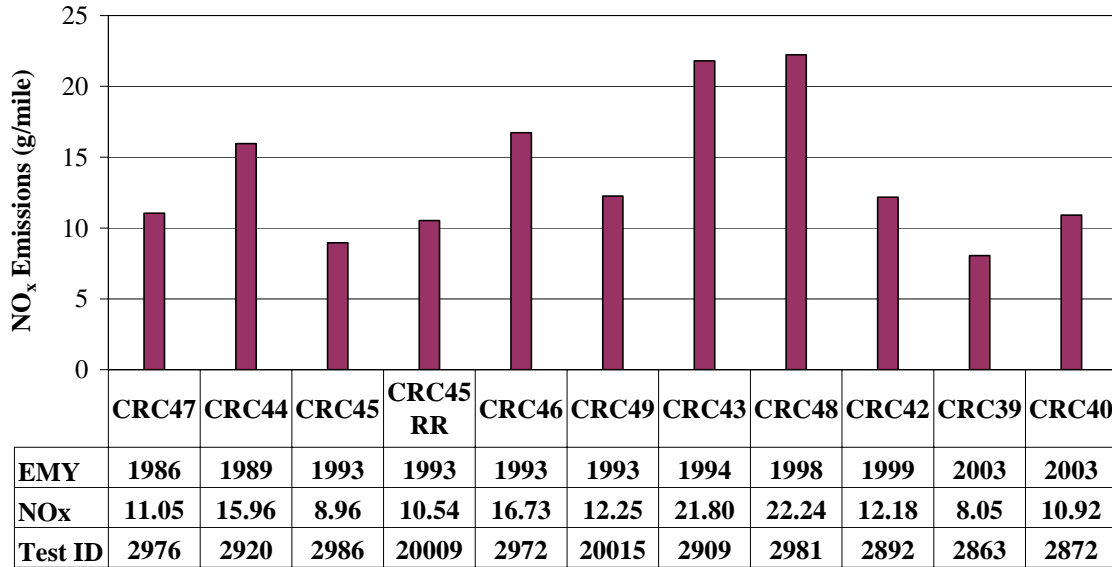


**Figure 4: NO<sub>x</sub> emissions for the HHDDT\_S Mode (56,000lb.).**

Figure 5 shows PM emissions for all HHDDT trucks operated through the Transient Mode at 56,000 lb. test weight. E55-E55CRC-45 both before and after repair and retest demonstrated significantly higher PM emissions than the other test vehicles.

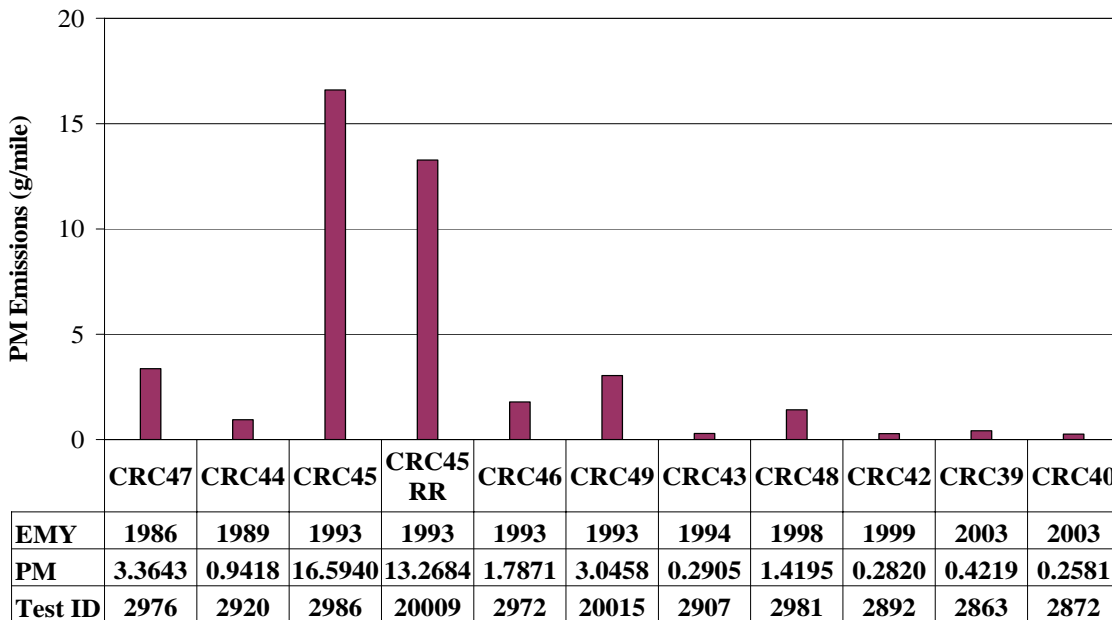


**Figure 5: PM emissions for the Transient (Trans3) Mode (56,000 lb.).**

Figure 6 shows PM emissions for all HHDDT trucks operated through the HHDDT\_S Mode at 56,000 lb. test weight. Once again E55CRC-45 both before and after repair and retest demonstrated significantly higher PM emissions than the other test vehicles. The PM of E55CRC-45 actually increased significantly after the repair on the HHDDT\_S (Figure 6), although its PM was lowered after repair on the Transient Mode (Figure 5). The newer vehicles generally produced the least PM. High CO is also often associated with high PM, because both can arise from insufficiently lean combustion. There was a 125% increase in CO emissions (from an average of 1.95g/mile to 4.39 g/mile) following the repair of E55CRC-45. E55CRC-47 was the oldest HHDDT in the test fleet and had the only two stroke engine in the fleet. With the high emitter E55CRC-45 excluded, this two stroke engine provided the highest PM emissions on the HHDDT\_S (Figure 6), but was similar in PM output to E55CRC-49, a 1993 four stroke diesel, on the Transient Mode (Figure 5).

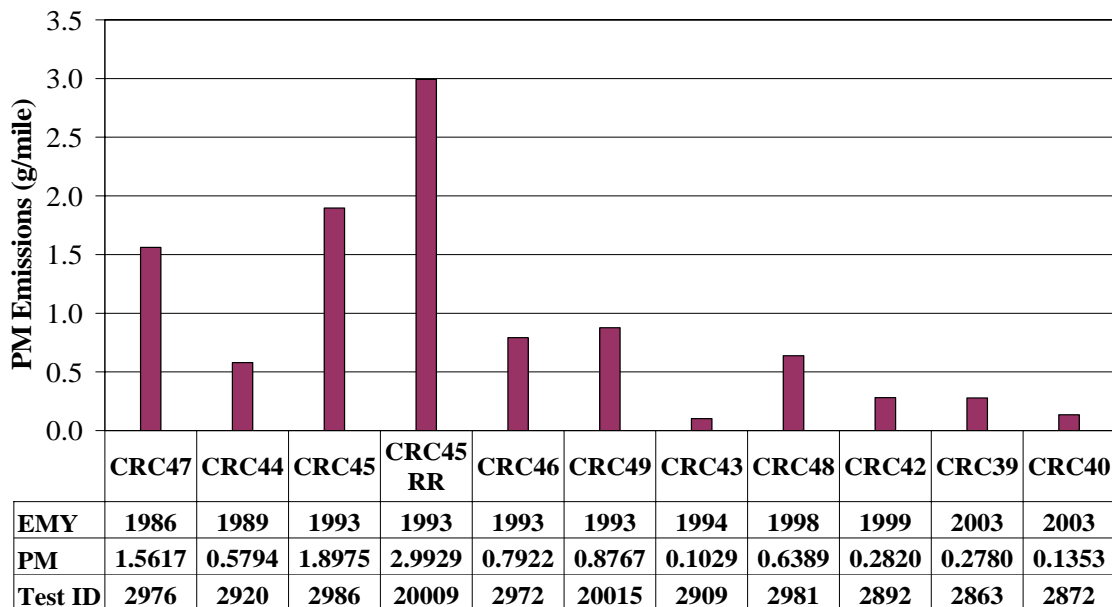
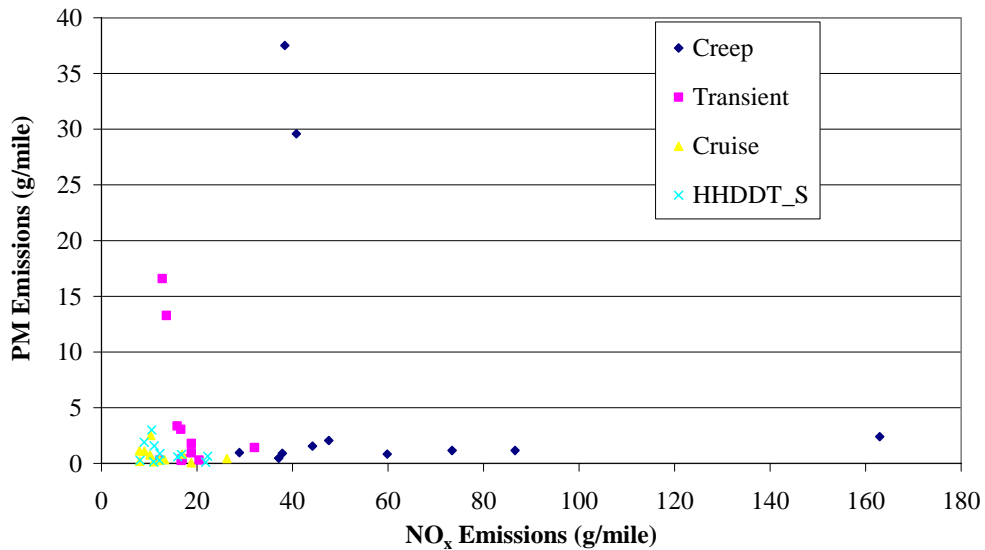


Figure 6: PM emissions for the HHDDT\_S Mode (56,000lb.).

### PM Versus NO<sub>x</sub> Plots

Plots of PM vs. NO<sub>x</sub> have been prepared showing a point for the distance-specific emissions for each truck on all modes at 56,000 lb. Figure 7 shows the Creep Mode yielding the highest distance specific emissions in most cases. The two most outlying points on the PM axis are from E55CRC-45 before and after repair. The single most outlying point on the NO<sub>x</sub> axis is from E55CRC-48.



**Figure 7: PM versus NO<sub>x</sub> for the HHDDT Modes (excluding Idle) for all Phase 2 trucks at 56,000 lb. test weight.**

### MHDT Data Gathered

This section discusses results of the testing of the MHDT. The MHDT Schedule includes the MHD TLO, MHD THI, and MHD TCR. Figure 8 presents NO<sub>x</sub> emissions for the Lower Speed Transient Mode from the MHDT. In this, and all other figures in this section, ‘laden’ refers to 75% of the gross vehicle weight rating (GVWR) and ‘unladen’ refers to 50% of the GVWR. NO<sub>x</sub> emissions from these vehicles are similar to those of the HHDT’s Transient Mode. E55CRC-57 shows unusually high unladen NO<sub>x</sub> emissions. This vehicle failed to meet the target trace, as shown in Figure 9. This vehicle apparently had an issue with a temperature sensor that indicated an overheated engine to the ECU. The ECU would then command a limp home mode resulting in the vehicle’s inability to follow the test target speed. The clutch actuated cooling fan would be activated only after the engine actually was warm. At that point the driver could return the vehicle speed to one consistent with the target trace. Conversation with Robert Graze, of Caterpillar, confirmed that the WVU diagnosis, of a temperature sensor misrepresenting the temperature to the ECU, was reasonable.

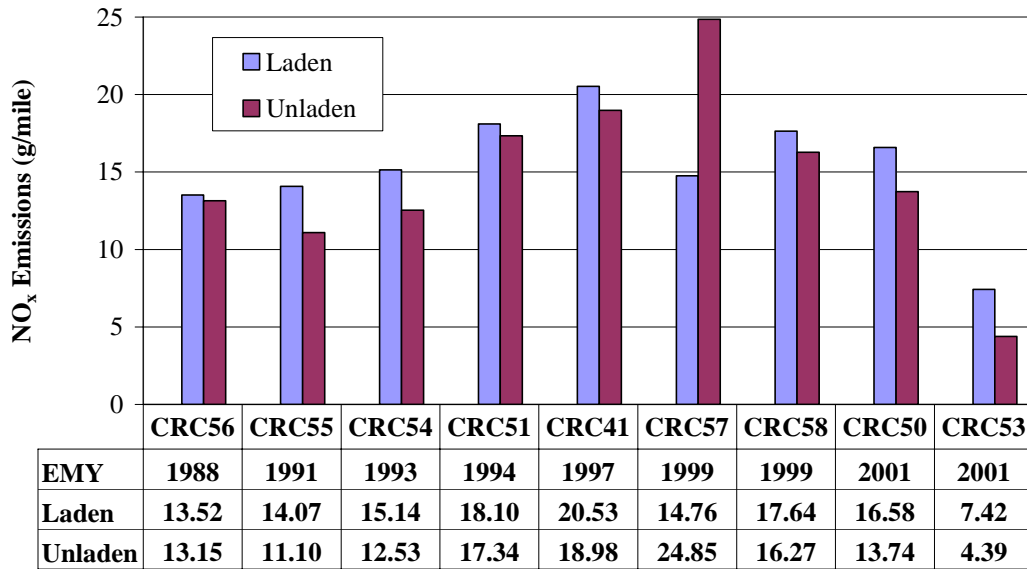


**Figure 8: NO<sub>x</sub> emissions for the Lower Speed Transient Mode (both laden and unladen).**

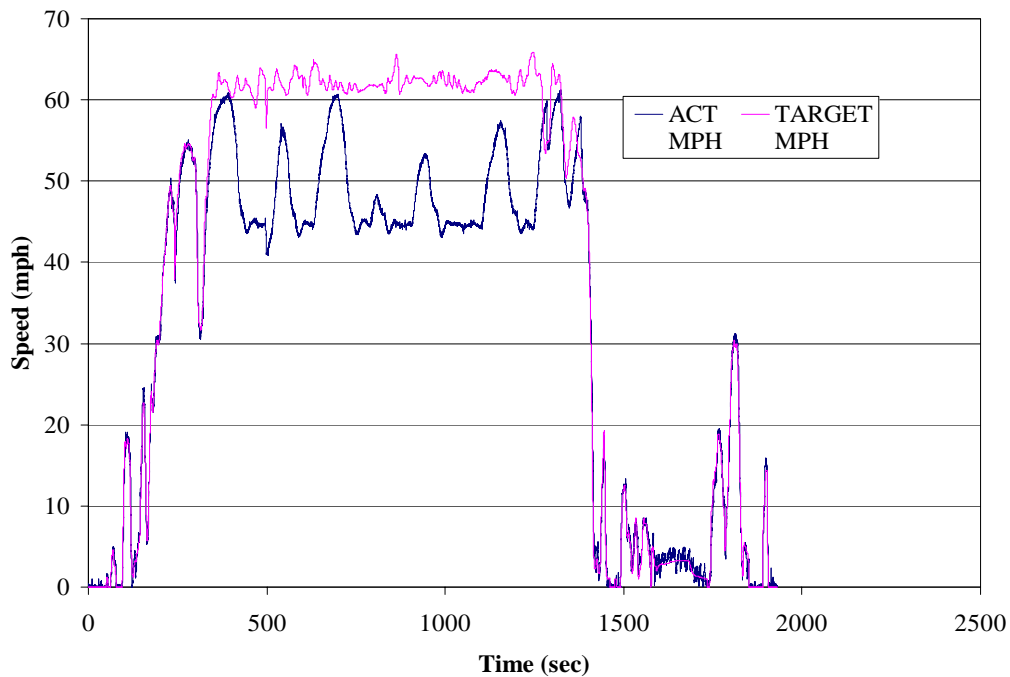


**Figure 9: Shows the inability of E55CRC-57 to meet the target trace.**

Figure 10 shows that the NO<sub>x</sub> emissions for the Higher Speed Transient Mode were consistently lower than for the Lower Speed Transient Mode. As in the previous mode, E55CRC-53, with a gasoline engine, produced the lowest NO<sub>x</sub> emissions at fewer than 4 g/mile. The older gasoline vehicle, E55CRC-54, emitted NO<sub>x</sub> at a level characteristic of

the diesel trucks. In Figure 8, and Figure 10 to 17, it is important to realize that varying test weights from truck to truck also influence distance-specific emissions levels.

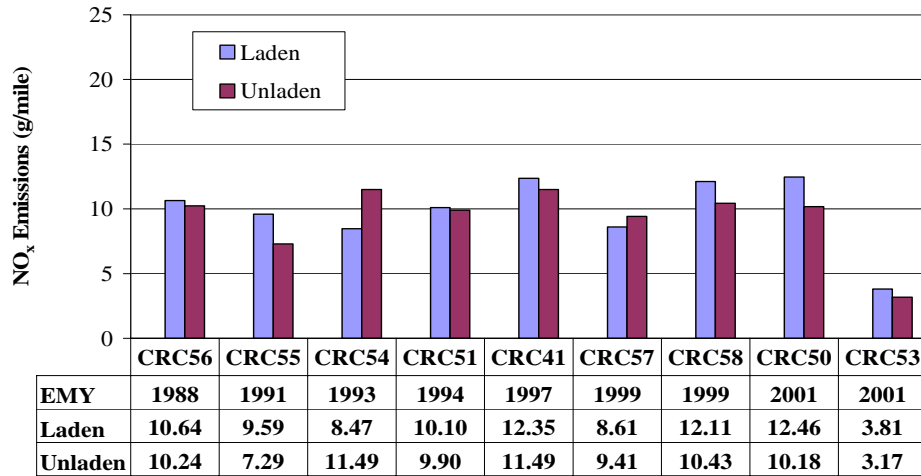


**Figure 10: NO<sub>x</sub> emissions for the Higher Speed Transient Mode (both laden and unladen).**

As seen in Figure 11, NO<sub>x</sub> emissions during the cruise cycle were slightly lower than for either of the Transient Modes and close to those of the High Speed Cruise shown in Figure 12. The older gasoline - fueled truck (E55CRC-54) emitted NO<sub>x</sub> at a higher rate than the diesel fleet on the Cruise Mode.

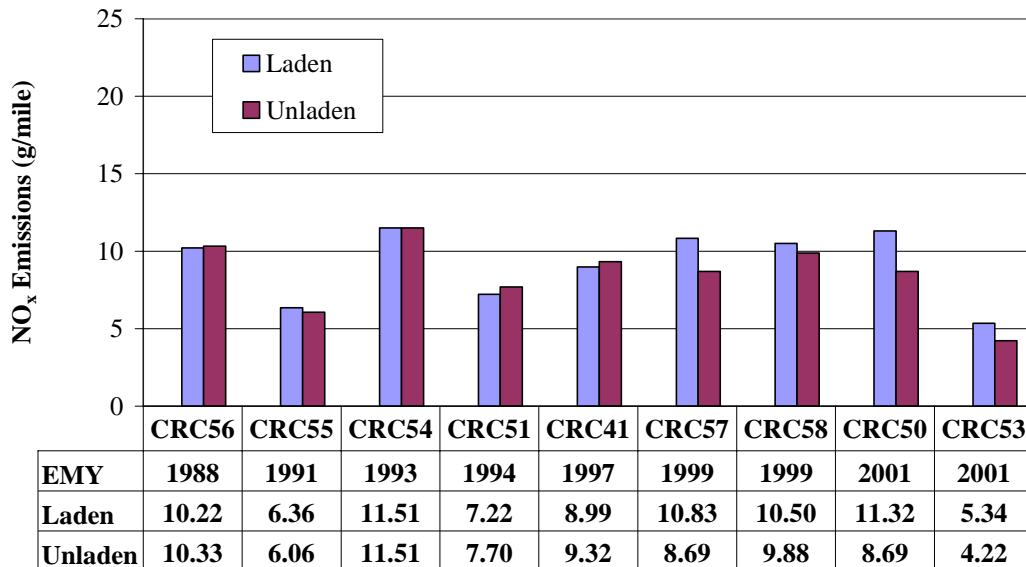


**Figure 11: NO<sub>x</sub> emissions for the Cruise Mode (both laden and unladen).**

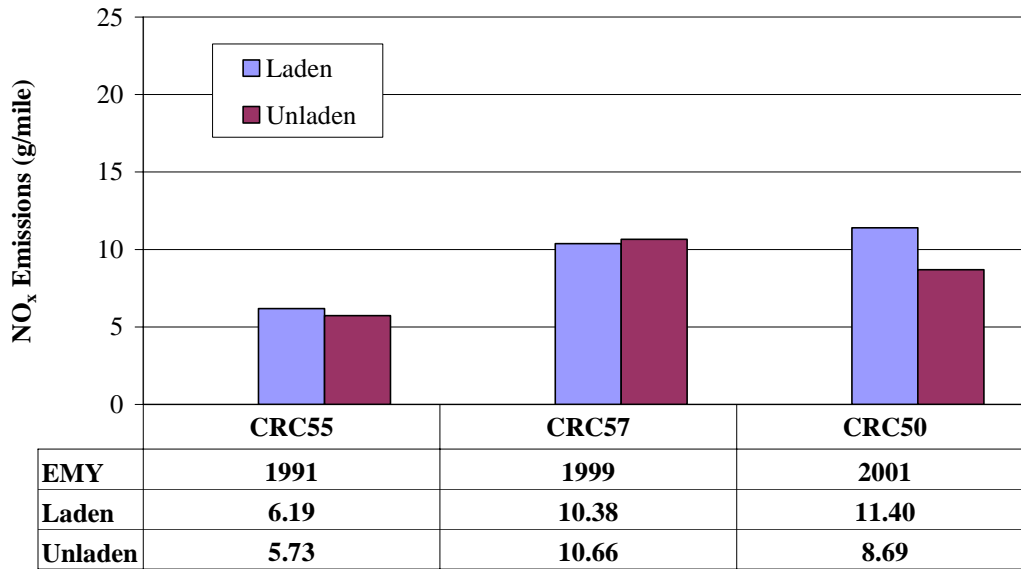


**Figure 12: NO<sub>x</sub> emissions for the HHDDT\_S Mode (both laden and unladen).**

Figure 13 to 16 show PM emissions for the Lower and Higher Speed Transients, the Cruise Mode, and the High Speed Cruise Mode. As expected, PM values from the gasoline trucks, E55CRC-53 and E55CRC-54, were consistently well below those of the diesel vehicles. Of the diesel engines, E55CRC-50, the newest vehicle, outperformed all others except the malfunctioning E55CRC-57 that could not maintain the required speed for the Cruise Mode. The influence of test weight (laden vs. unladen) on PM was noticeably greater than for NO<sub>x</sub>.

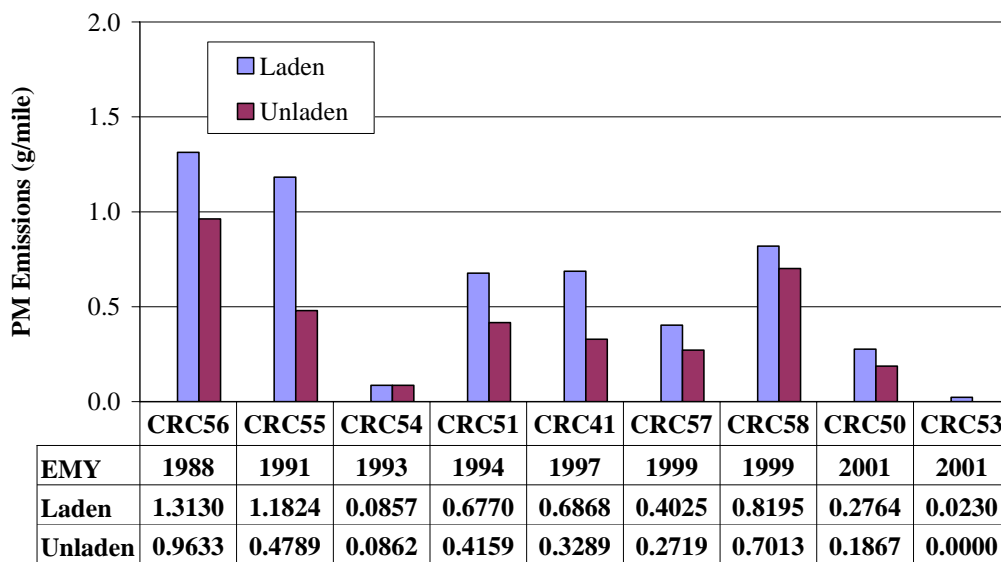


**Figure 13: PM emissions for the Lower Speed Transient Mode (both laden and unladen).**

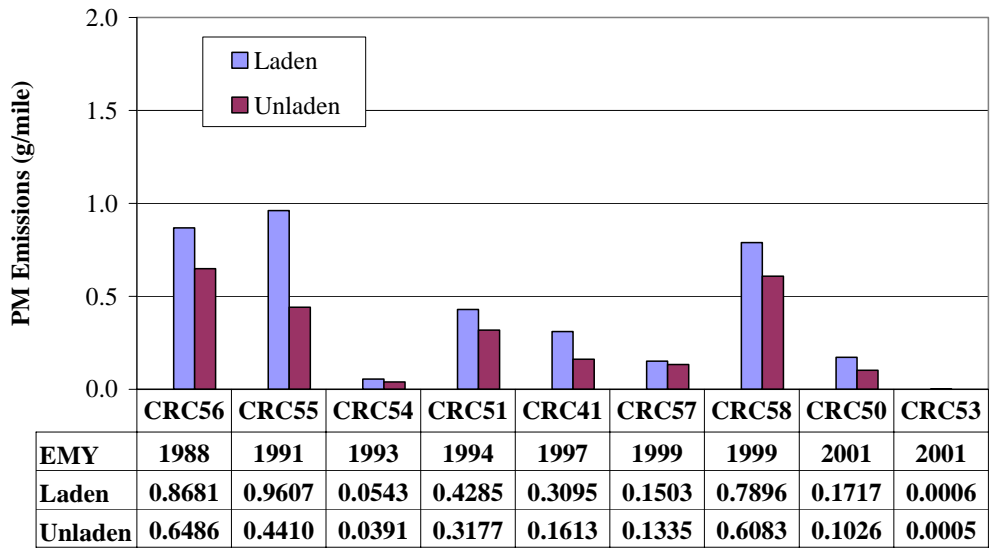


**Figure 14: PM emissions for the Higher Speed Transient Mode (both laden and unladen).**

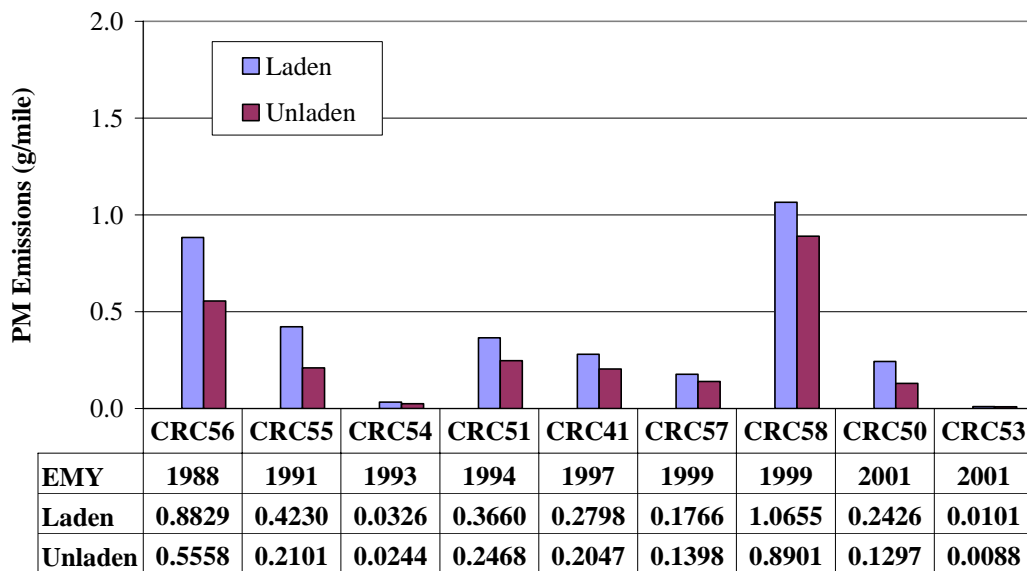


**Figure 15: PM emissions for the Cruise Mode (both laden and unladen).**

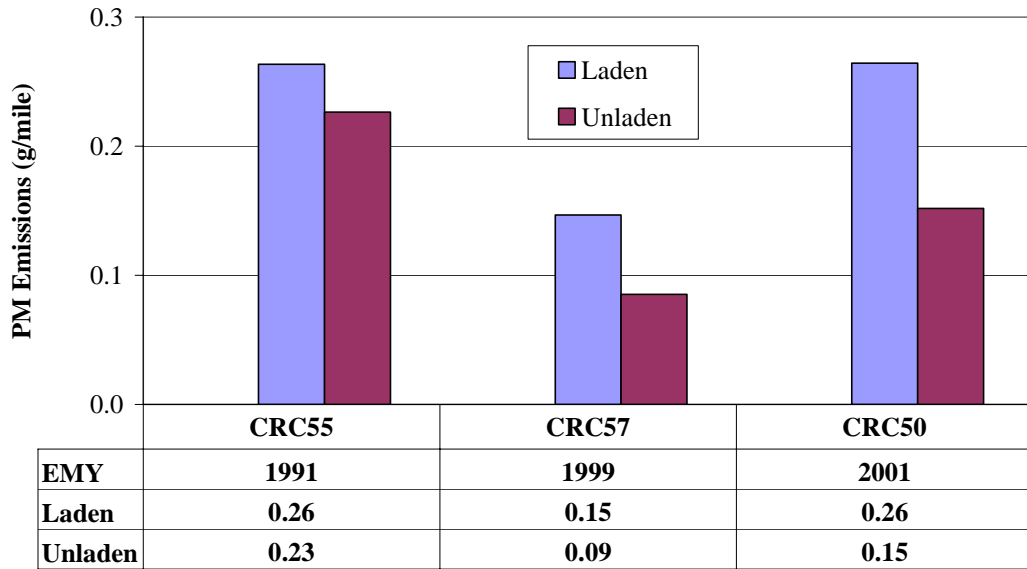


Figure 16: PM emissions for the HHD T\_S Mode (both laden and unladen).

### PM Versus NO<sub>x</sub> Plot

Figure 17 presents the PM and NO<sub>x</sub> laden truck emissions for the four test modes. These data emphasize that PM varies over a greater range than NO<sub>x</sub> for the fleet on the two Transient Modes. Figure 18 presents the unladen truck emissions.

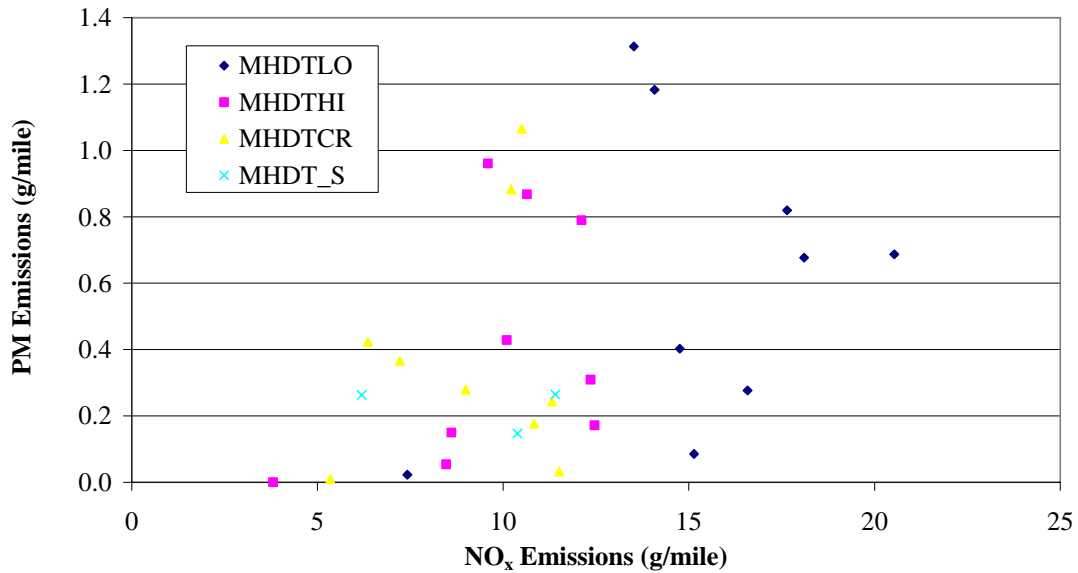
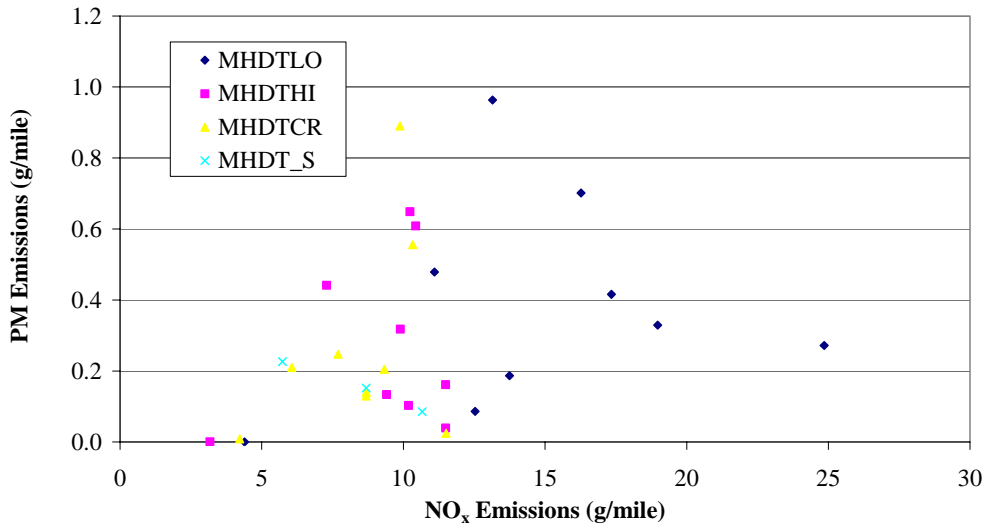


Figure 17: PM versus NO<sub>x</sub> for the MHD T Modes for Phase 2 trucks (laden).



**Figure 18: PM versus NO<sub>x</sub> for the MHD Modes for Phase 2 trucks, except E55CRC-45 and E55CRC-45RR (unladen).**

### Continuous Data

All dynamometer speeds and torques, all regulated gaseous emissions, exhaust and tunnel temperatures, and TEOM data are available on a continuous basis. These data are available to the sponsors separately from this report. Figure 19 to 21 present examples of continuous NO<sub>x</sub>, HC and CO emissions from E55CRC-42 on the Transient Mode at 56,000 lb. test weight and Figure 22 shows the exhaust temperature of this vehicle.

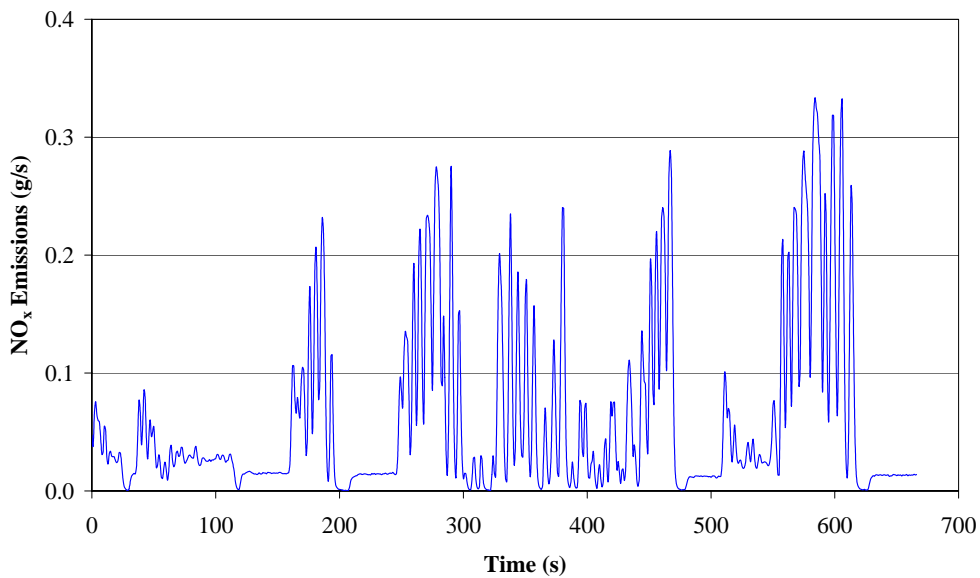


**Figure 19: Example of a continuous NO<sub>x</sub> emissions plot in g/second for E55CRC-42 at 56,000 lb. following the Transient Mode schedule.**

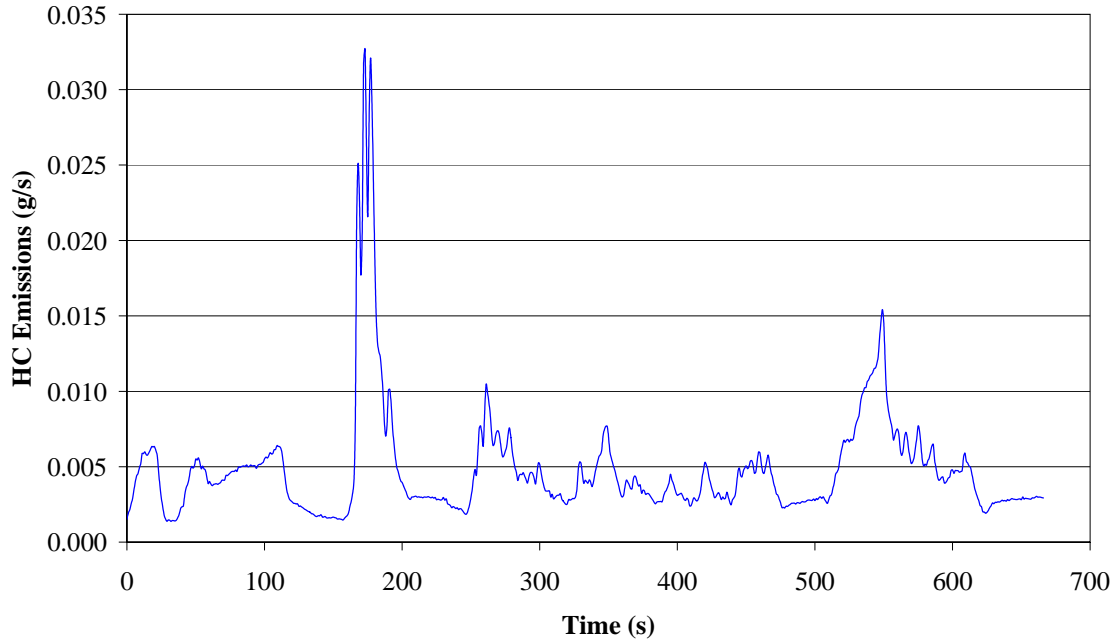


**Figure 20: Example of a continuous HC emissions plot in g/second for E55CRC-42 at 56,000 lb. following the Transient Mode schedule.**

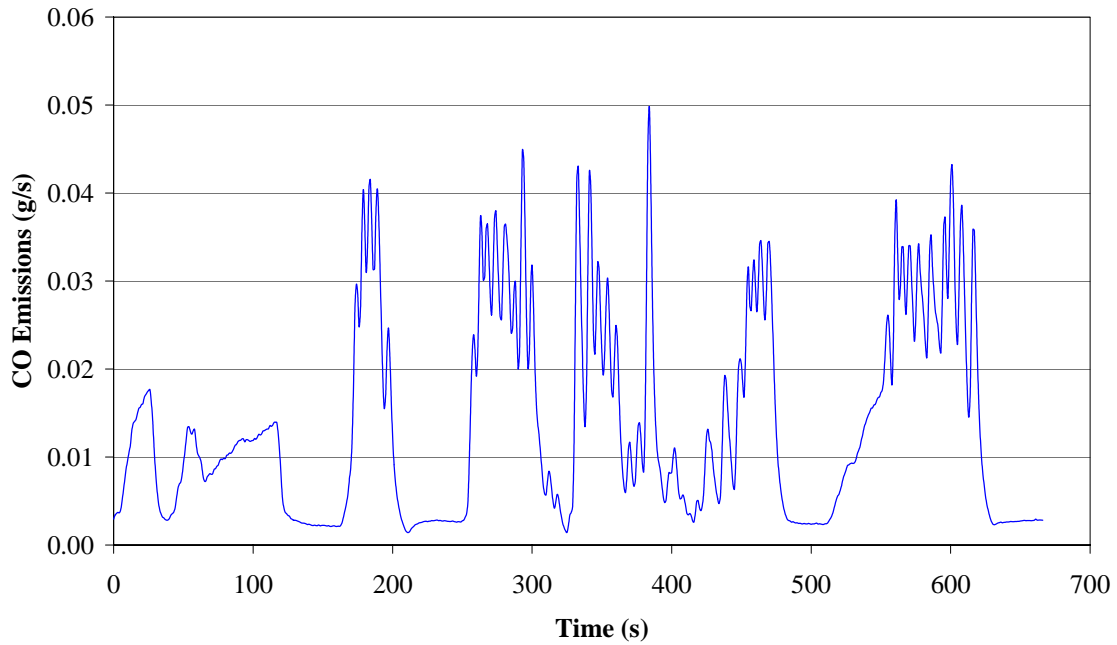


**Figure 21: Example of a continuous CO emissions plot in g/second for E55CRC-42 at 56,000 lb. following the Transient Mode schedule.**

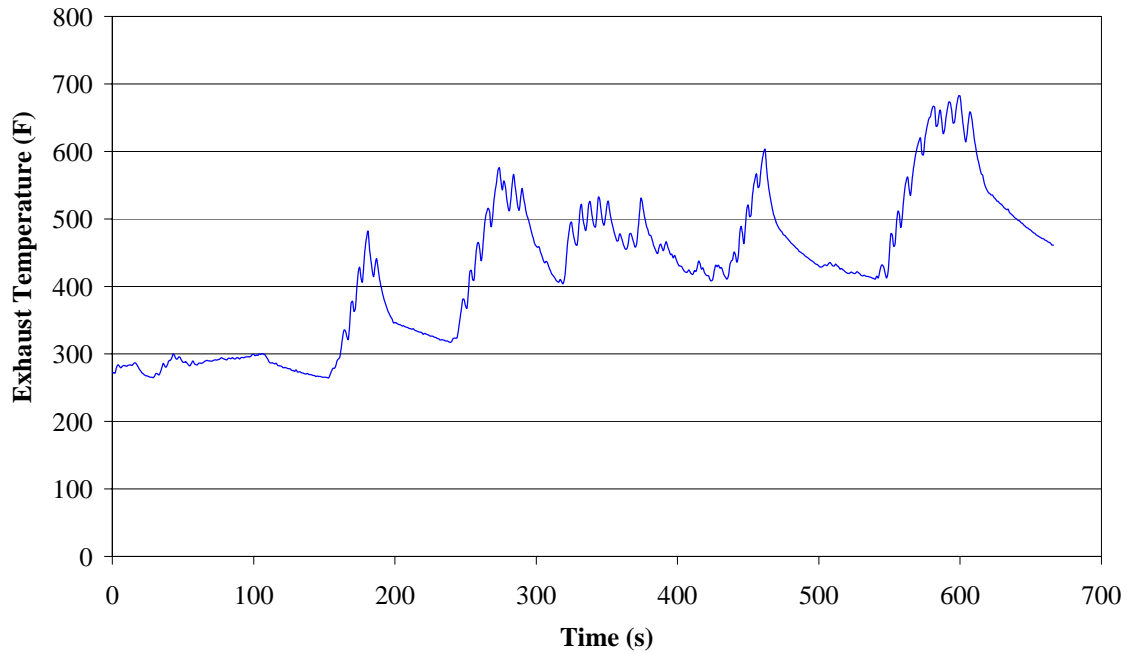


**Figure 22: Example of a continuous exhaust temperature reading for E55CRC-42 at 56,000 lb. following the Transient Mode schedule.**

### **Correlation of PM Filter and TEOM Data**

TEOM data, computed from the difference between the TEOM filter end weight and beginning weight, were compared with the 70mm filter data. Agreement was generally good as shown in Figure 23. This plot provides confidence in PM data gained from a single test run. The TEOM underreported PM mass, relative to the filter, by about 7%. Prior publications have shown that the TEOM reports less mass than the traditional filter [4].

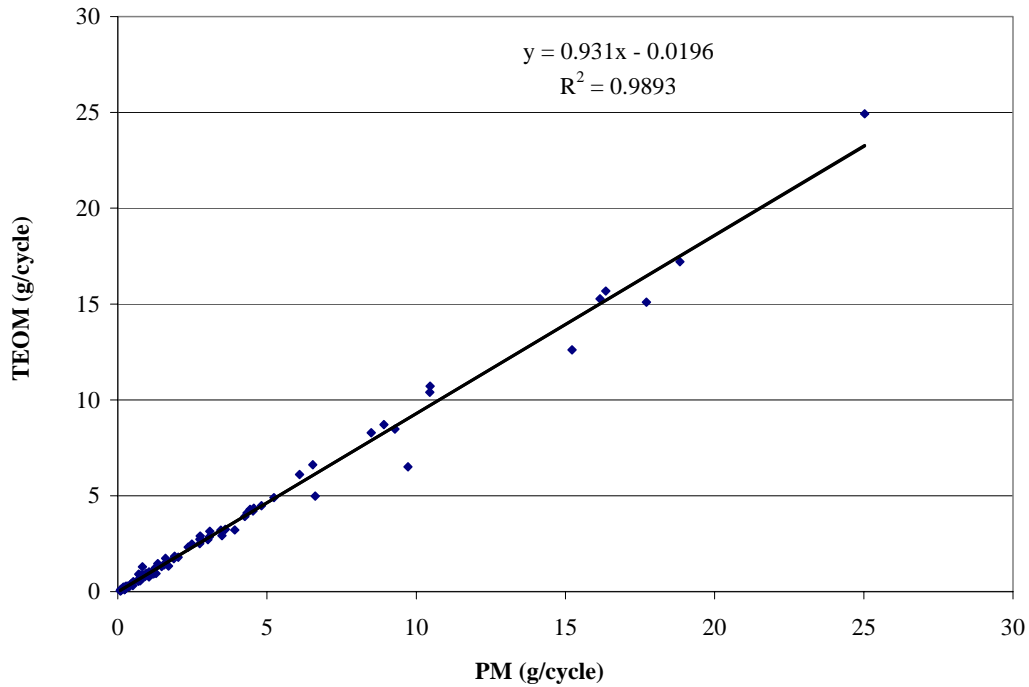


**Figure 23: Comparison of TEOM filter weight to 70mm filter weight.**

**Correlation of NO<sub>x</sub> Data from two Analyzers**

Figure 24 compares the data between the two NO<sub>x</sub> analyzers for every run. Both analyzers were in “NO<sub>x</sub>” mode so that both NO and NO<sub>2</sub> were measured. Two points showed unacceptable disagreement between the two analyzers. One of the runs, sequence 20181 run 2, was an MHD TLO (10.7 % difference). The second, sequence 2868 run 1, was the first of a set of two Idle33 runs (11.4% difference) during a speciation run. The deviation of other points was small, typically differing between the two analyzers by less than 5%.

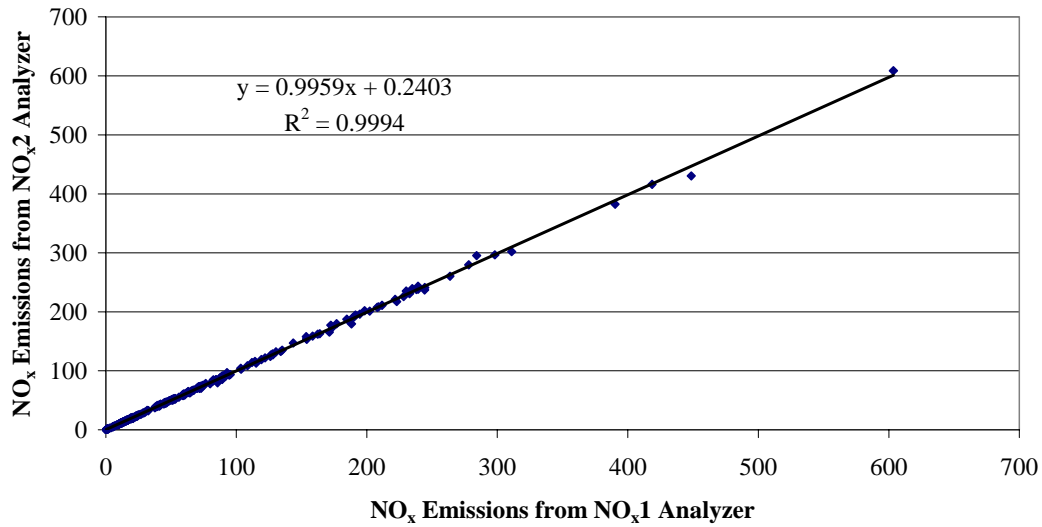


**Figure 24: Comparison of NO<sub>x</sub> readings from the two TransLab analyzers.**

### MHDT Effect of Test Weight

Figure 25 to 28 present the effect of test weight on emissions. While there were substantial truck-to-truck variations, the average effect of weight across the Phase 2 fleet was a rise in NO<sub>x</sub> of 9% for the Higher Speed Transient Mode and 8% for the Cruise Mode as the weight increased from 50% to 75% of the GVWR. The research effort to establish the MHDT schedule [3] found, in agreement with the present study, that effect of weight on NO<sub>x</sub> was smaller than previously established for HHDDT. The average effect on PM indicated an increase for the Higher Speed Transient Mode of 50% and 47% for the Cruise Mode.

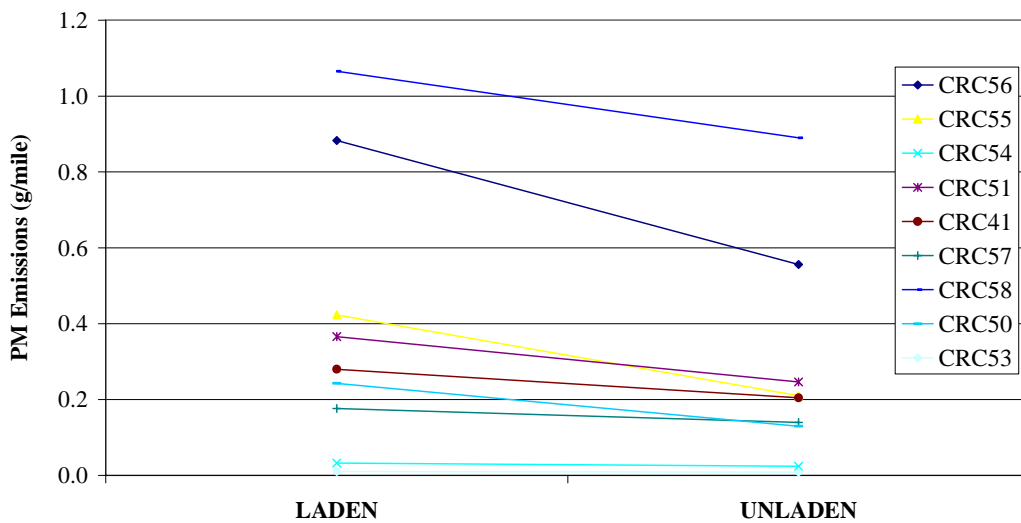


**Figure 25: PM emissions for Cruise Mode (laden and unladen)**

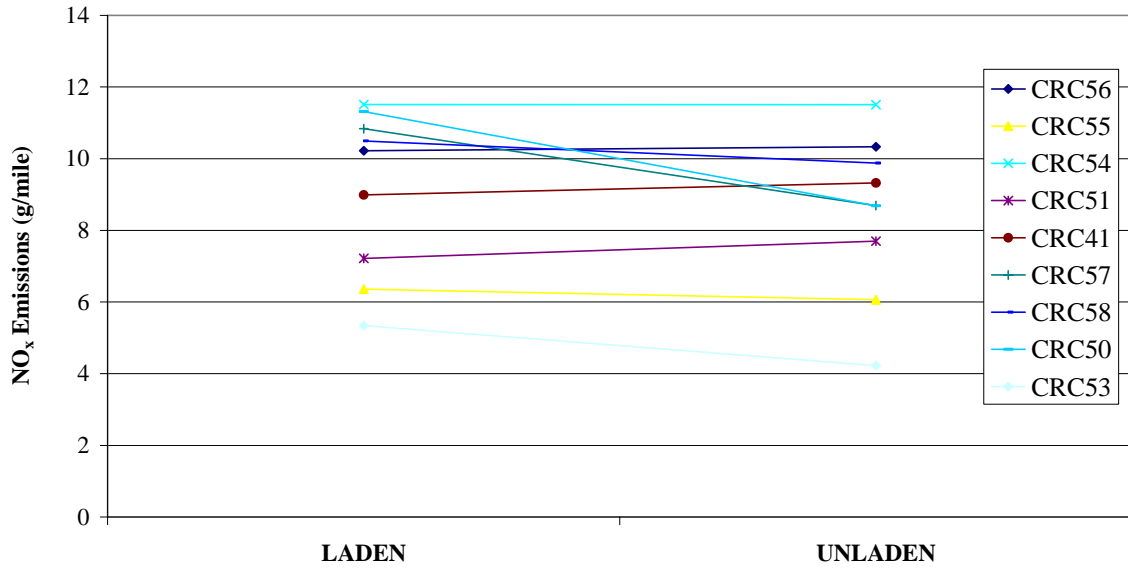


**Figure 26: NO<sub>x</sub> emissions for Cruise Mode (laden and unladen)**

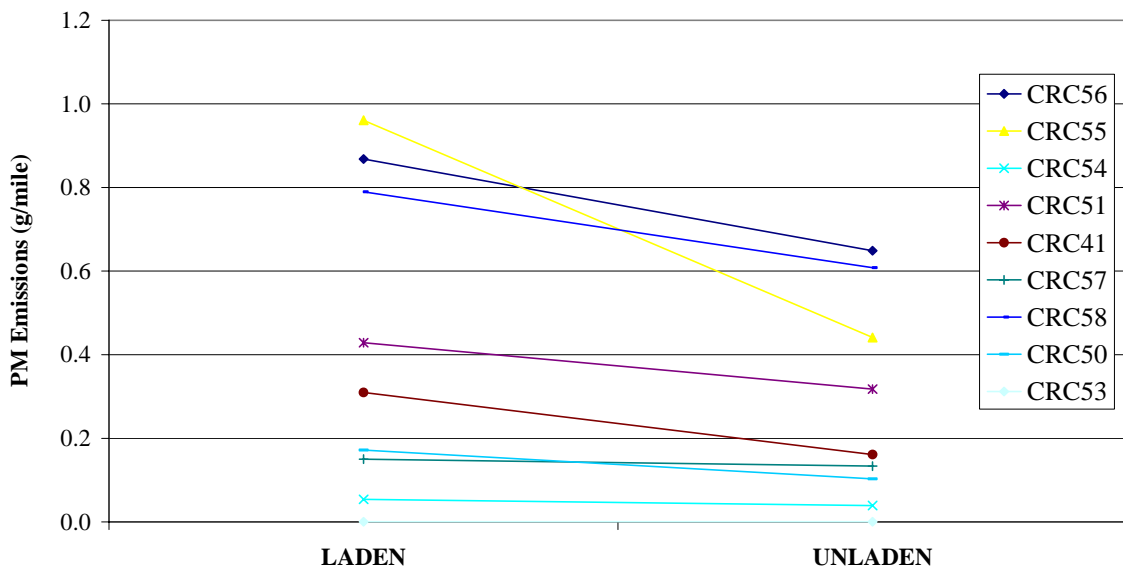


**Figure 27: PM emissions for the Higher Speed Transient Mode (laden and unladen).**

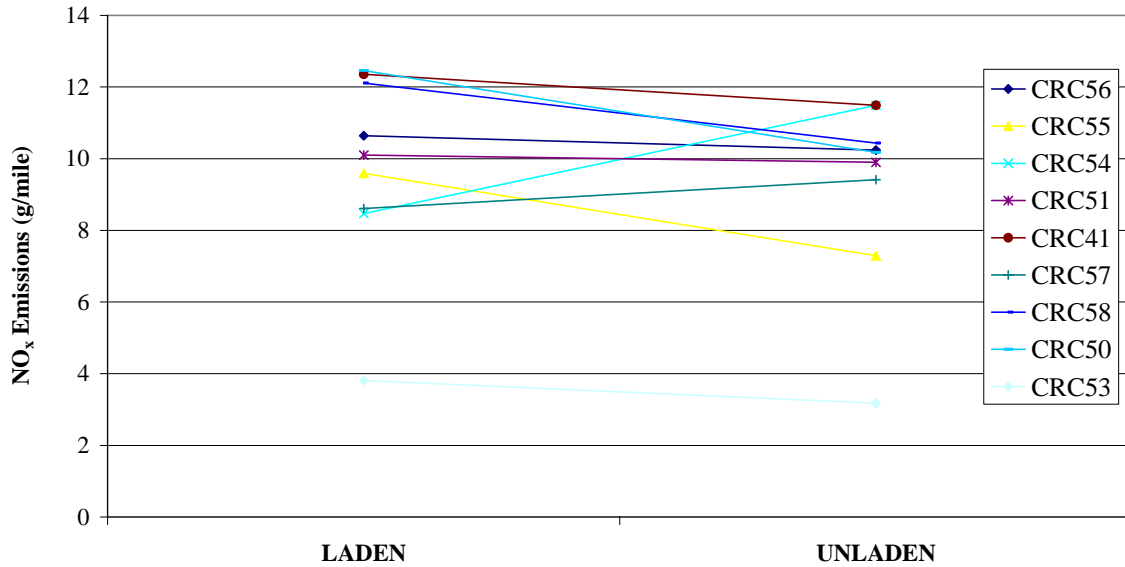


**Figure 28: NO<sub>x</sub> emissions for the Higher Speed Transient Mode (laden and unladen).**

### Comparison with Data from Prior Phases

The Phase 2 data presented in this report were compared with data from the prior phases. Figure 29 shows data for carbon dioxide emissions, in units of g/mile, for all HHDDT operated through the UDDS at 56,000 lb. test weight. There is little variation in the CO<sub>2</sub> emissions values over MY or by phase, because these are governed by the engine efficiency and cycle energy demands. These data build confidence in the repeatability of data between phases, and suggest that both the dilution tunnel flowrate calibration and the carbon dioxide analyzer function remained consistent between phases. In contrast, Figure 30 shows that CO varied substantially between vehicles. When the CO emissions are averaged for the two most populated bins, as shown in Figure 31, Phases 1 and 2 agree reasonably well for the 1994-97 MY group, but differ substantially for the 1990-93 model year group. Since CO is known to be a species that varies widely from truck to truck, this suggests that too few vehicles were selected in each phase to form a reliable opinion on average CO emissions. NO<sub>x</sub> emissions are less variable over the fleet than CO emissions, as shown in Figure 32 and Figure 31. However, Figure 31 still shows variation between phases. The NO<sub>x</sub> data for each phase are not in doubt: the carbon dioxide comparison (Figure 29) confirms consistent dilution tunnel flow, while the NO<sub>x</sub> data were guaranteed to have reasonable accuracy by employing two separate NO<sub>x</sub> analyzers in the program. PM data also vary between phases, as shown in Figure 31, so that one must conclude that the fleets in each phase are also too small for use in reaching conclusions on NO<sub>x</sub> or PM averages. Further data on NO<sub>x</sub> variability for the Transient Mode and Cruise Mode at 56,000 lb. test weight appear in Figure 33 and Figure 34.

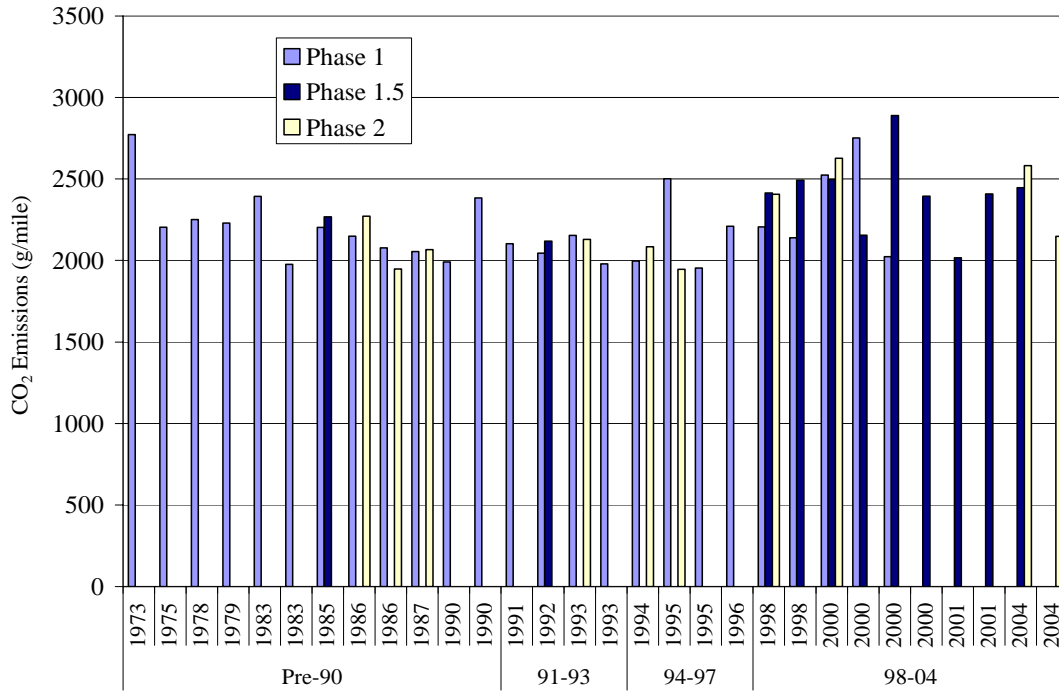


**Figure 29: Variation of HHDDT carbon dioxide emissions by vehicle model year and by phase of the program for the UDDS at 56,000 lb. test weight.**

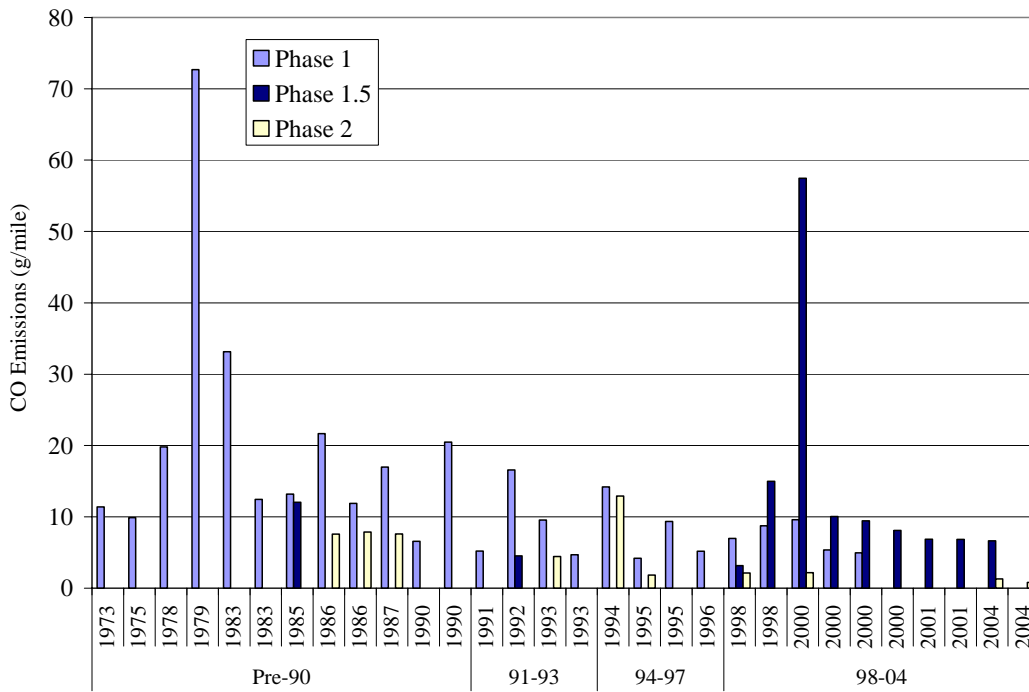


**Figure 30: Variation of HHDDT carbon monoxide emissions by vehicle model year and by phase of the program for the UDDS at 56,000 lb. test weight.**

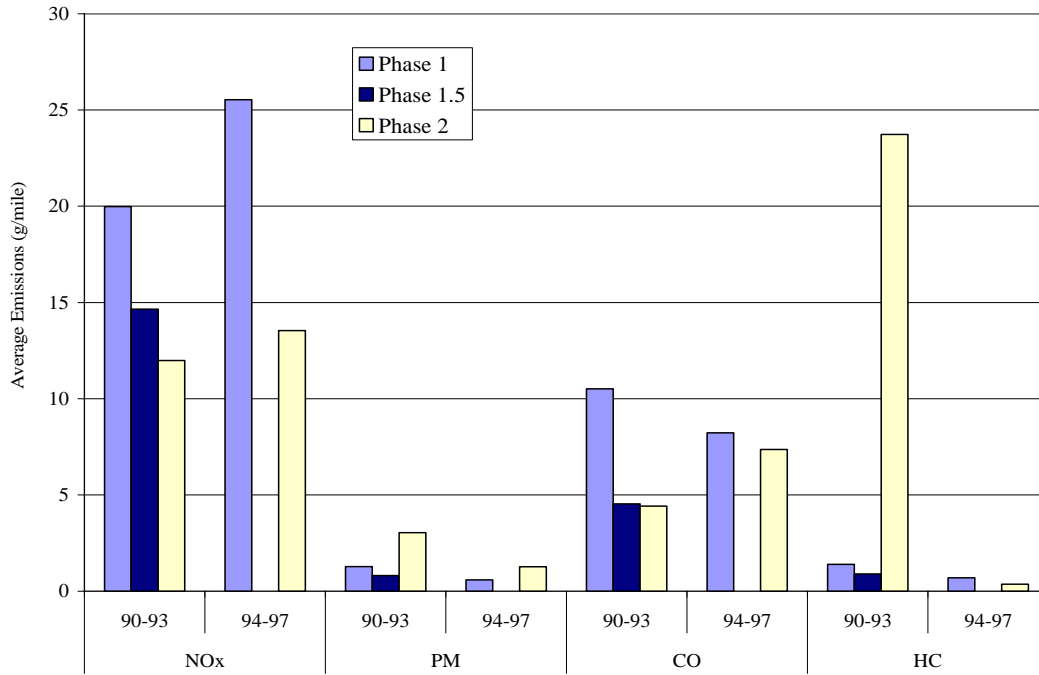


**Figure 31: Summary of HHDDT average emissions on the UDDS (56,000 lb. test weight) for vehicles in the 1990-93 and 1994-97 age groups.**

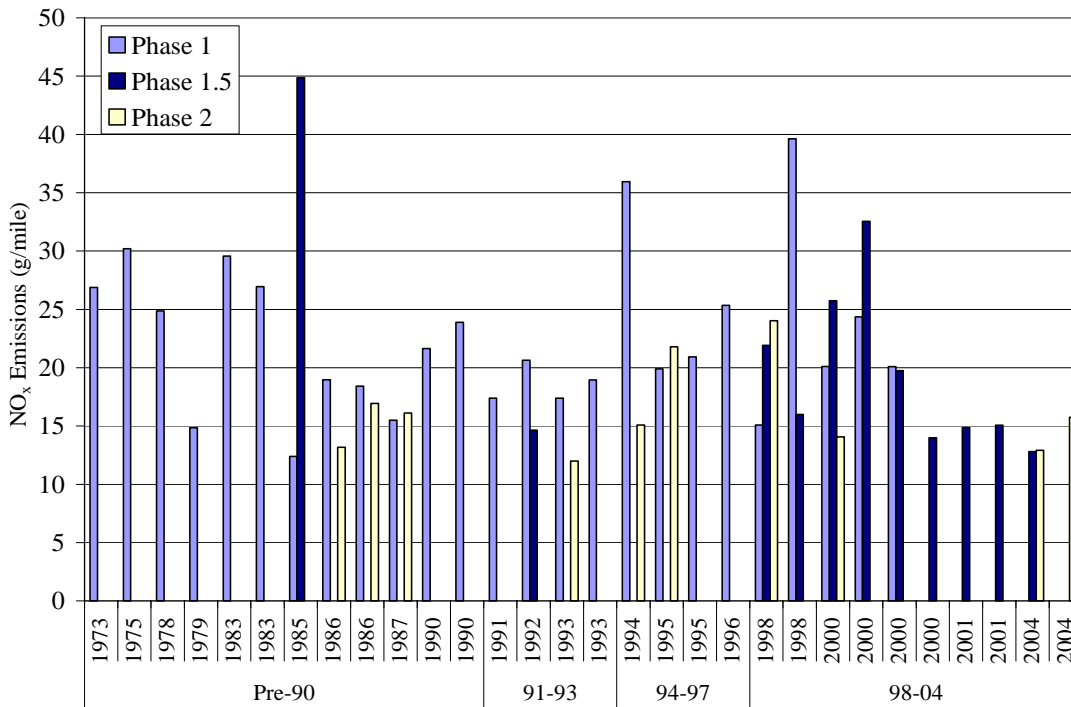


**Figure 32: Variation of HHDDT oxides of nitrogen emissions by vehicle model year and by phase of the program for the UDDS at 56,000 lb. test weight.**

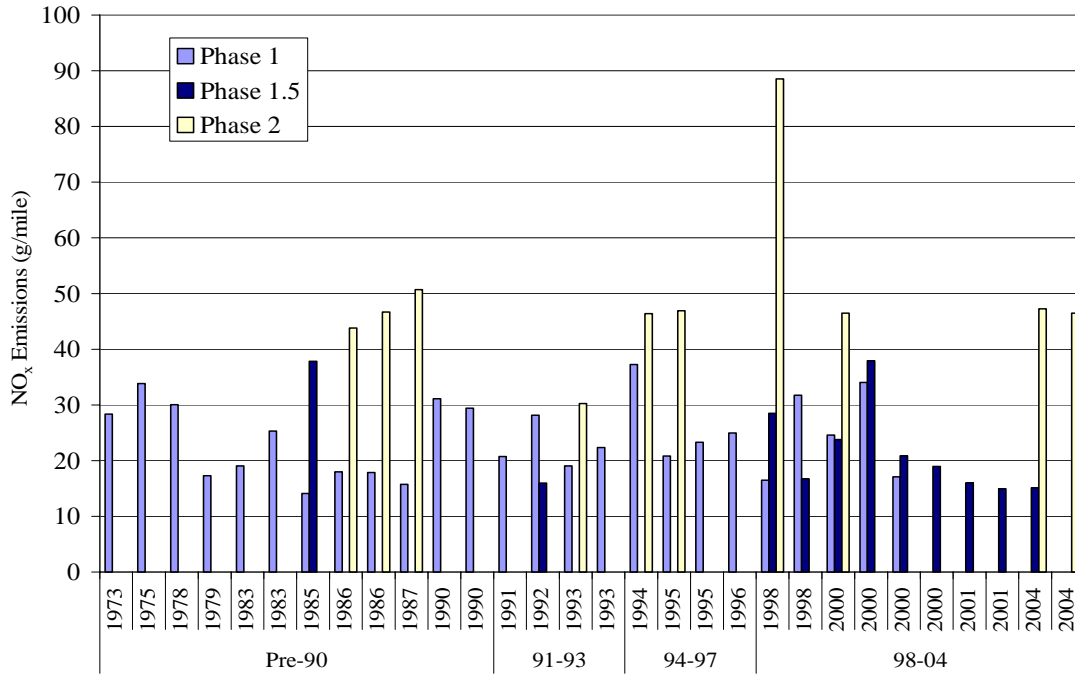


**Figure 33: Variation of HHDDT oxides of nitrogen emissions by vehicle model year and by phase of the program for the Transient Mode at 56,000 lb. test weight.**

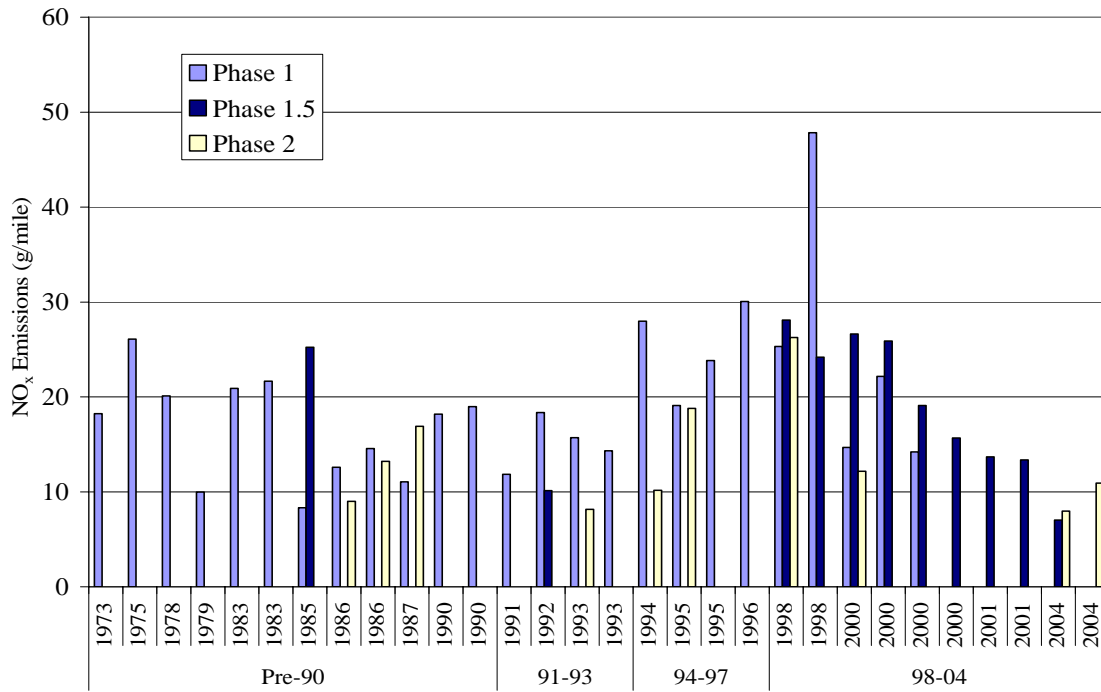


**Figure 34: Variation of HHDDT oxides of nitrogen emissions by vehicle model year and by phase of the program for the Cruise Mode at 56,000 lb. test weight.**

## Chemical Speciation and PM Size Measurement

This section presents the methods, results and discussion for the measurement of non-regulated emissions from a subset of the vehicles in the Phase 2 program. PM size was measured using both the Scanning Mobility Particle Sizer (SMPS) from TSI and a new instrument, the Differential Mobility Spectrometer (DMS500) from Cambustion. In addition, both the gaseous and PM fractions of the exhaust were speciated to determine the distribution of organic compounds and certain metals and ions in the exhaust. The Desert Research Institute (DRI) played a major role in this chemical speciation. An exhaust stream was also provided for analysis by ARB-funded researchers. This included using a particle mass spectrometer (ATOFMS), but data from these ARB-funded research measurements are not presented in this report.

### *Description of Dilution Systems*

#### WVU Constant Volume Sampling System (CVS)

Dilution systems serve to mix the exhaust with ambient air to promote PM formation, and serve to provide a consistent flowrate of dilute exhaust to permit computation of mass flowrates of gaseous species. One system employed by WVU in this study was the Critical Flow Venturi-Constant Volume Sampler (CVS), which is described below, and which was used for the bulk of the speciation research. The CVS system was also used for the regulated emissions presented above. A separate partial (mini) dilution system was used for some of the particle sizing research, and this system is also described below. In addition, Desert Research Institute, who were subcontracted by WVU to conduct speciation research, employed a residence time system ahead of their speciation media.

The CVS system was in accordance with the requirements of the Code of Federal Regulations 40 [5]. The CFR requires two basic conditions to be satisfied for measuring mass emissions; the total volume of both exhaust and dilution air must be measured and a proportional sample must be collected for analysis. Figure 35 shows the schematic of the WVU sampling train and Table 7 provides a list of the samples and analyzers using this system.

**Table 7: Sampling System Description and Media Type, used in conjunction with the CVS tunnel**

<b>ID</b>	<b>Sample Description</b>	<b>Media Type</b>
1	HC	Heated FID Analyzer
2	CO/CO <sub>2</sub>	NDIR Analyzers
3	NO <sub>x</sub>	Chemiluminescent Analyzer
4	TEOM	TEOM Filter
5	TPM	70 mm T60A20 Filters (Primary and Secondary)
6	PM <sub>10</sub> Fraction for Gravimetric Analysis	47 mm TX40HI20WW Filters
8	DRI Residence Time Dilution Tunnel	Various media for chemical speciation
9	Particle Analysis by Mass Spectroscopy	ATOFMS
10	Real-time PM Size Distribution	DMS 500

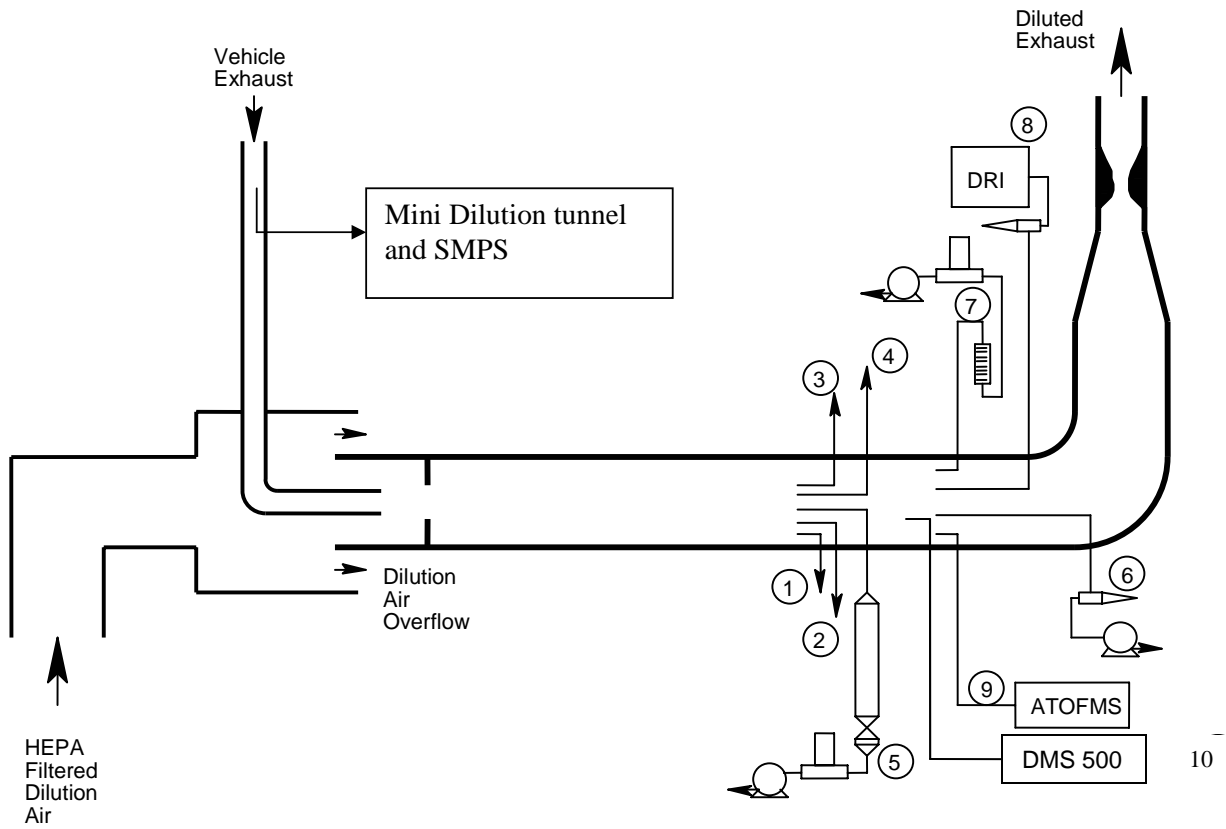


**Figure 35: WVU Sampling Train Schematic**

Further requirements include that the system should not artificially lower the engine back pressure. Continuous static pressure measurements are required. The temperature measuring system needs to have an accuracy of  $\pm 3.4^\circ$  F and the pressure measuring system  $\pm 3$ mm of Hg. Tunnel flow must be kept turbulent to allow complete mixing of the exhaust gas and the dilution air, and the length of the tunnel must be kept at least ten times the diameter to ensure fully developed turbulent flow. The tunnel should be fabricated of electrically conductive material and must be grounded so that particle losses do not occur due to electrostatic deposition.

The dilution tunnel was constructed of 22 gage 304 stainless steel and was 0.45 m (18 inches) in diameter and all sampling was done after 4.5 m (180 inches). The whole tunnel was wrapped in insulation to minimize particle losses by thermophoretic deposition. A 56 KW (75 hp) blower was used to draw the exhaust and dilution air. Dilution air was not heated and the air was filtered through a HEPA filtration system. The flow was regulated by a 42,500 lpm (1500 scfm) critical flow venturi under choked conditions. A differential pressure gage monitored the pressure drop at the throat to ensure that choked flow occurred at the venturi throat. The mass and flows do vary slightly due to a variation in tunnel temperature. The equation for determining sonic flow rate is:

$$Q = \frac{K_v \times P}{\sqrt{T}}$$

where  $K_v$  is the calibration coefficient, P is the absolute pressure and T is the absolute temperature. Both P and T were measured upstream of the CFV. The total flow rate could be varied by changing out the venturi. Calibration checks were made according to the procedure stated in the CFR 40 [5] whenever a venturi was changed.

#### Residence Time Dilution System

A Residence Time Dilution System was employed by the DRI researchers for chemical speciation, in conjunction with the main CVS dilution tunnel. The system was based on a dilution stack sampler designed and tested by a group led by Dr. G.R. Cass [6]. Figure 36 shows a schematic of the DRI sampler from reference [6]. Samples of dilute exhaust were withdrawn from the CVS tunnel through a cyclone separator, inserted into the dilute exhaust stream. The dilute exhaust gases were transported through a heated Teflon line to the residence time dilution tunnel. Additional dilution was not provided in this study due to insufficient quantity of sample collected on the filters and other media. After passing through a tunnel length equal to  $\sim 10$  tunnel diameters, a fraction of the diluted exhaust entered a large chamber, where additional residence time was provided before the samples were collected. The samples were drawn through cyclone separators (Bendix-Unico 240) with a 50% cut-point of 2.5 micrometers aerodynamic diameter at a volumetric flow rate of 113 liters/minute and collected using the DRI Sequential Filter Sampler (for inorganic species) and/or the DRI Sequential Fine Particulate/Semi-Volatile Organic Compound (PSVOC) Sampler for organic species. The rest of the diluted exhaust passed through a high-volume sampler filter before being exhausted.

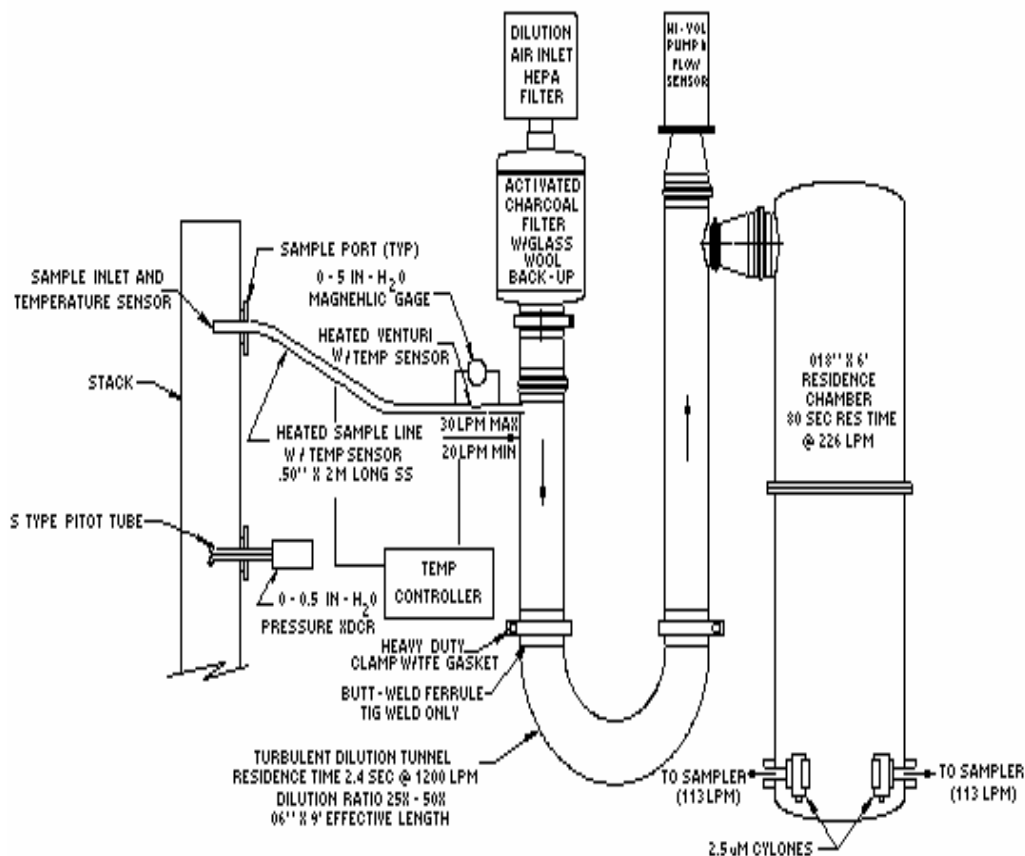


**Figure 36: Schematic of the DRI Residence Time Dilution Tunnel [6]. In the present application the DRI system sampled from the main CVS dilution tunnel.**

### Mini Dilution System

The Scanning Mobility Particle Sizer (SMPS) employed a mini dilution tunnel to dilute the raw exhaust for sampling. The DMS 500 did not employ this mini dilution tunnel, but was used to sample directly from the main CVS tunnel.

The mini dilution system shown in Figure 38 incorporated a tunnel with its length maintained at ten times its diameter to facilitate good mixing and uniform distribution at the sampling zone. An orifice plate was provided at the inlet of the dilution system to ensure proper turbulence. The tunnel was wrapped with heating tape and insulation to maintain a temperature of 46° C (115° F) to prevent water condensation. A dilution ratio of 1:30 was maintained throughout this study. A 12 cm (5 inch) exhaust coupling with a 2 cm (3/4 inch) probe welded on its body was used to draw a partial sample from the raw exhausts shown in Figure 37. One end of the probe had a quick disconnect fitting for ease of coupling the probe to the mini dilution tunnel. The sample line from the probe to the mini dilution tunnel was kept as short as possible and well insulated. Dilution air was supplied immediately before the mixing orifice by a separate pump. The dilution air was passed through a refrigerated dryer and a HEPA filter to provide particle and moisture free air. A separate vacuum pump was used to draw in the exhaust sample.

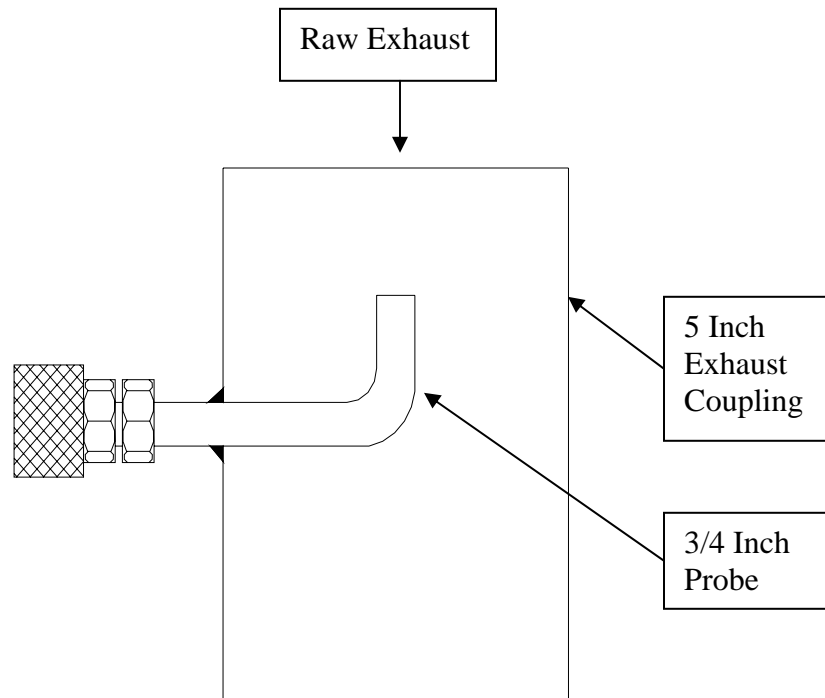


**Figure 37: Exhaust Coupler with Sampling Probe**

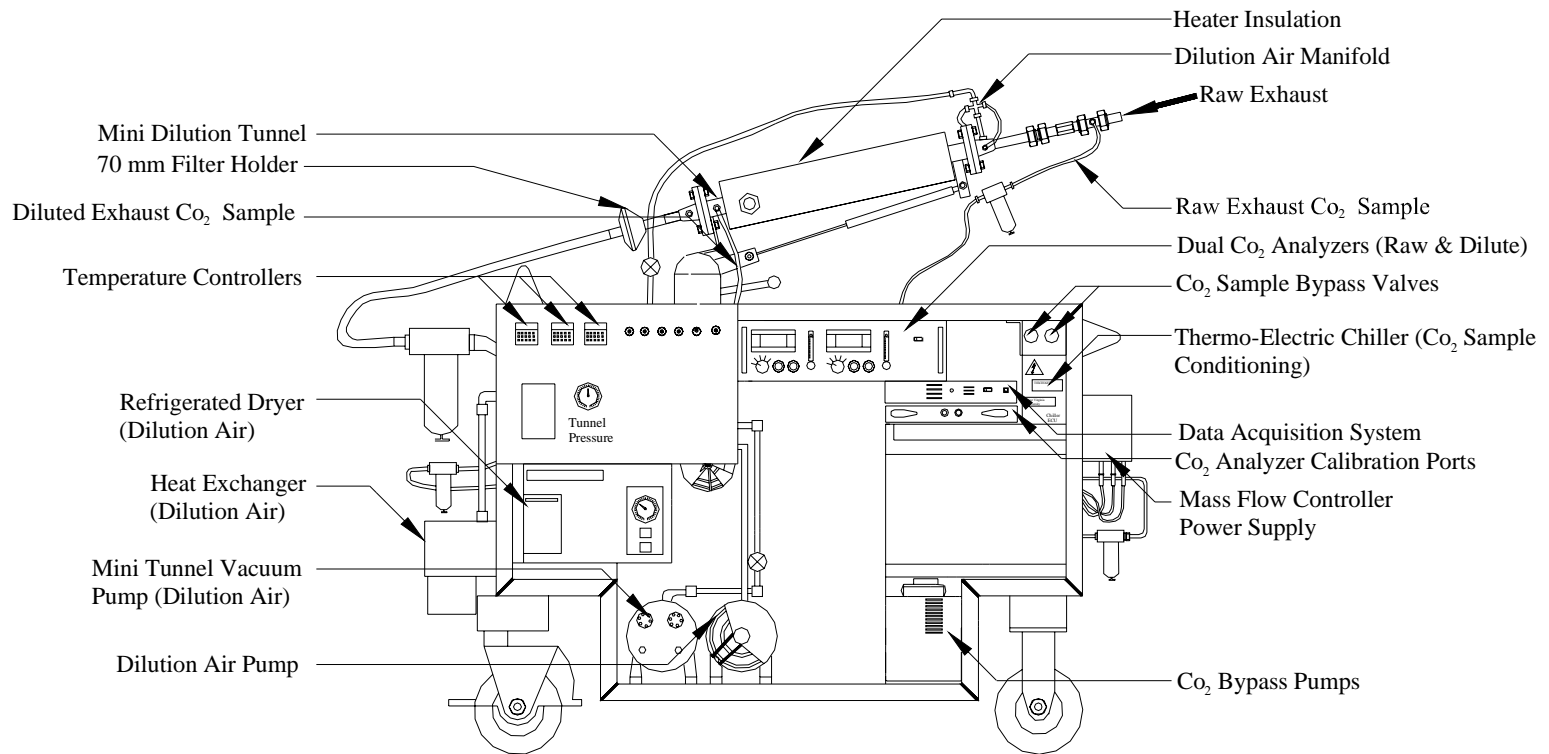


**Figure 38: West Virginia University-Mini Dilution System**

Both the dilution air and total air flow rates were controlled by two Sierra mass flow controllers calibrated from 0 to 200 slpm (0 to 7 scfm). Sampling probes were installed ten diameters downstream of the mixing orifice to ensure uniform concentration. A dual range CO<sub>2</sub> analyzer was used to measure the raw and dilute CO<sub>2</sub> concentrations. A 10-point analyzer calibration was employed using 15% and 1% CO<sub>2</sub> bottles. The analyzer was checked everyday for a zero and span using nitrogen as zero gas and 15% and 1% CO<sub>2</sub> bottles as span gas for the analyzers. The raw and dilute exhaust gases were filtered by inline filters and chilled by thermoelectric chillers for removal of particulates and moisture, respectively. The filters were checked every day and replaced if necessary. A purge air supply for the CO<sub>2</sub> analyzers was provided by an external oil free compressor through a HEPA filter. This purge air was useful in flushing the analyzer of any residual gas present, which may provide erroneous readings.

The mass flow controllers and the CO<sub>2</sub> analyzers were connected to a data acquisition system (National Instruments DAS 6020-E BNC). A program in Visual Basic was developed by WVU to control the DAS pad and to save continuous data from the analyzer and the mass flow controller. Other parameters such as tunnel pressure, and temperature were also recorded on a continuous basis. The DAS pad also maintained the user defined dilution ratio. The desired dilution ratios were achieved in two ways, first a flow-based system and the other is a CO<sub>2</sub> based system. With the flow based system, the dilution ratio was calculated using the following equation:

$$DR = \text{total} / (\text{total} - \text{dilute})$$

The dilution ratio was maintained by adjusting both the total and dilute flow rates. The total and dilute flow rates were measured and set by the mass flow controllers. The CO<sub>2</sub>-based system measured the raw and dilute CO<sub>2</sub> concentrations and the dilution ratio was the simple ratio of raw to dilute concentrations. The dilution ratio was maintained by controlling the mass flow controllers based on the CO<sub>2</sub> readings. Through experience it had been determined by WVU that the flow based system was more accurate in controlling the dilution ratio and the CO<sub>2</sub> readings were used to verify the set dilution ratio. It may be argued that the dilution ratios may be better controlled using CO<sub>2</sub> concentrations than using mass flow controllers. WVU has both systems on the mini-dilution tunnel that is used for PM sizing work. Problems associated with deskew times, gas dispersion in the tunnel, and chillers complicate the CO<sub>2</sub>-based control method, especially during transient tests. Over steady state tests, the CO<sub>2</sub>-based dilution ratio control can be very accurate. One probe was installed next to the dilute CO<sub>2</sub> probe for particle size distribution measurements using the SMPS. Carbon impregnated electrically conductive Tygon tubing was used to transfer the sample from the tunnel to the instrument. This tubing was used to prevent any particle losses due to electrostatic deposition on the walls of the sampling tube.

Exhaust pulsations from the engine were encountered during this study and an exhaust pulsation damper was devised, as shown in Figure 40. The damper was a simple 5 gallon tank with one end cut off and sealed with a rubber diaphragm. The rubber diaphragm was helpful in reducing the exhaust pulsations. The top of the tank had a tee connection which incorporated a straight probe as seen in Figure 39, to minimize particle losses into the

damper. This system provided a pulsation free stream of sample with minimal particle loss. The damper was flushed with particle free air and evacuated after every test to remove any remaining particles or even volatile compounds, which may have found their way into the damper. This was done because the volatile compounds may adhere to the walls of the damper and subsequently form particles and create sampling artifacts.

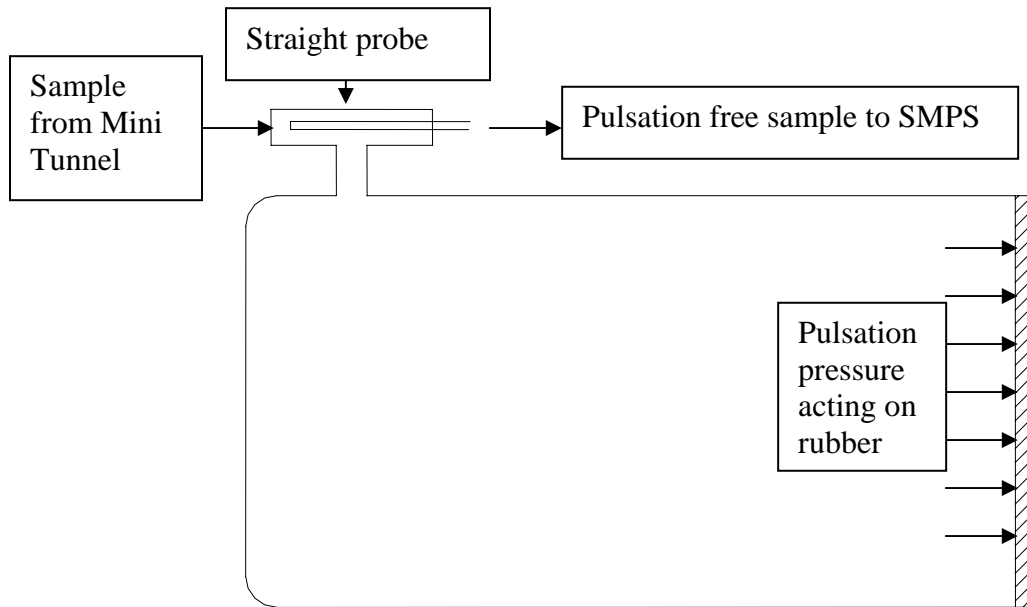


**Figure 39: Schematic Representation of the Damping System**

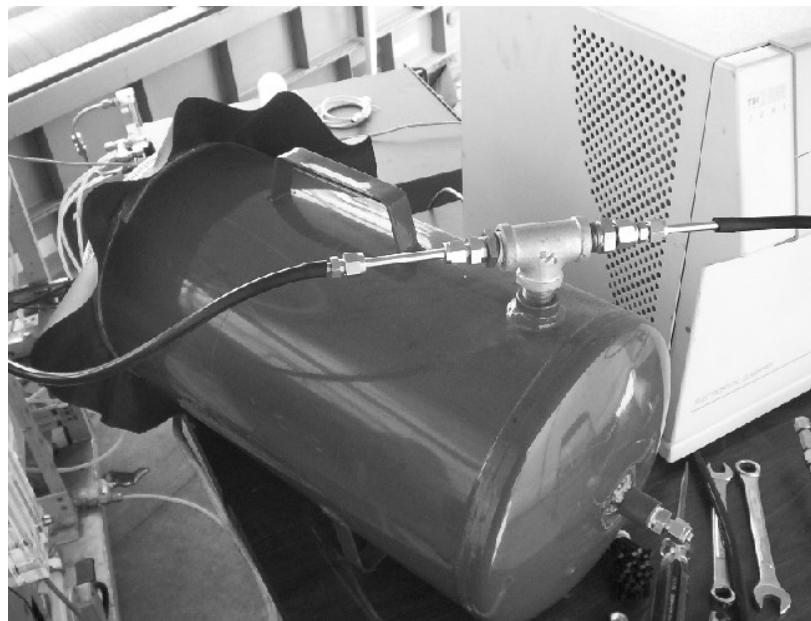


**Figure 40: Exhaust Pulsation Damper**

## Particle Sampling

### Total Particulate Matter

Total Particulate Matter (TPM), as defined by the US EPA, is sampled by filtering diluted diesel exhaust at filter face temperatures of less than 52°C (125° F). TPM has been reported as a regulated emission species.

A 70mm filter holder was connected that contained two 70mm T60A20 fiberglass filters, the primary and secondary filters to capture the regulated TPM.

### Particle Sizing with the SMPS

The SMPS consists of two basic components, the Electrostatic Classifier or the Mobility Analyzer and a Condensation Particle Counter. The use of the classifier to produce monodisperse aerosols is illustrated in Figure 41. The classifier or mobility analyzer separates particles based upon their electrical mobility and the resulting particles are transported to the particle counter to obtain number concentrations. In mobility analyzers particles are first charged, and then the aerosol is classified in a high electric field according to the electrical mobility of the particles. The particle size distribution is obtained on the basis of the relationship between mobility and sizes. The ultimate size parameter determined from electrical mobility measurements is the equivalent mobility diameter.

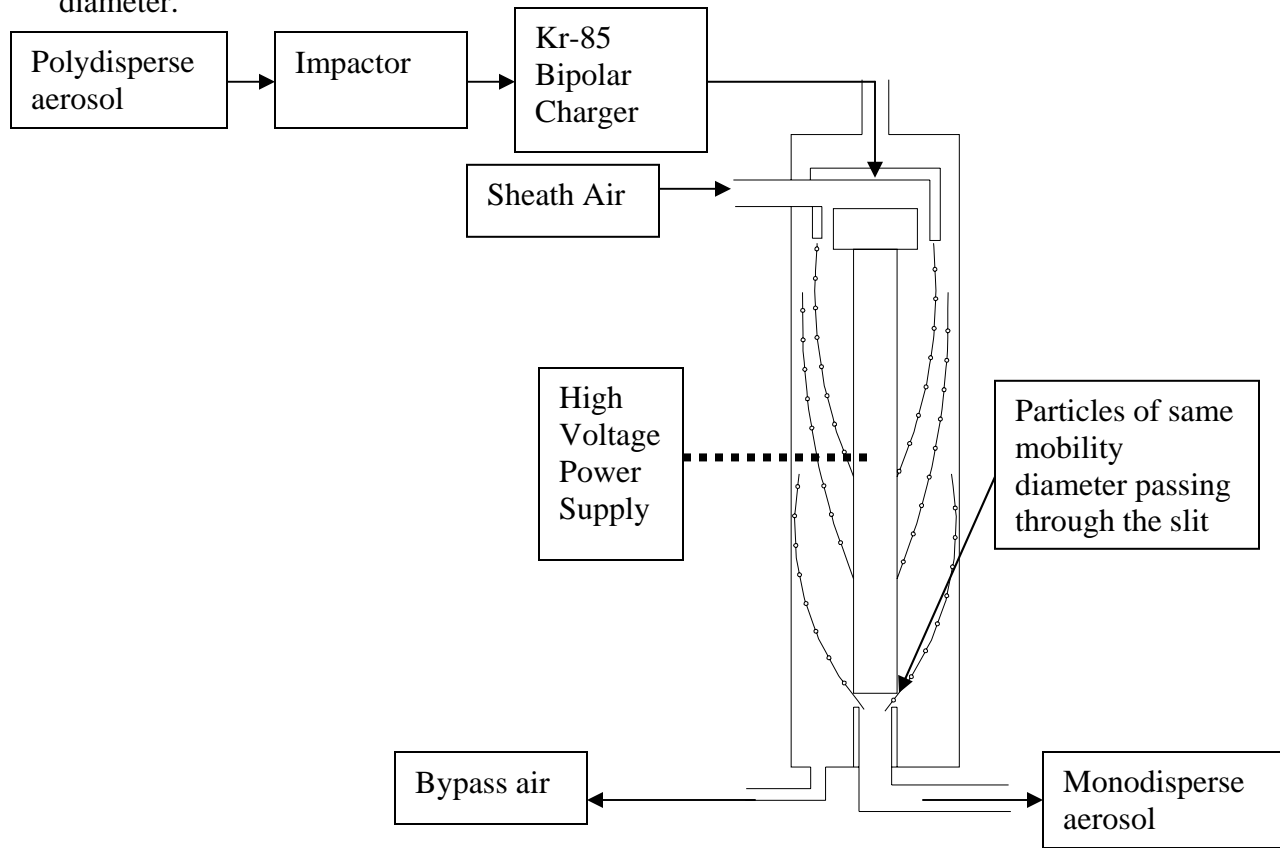


**Figure 41: Differential Mobility Analyzer**

The inlet of the classifier has an impactor which removes all particles above  $1\mu\text{m}$  since large particles tend to have multiple charges and stripping these charges is very difficult. The impactor has a nozzle and an impactor plate and different size orifices (0.071 and 0.0475 cm) are used depending on the flow rate. The polydisperse aerosol passes through the bipolar charger containing a radioactive source (Krypton), which exposes the aerosol particles to high concentrations of bipolar ions. The particles and ions undergo frequent collisions due to random thermal motion of the ions. After reaching a state of equilibrium, the particles carry a bipolar charge distribution. The polydisperse aerosol passes into the DMA between the sheath flow, which creates an air curtain, and the outer cylinder. The central rod is charged with a high negative voltage and the positive particles are attracted to the rod. Particles with high mobility precipitate at the top end of the rod and particles with low mobility exit the DMA along with the bypass air. Only particles with a narrow mobility range exit the DMA through the slit as monodisperse aerosol, which pass on to the Condensation Particle Counter for concentration measurements.

To obtain a full scan of the particle sizes, the voltage in the central rod of the classifier is increased exponentially which is termed the up-scan of the DMA and the voltage is dropped to zero which is termed as the down-scan. The up-scan and down-scan times are typically 120 and 15 seconds, respectively. These times can be increased by the user to obtain a better resolution if the particle concentrations are steady.

The Condensation Particle Counter (CPC), also called the condensation nucleus counter (CNC), is the most common instrument used to determine number concentrations of diesel particles. Upon entering the CPC the aerosol stream is saturated with alcohol (typically butanol) vapor. As the mixture is cooled in the condenser tube, the vapor becomes supersaturated and condenses on particles. As a result, the particles grow to a diameter of about  $10\mu\text{m}$ , allowing for optical detection. Particle size detection limit in the CPC is related to the increasing saturation ratio which is required with decreasing particle diameters. Modern CPCs have detection limits of around 3-10 nm.

CPCs can be operated in two modes: (1) the counting mode and (2) the opacity mode. In the counting mode, pulses of scattered light from individual particles are counted. This mode provides the most accurate measurements, but can be used only at low particle concentrations. In the opacity mode, used for concentrations above  $10^4/\text{cm}^3$ , number concentrations are determined from the total scattering intensity. This mode, generally subject to a larger error, requires that all particles grow to the same diameter and that the optical system be frequently calibrated. The CPC instrument is very sensitive to the ambient temperature, which affects the degree of supersaturation, as well as to positioning and vibrations. For these reasons, it is suitable primarily for laboratory measurements and its use for in-field measurements is more challenging. The CPC is used for particle detection in many aerosol size distribution measurement instruments.

Both the CPC and the Electrostatic Classifier make up the SMPS system. The CPC and the classifier are interfaced with an analog BNC connector cable. A personal computer with custom software provided by TSI was used to record data and control the classifier. A TSI model 3936 SMPS system was used for this study (Figure 42). DMA models 3081

(Long DMA) and 3085 (Nano DMA) were used interchangeably to obtain a full particle size distribution down to 4nm and up to 800nm. A Model 3025A CPC was used for particle counting since it could detect particles with diameters as low as 3nm and had a response time of one second.

The SMPS is basically designed for steady state operations, where the exhaust characteristics are invariant with time; that is, the engine is at a constant load and RPM or when the vehicle is operated at a constant speed. During these steady states, concentrations of all particles are almost constant, but the concentrations vary whenever the load or speed of the engine/vehicle varies. For transient measurements of the engine/vehicle, the engine/vehicle was first operated on a steady state mode and a full size scan was obtained. Particle sizes were chosen from the full scan and the number of particles chosen was dependent upon the number of times the vehicle was operated through the transient cycle. For transient tests, the classifier operated in manual mode, which allowed the user to enter a particular particle size and track the concentration of that particular size for the entire test.



**Figure 42: TSI Model 3936 SMPS System**

To assure accurate measurements, the SMPS was flow calibrated before the start of the project. An electro spray aerosol generator was used to calibrate the SMPS. The generator was capable of producing 15, 30 and 70nm sucrose particles. Leak checks were performed every day to ensure that the SMPS had no leaks. Two types of leak checks were performed, a HEPA filter check and a zero voltage check. Since HEPA filters have high filtration efficiencies, a HEPA filter was connected to the inlet of the SMPS and a full size scan was performed. If any particles were detected above the noise level of the instrument, which was typically  $1 \times 10^3$  particles/cm<sup>3</sup>, then a thorough leak check was performed according to the instrument instruction manual. The second method required the voltage on the collector rod to be set at zero and checked for any particles being measured by the CPC. Since the voltage on the collector rod determines the particle size that exits the classifier, a zero voltage on the rod should ensure no particles exit the classifier. Both these methods were used everyday to make sure the SMPS had no leaks. If any leak was detected in the system, the manufacturer's leak check procedure was used to track and solve the problem. The inlet nozzle on the classifier was cleaned everyday with alcohol to remove any particle deposits, which may block the flow. The impactor

plate was also cleaned with alcohol and a thin layer of vacuum grease was applied to prevent particle bounce.

Particles are classified in the DMA by increasing the voltage exponentially and the particles leaving the classifier are increasing in size. The particles are then counted by the CPC and the values for concentrations for each particle size are stored in the PC as raw counts. The particle size obtained from the raw data assumes that each particle has a single charge on it after passing through a bipolar charger, which is not actually true. Multiple charges on a particle increase its mobility and can be incorrectly binned into the smaller diameter range. TSI uses an inbuilt algorithm in its SMPS software (Aerosol Instrument Manager-SMPS) to correct for multiple charges based on Fuchs-Gunn aerosol charging theory and a truncated triangular transfer function based on Knutson and Whitby [7].

The software provided by TSI to record only CPC concentrations (Aerosol Instrument Manager-CPC) does not provide any algorithm for the reduction of data. The single particle charge correction, transfer function and efficiencies of the CPC and impactor have to be applied to the raw data. Two programs were developed in MathCAD, one to reduce the CPC data and the other to correct the SMPS data for the dilution ratio [Appendix J]. The final data for the SMPS were presented as particle size based concentration variations with concentrations in normalized units of particles/cm<sup>3</sup> (dN/dlogDp). A log normal distribution was found to fit the data from the SMPS very well. The final data from the CPC were presented as time-based concentration variations of a selected particle size with concentrations in normalized particles/cm<sup>3</sup> (dN/dlogDp).

#### Particle sizing with the DMS500

A second instrument used to measure the size and number distributions of PM was a differential mobility spectrometer, DMS500 [8,9]. The DMS500 was directly connected to the secondary dilution tunnel and was used to sample at a point close to the standard 70mm filter of the laboratory. Only primary dilution in the CVS tunnel was employed. Secondary dilution was not needed in the tests because the filter face temperature remained below 52°C with just primary dilution. The working principle of the DMS500 is that it draws sample flow from the dilution tunnel containing aerosols/ particles. It is capable of measuring 41 particle size bins (3.16nm – 1000nm) as a continuous number count at a maximum frequency of 10Hz. The size bins start at a diameter of 3.16nm and increase in the geometric ratio of 1.15 for each next size bin up to the end limit of 1000nm. The impactor at the inlet removes particles greater than 1000nm and then the particles are charged by a corona charger. The charging of the particles is argued to depend only on size and not on material composition. The dilute exhaust then flows as a uniform laminar sheath through an annular geometry between the inner and outer electrodes, as shown in Figure 43, and the charged particles are carried in this dilute exhaust flow. The particles are then deflected towards grounded electrometer rings by their repulsion from a central high voltage rod. Their landing position on the electrometer rings is a function of the particle's charge and momentum. The particles give up their charge to the electrometer amplifiers through the rings and the resulting currents are output as particle number and size distribution through the user interface. There are

studies showing the good accuracy of the DMS500 when compared with the SMPS and ELPI [10].

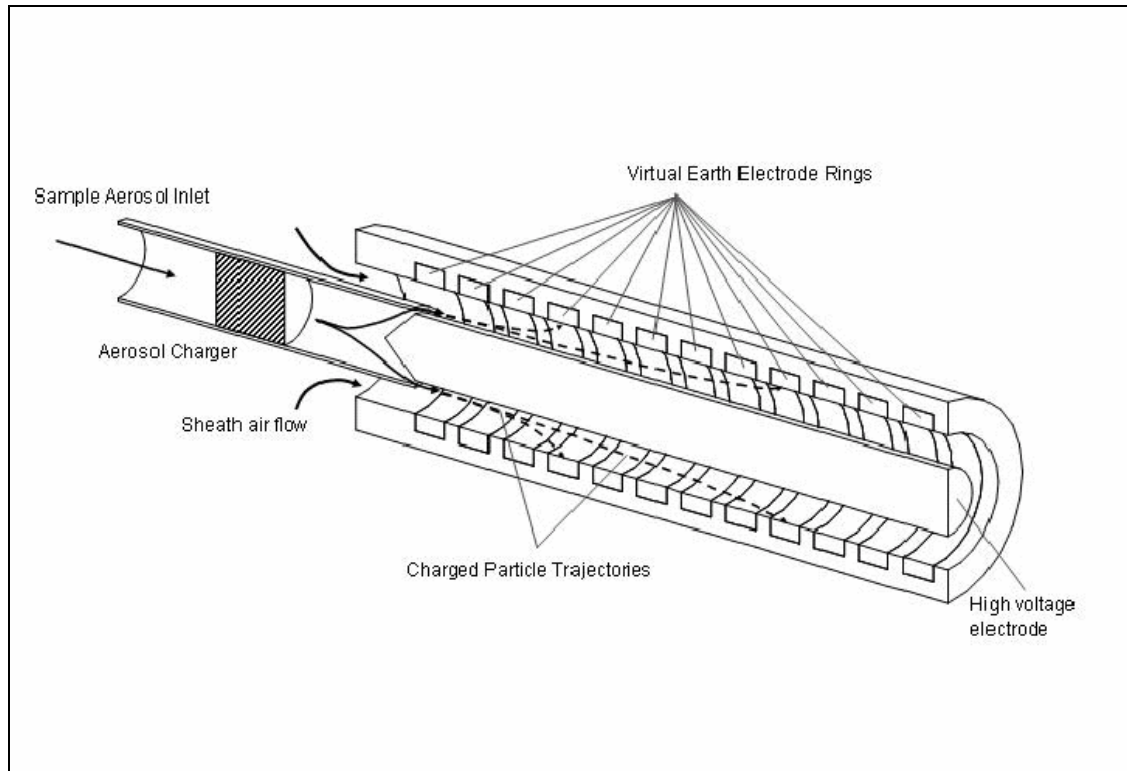


**Figure 43: Working principle of the DMS500[8].**

### ***Unregulated Emissions (West Virginia University and Desert Research Institute) Measurement***

West Virginia University (WVU) and Desert Research Institute (DRI) (subcontractor to WVU) were jointly responsible for the unregulated emissions measurement. Listed below are the specific tasks/activities conducted by WVU and DRI, related to PM<sub>10</sub> sampling and chemical sampling.

#### West Virginia University

In addition to the gaseous sampling probes and a secondary dilution tunnel, WVU installed the following on the primary dilution tunnel:

1. PM<sub>10</sub> cyclone with TX40 filters for gravimetric analysis (PM<sub>2.5</sub> sampling was conducted by DRI using the DRI residence time chamber).
2. Probe for the DRI's residence time dilution chamber.

WVU collected the PM<sub>10</sub> fraction using a cyclone for all six vehicles. Size-selective cyclone samplers (URG Model 2000-30 EA, 28.3 lpm,  $_{50}d_{ae}=10\mu\text{m}$ ) were used to collect samples for PM<sub>10</sub>. The PM<sub>10</sub> cyclone was an inertial particle separator that used centrifugal force to remove heavier particles from a gas stream ( $>10\mu\text{m}$  and  $>2.5\mu\text{m}$ ,

respectively). The diluted exhaust sample entered the cyclone tangentially, and was drawn through the cyclone body and the in-line filter by a vacuum pump. Maintenance of this exact flow rate can be difficult if the conditions at which the samples were being collected are not near standard. Cyclone use in a dilution tunnel required a feedback control system to adjust the flow to account for variations in temperature and pressure. This signal was used to command a mass flow rate controller that would be responsible for maintaining the required constant actual flow rate.

### Desert Research Institute

Chemical speciation samples were collected by DRI, using the residence time dilution chamber. DRI used a Model Bendix-Unico 240 PM<sub>2.5</sub> cyclone to draw dilute exhaust samples from WVU's dilution tunnel into the DRI's residence time dilution chamber. The cyclones were an integral part of the residence time chamber. The cyclone in the DRI residence time chamber operated at a volumetric flow rate of 113 lpm (4 cfm). However, there was no additional dilution performed within the DRI chamber. The list of chemical compounds analyzed and the media used to collect them are given below:

1. Volatile organic compounds (VOC) – Canisters; field GC
2. Methane - Canisters
3. Semi-volatile organic compounds (SVOC) – PUF/XAD and TIGF filters
4. SVOC, low molecular weight compounds – Tenax tubes
5. Nitro- PAHs – PUF/XAD and TIGF filters
6. Carbonyls – DNPH cartridges
7. Nitrosamines - Thermosorb cartridges
8. PM soluble organic fraction (SOF): organic compounds – TIGF filters
9. Elemental analysis and gravimetric analysis (PM<sub>2.5</sub>) – TIGF filters
10. Ammonium and anions (Nitrate, Nitrite, Chloride, Sulfate) – Quartz filters
11. EC/OC – Quartz filters
12. PM<sub>2.5</sub> fraction for gravimetric analysis

Details of the sample collection and the analytical procedures followed by DRI are provided in Appendix K.

### ***Speciation Fleet and Approach***

The sampling of non-regulated species occurred at the same time that regulated species were sampled. Five HHDDT with a Gross Vehicle Weight Rating (GVWR) of 80,000 lbs were selected specifically for non-regulated sampling. These were E55CRC-39, E55CRC-40, E55CRC-42, E55CRC-43 and E55CRC-44. A sixth vehicle, E55CRC-41 was a MHDT and hence cannot be used for comparison purposes directly with the HHDDT in this study. The details of the test vehicles, engines, model years and the test fuel used is given below in Table 8.

**Table 8: Test Vehicle Details**

Vehicle ID	Vehicle Manufacturer	Vehicle Model Year	Engine Manufacturer	Engine Model	Engine Model Year	Primary Fuel
E55CRC- 39	Volvo	2004	Cummins	ISX 530	2004	CARB
E55CRC- 40	Freightliner	2004	Detroit Diesel	Series 60	2003	CARB
E55CRC- 41	Ford	1998	Cummins	B5.9	1997	CARB
E55CRC- 42	Freightliner	2000	Caterpillar	3406	1999	CARB
E55CRC- 43	Peterbilt	1995	Detroit Diesel	Series 60	1994	CARB
E55CRC- 44	Volvo	1989	Caterpillar	3406	1989	CARB

No aftertreatment devices were used on any vehicle. The vehicles were tested in an “as received tank fuel” condition in the same way as for regulated emissions characterization. Fuel samples for every vehicle were collected at the end of the test period and were sent for chemical analysis to Core Laboratories for analysis of cetane number, total sulfur content, aromatic content and viscosity. Another sample of the fuel was sent to DRI for analysis of inorganic and organic compounds. Oil samples were collected for every vehicle and were sent to oil sciences laboratory for 27-point analysis and sulfur content. Another sample of the oil was sent to DRI for organic and inorganic analysis.

This non-regulated emissions study employed the same test schedules that were used for the regulated emissions measurement.

The Idle Mode was extended to run three times longer than the normal Idle Mode to facilitate sufficient sample collection on the speciation media. No speciation or particle sizing data were recorded for the Creep mode. The Transient was run normally for 688 seconds. The Cruise Mode was run normally for 2083 seconds. Chemical speciation and particle sizing data were recorded for the Idle, Transient, Cruise and High Speed Cruise Modes.

Each mode was repeated twice for every vehicle. Similar multiple modes were composited by DRI on the same media to ensure sufficient sample collection. The SMPS operated in a full-scan mode during the HHDDT schedule. For the Transient Mode, the SMPS was locked onto a particle size of interest and concentration variation for that mode was measured. Particle sizes were selected based on the steady state size distribution. A steady state run at 40 kmph (25 mph) mode, not required for regulated emissions testing, was executed prior to any other tests for the sole purpose of obtaining a full particle size distribution by the SMPS. The steady state speed of 40 kmph (25 mph) was selected based on the average speed of the transient cycle. The DMS500 was operated during the modes because it was not restricted to steady-state measurements.

### **Speciation and Sizing Results**

This section discusses exhaust particle size distributions (SMPS and DMS500) and chemical speciation results for five heavy heavy-duty diesel trucks operating on various modes of the California HHDDT cycle. Particle size distribution results from the SMPS were corrected for dilution ratios. Since dilution ratio on the main tunnel was not

accurately known, DMS500 data presented in this report are for dilute flow in the main CVS tunnel. Particle size distribution is highly dependent on the method of dilution (dilution ratio and residence time) and on the dilution air properties (temperature, humidity and possibly, particle loading). Therefore, the particle size distributions measured in this program using both the SMPS and the DMS500 may not be representative of the particle size distribution generated by the exhaust plume of the vehicle in real on-road use. The raw uncorrected results obtained from DRI's analytical laboratory for chemical speciation were presented in ng/m<sup>3</sup>. All speciation data were reduced by correcting for flow rates in the sampling system. The mass values for chemical speciation were found using the equation

$$\text{g/cycle of chemical species} = (\text{V}_{\text{tunnel}} * \text{Speciated sample in ng/ m}^3) / 1.00\text{E}+09.$$

$$\text{V}_{\text{tunnel}} = \text{V}_{\text{mix}} + \text{Total PM volume} + \text{PM}_{10} \text{ volume} + \text{DRI volume (m}^3\text{)}.$$

V<sub>mix</sub> was the total integrated volume sampled from the venturi for a particular cycle. Total PM volume was the integrated volume sampled from the secondary dilution tunnel for a particular cycle. PM<sub>10</sub> volume was the integrated volume sampled from the PM<sub>10</sub> cyclone for a particular cycle. DRI operated three PM<sub>2.5</sub> cyclones at 113 lpm each; e.g., 0.34 m<sup>3</sup>/min total. To obtain the total DRI sample volume, 0.34 m<sup>3</sup>/min was multiplied by the sample time. The PM<sub>10</sub> and DRI flows were small with respect to tunnel flow.

Chemical speciation results are usually reported in g/mile, but since Idle Mode was also considered for comparison purposes, all speciation data are presented in g/hour. Only for chemical speciation, both the Cruise Modes were integrated and results reflect the combination of both the normal and High Speed Cruise Modes.

The data are depicted as "Tunnel Background" and "Test, Uncorrected" to illustrate the magnitude of reductions, while being mindful of the role the tunnel background plays when the primary emissions are so low.

Results presented for chemical speciation were not corrected for background values, which is a departure from regulatory compliance reporting, and is different from the treatment of regulatory emissions presented in this report. Background data are provided separately. There are two barriers to representing data with background correction. First, the exhaust dilution ratio in the main CVS was not known. The background correction for regulated species is performed using a dilution factor, prescribed in the Code of Federal Regulations (CFR), and this factor is not equal to the ratio. Second, background levels of each species are known to vary with time, so that accurate quantitative correction is not possible without parallel sampling trains. Finally, the role played by the tunnel background, and tunnel history effects in speciation results is an unknown.

### ***E55CRC-39***

E55CRC-39 was powered with a Cummins ISX 530 model year 2004 engine. Particle sizing and chemical speciation results are presented below for various modes of the HHDDT schedule. Figure 44 and Figure 45 present the SMPS particle size distribution for Idle and steady modes.

A very distinct clear bimodal distribution was noted for the Idle Mode with a nuclei mode in the particle size range of 18nm and an accumulation mode of 157nm with concentrations in the range of  $3.5 \times 10^5$  and  $1.5 \times 10^5$ , respectively. The nuclei mode formation is attributed to low engine load at Idle conditions. Exhaust temperatures are low under idling conditions, which lead to formation of higher levels of volatile organic compounds.

These volatile compounds are usually in the gas phase in the tailpipe. As the exhaust is diluted and cooled in the atmosphere or the dilution system, these volatile compounds may either adsorb the nucleated sulfuric acid and/or undergo homogenous nucleation to form particles. Some semi-volatile particles adsorb onto existing soot particles and increase their size and these particles are measured as the agglomeration mode particles. Nuclei mode particles do not contribute much towards Idle mass emissions as seen in Figure 46, but their number concentrations are high.

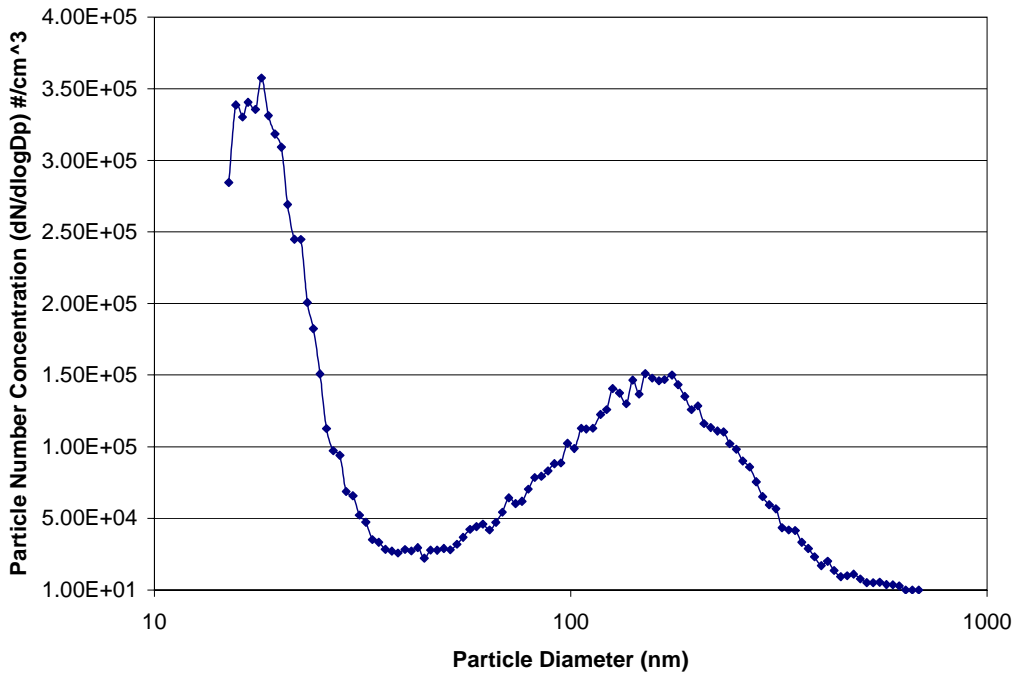


**Figure 44: SMPS Particle Size Distribution for E55CRC-39 Operating on an Idle Mode**

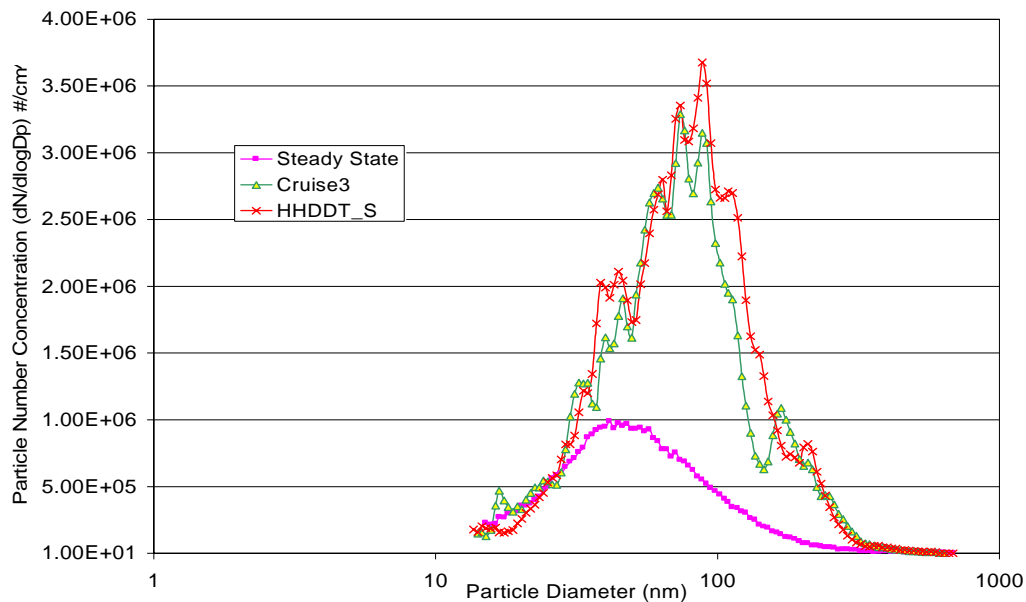


**Figure 45: SMPS Particle Size Distribution for E55CRC-39 Operating on Various Steady Cycles**

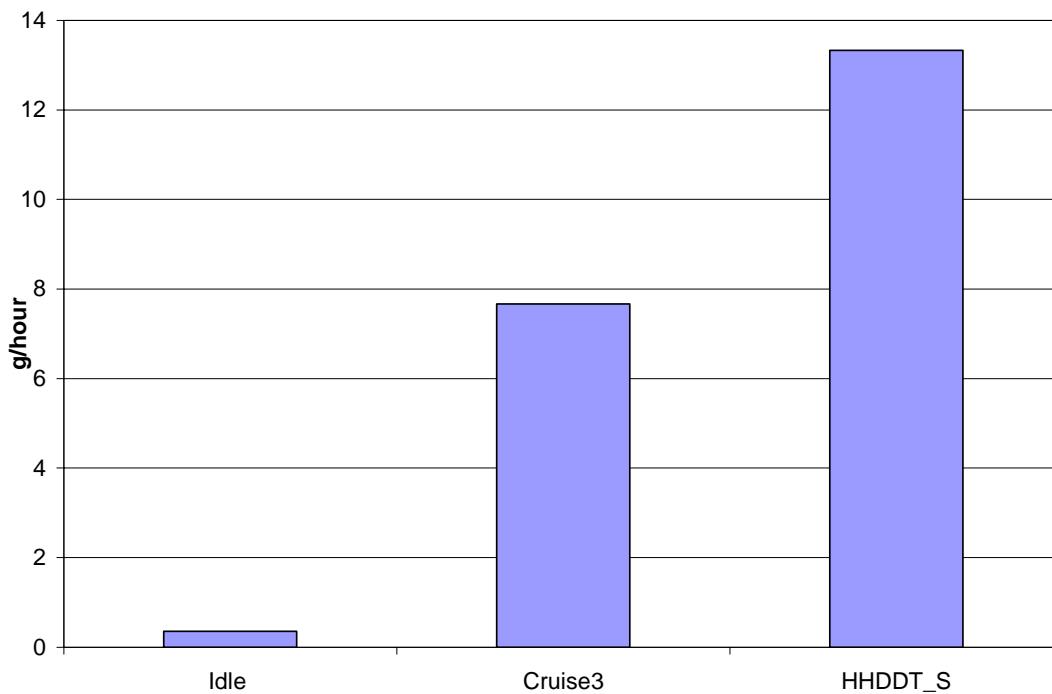


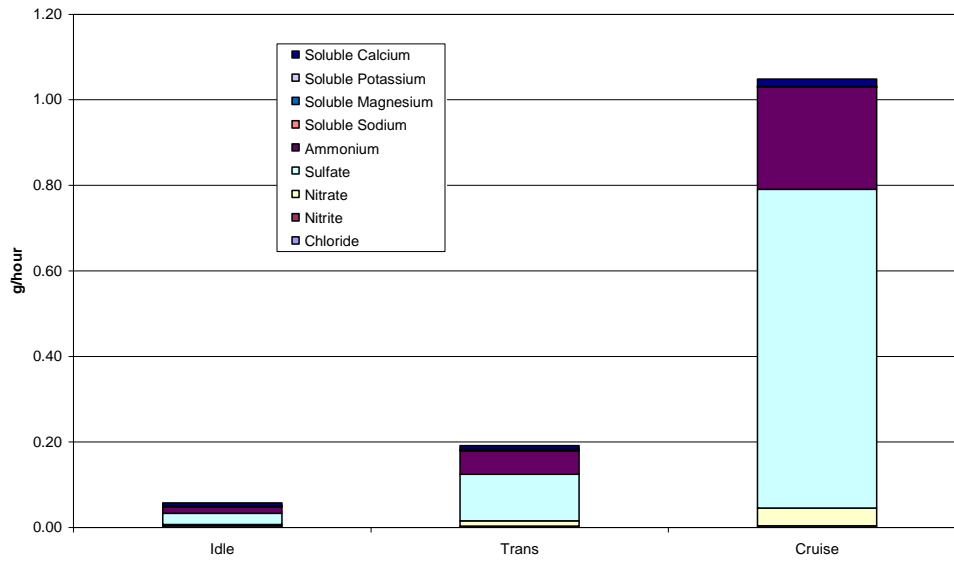
**Figure 46: PM Mass Emissions for E55CRC-39**

Chemical speciation of exhaust from E55CRC-39 showed that volatile organic compound emissions were very high in the Idle Mode at 0.68 g/hour when compared to the Cruise Mode at 0.21g/hour (Appendix M: Figure M1 to M5). In the semi-volatile group, polar

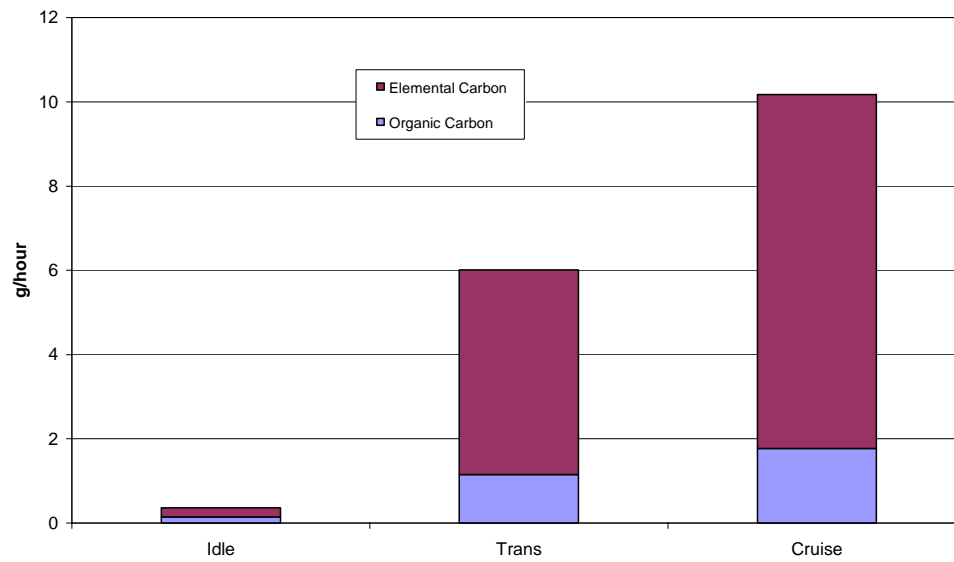
compound emissions for the Cruise Mode were very similar to Idle Mode emissions (Appendix M: Figure M9). The elemental carbon emissions for the Cruise Mode were very high at 8.3 g/hour when compared with the Idle Mode at 0.21 g/hour (Figure 48). At idle, the volatile compounds experience lower temperatures after being emitted or in the tail pipe. The saturation ratios (partial pressure/saturation pressure) are also higher in light of the fact that elemental carbon is present in very low quantities; hence, idle operation PM emissions are driven by the lower exhaust temperatures and higher saturation ratios. The lower concentration of elemental carbon contributes to nucleation of nano-particle formation. These analyses clearly indicate that, for this vehicle, the nano-particles or nuclei mode particles which are measured during the Idle Mode, are mostly made up of volatile compounds. The heavier organic species undergo condensation onto the hetero-molecular complex of water, sulfuric acid and lubricating oil based nano-sized ash particles. For the steady state mode at 40 kmph (25mph), the Count Median Diameter (CMD) of the particle size distribution was 48.89nm with a maximum concentration level of  $1 \times 10^6$  particles/cm<sup>3</sup>. For the High Speed Cruise and normal Cruise Mode, the particle size distribution was very similar with a CMD of 75.91 and 71.84nm, respectively. The concentration levels for the Cruise Modes were almost twice that of the steady state mode and almost ten times that of the Idle Mode.

The geometric standard deviation (GSD) for the steady state, Cruise and High Speed Cruise Modes were 1.83, 1.84 and 1.79, respectively. The geometric standard deviation represents the distance of shift from the mean of the whole distribution. GSD values close to 1.8 represent a good distribution about the mean for diesel exhaust. For the Idle Mode the GSD was 2.9 which indicates that the distribution was skewed and this can also be inferred from Figure 44. The shift towards a higher particle size in the Cruise Modes was likely due to a higher concentration of carbonaceous agglomerates in the exhaust, which also tend to suppress nano-particle formation (see Figure 45). Sulfate emissions were almost 20 times higher in the Cruise Mode than in the Idle Mode (Figure 48). Acetone emissions were unusually high for the Transient Mode at 212.4 g/hour (Appendix M: Figure M11).

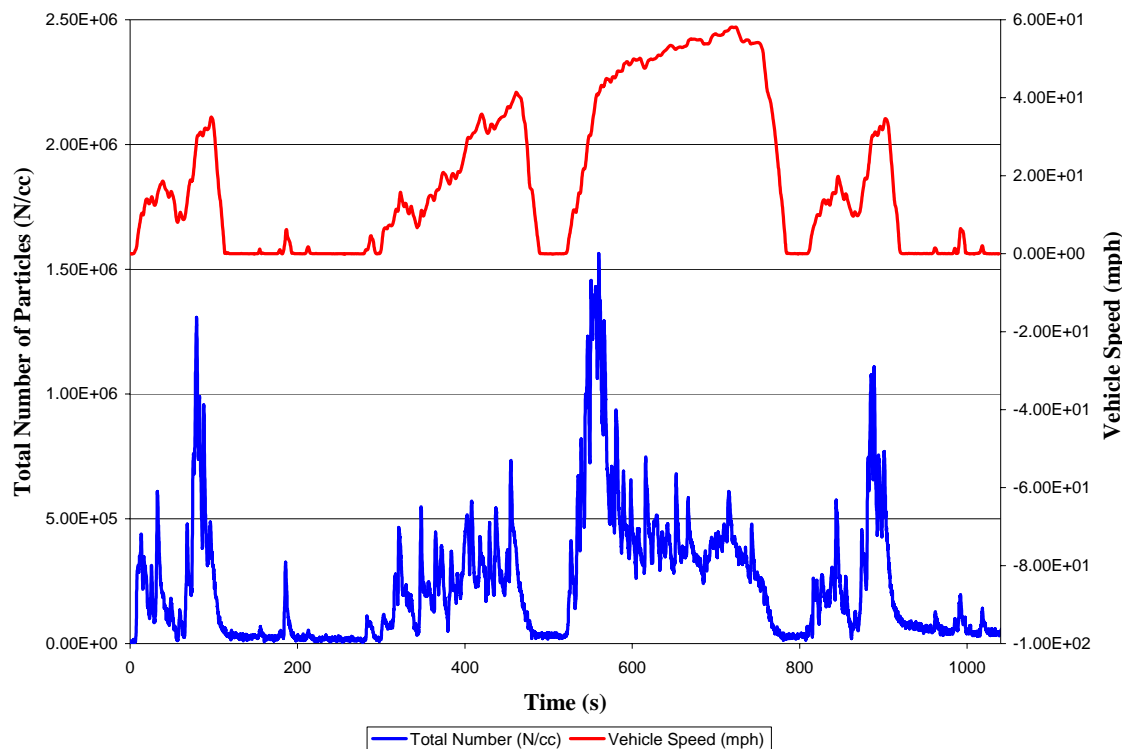
On a mass basis, the contribution of nitro-PAH and hopanes & steranes compounds (Appendix M: Figure M8 and M10) were not significant, although hopanes and steranes are valuable in source apportionment. Sulfates along with semi-volatile and carbonyl compounds usually adsorb onto carbon particles and form a cluster-like structure which increases the size of the particles, and the size spectrum is shifted towards the larger accumulation mode which is evident from Figure 45. These analyses show that accumulation mode particles formed during the Cruise Mode are mostly made up of semi-volatile compounds with a solid carbonaceous core.



**Figure 47: Ion Composite Results for E55CRC- 39**



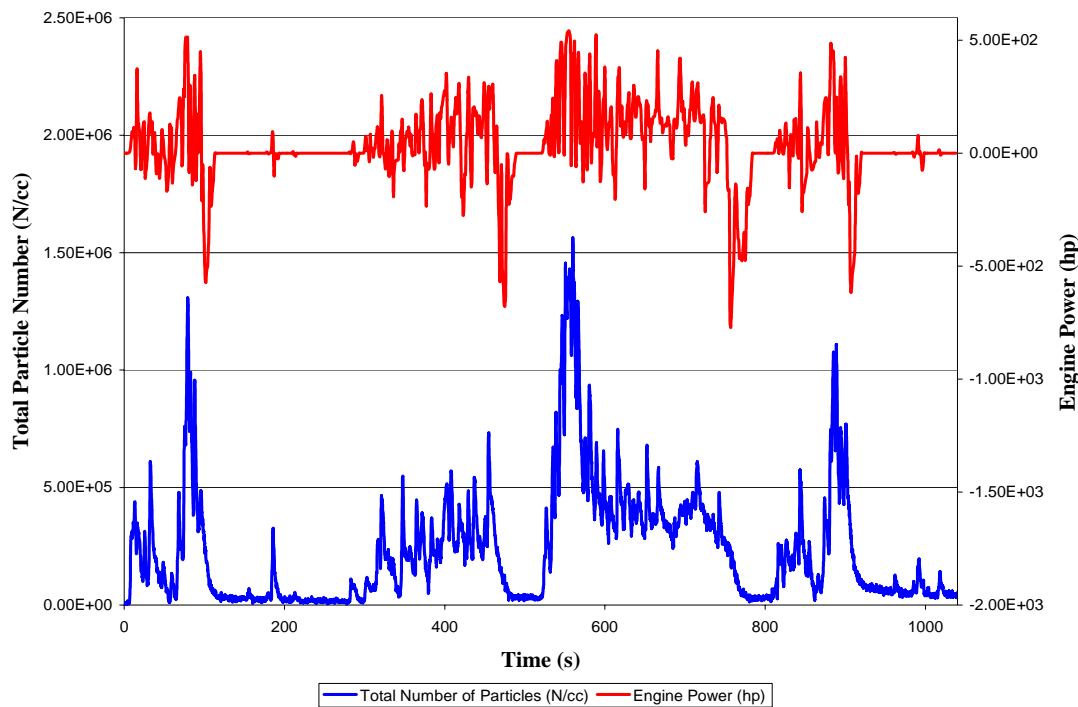
**Figure 48: Elemental Carbon and Organic Carbon PM Analysis for E55CRC-39**



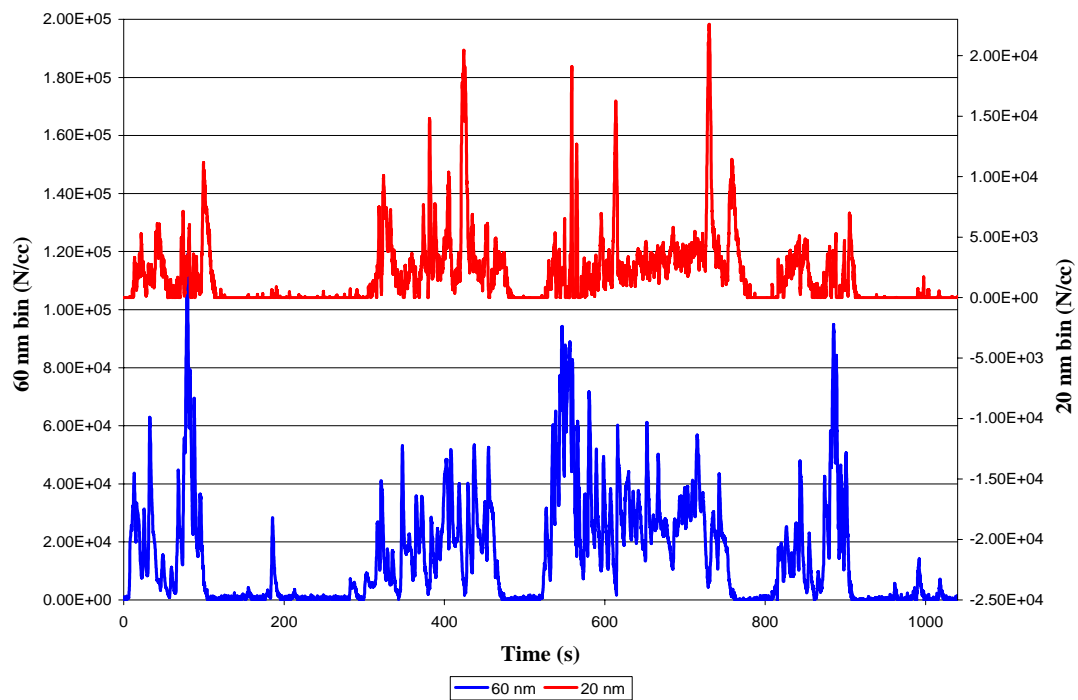
**Figure 49: DMS500 Total Number of Particles and Vehicle Speed vs. Time during the UDDS for E55CRC-39 tested at 56,000 lb.**

Comprehensive DMS500 data are available for E55CRC-39. Figure 49 shows the total number of particles and vehicle speed versus time during the UDDS for E55CRC-39. The total number goes as high as  $1.5 \times 10^6$  particles/cm<sup>3</sup> during steep accelerations and goes down to  $1.5 \times 10^4$  during idle conditions. There is no strong correlation between the total number and engine speed, but as can be observed from Figure 49, during accelerations, the total number was high and when the high speed was continued for a period, the total number started to drop, e.g., between  $t = 600$  and  $700$ s. During decelerations, the total number dropped to a minimum and continued that way during the idle period.

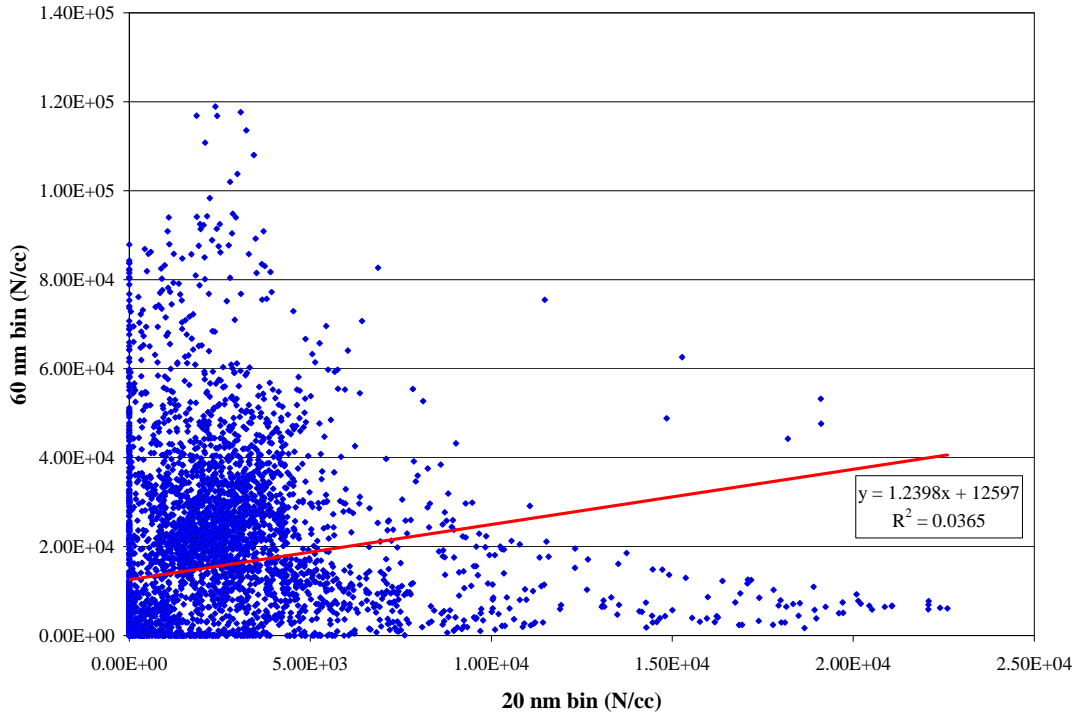
Figure 50 shows the total number of particles and engine power versus time. Figure 51 shows the distribution of the total number concentration of particles in the 60 and 20nm bins versus time. The 60nm bin contains particles of diameters between approximately 55 and 65nm, and the diameters for the 20nm bin range between 17.5 and 22.5nm. As can be observed from the plot, the overall number of 60nm particles, which represent the accumulation mode particles, are almost an order of magnitude higher than the total number of particles in the 20nm bin. Figure 52 shows the total number of particles in the 60nm bin versus the total number of particles in the 20nm bin. There is a much sharper increase in the total number of particles in the 20nm bin during decelerations and a sharper increase in the total number of particles in the 60nm bin during accelerations. As can be seen, there is no clear correlation between the two size bins as measured by the DMS500, confirming that the PM formation processes differ between the two sizes of PM.



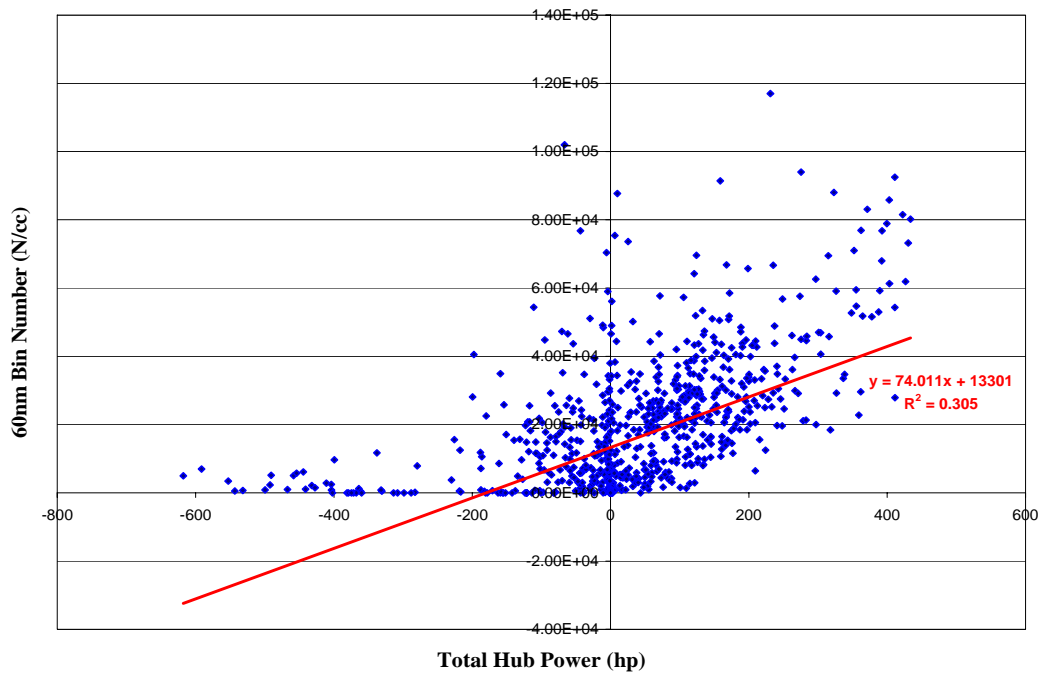
**Figure 50: DMS500 Total Number of Particles and Engine Power vs. Time during the UDDS for E55CRC-39 tested at 56,000 lb.**



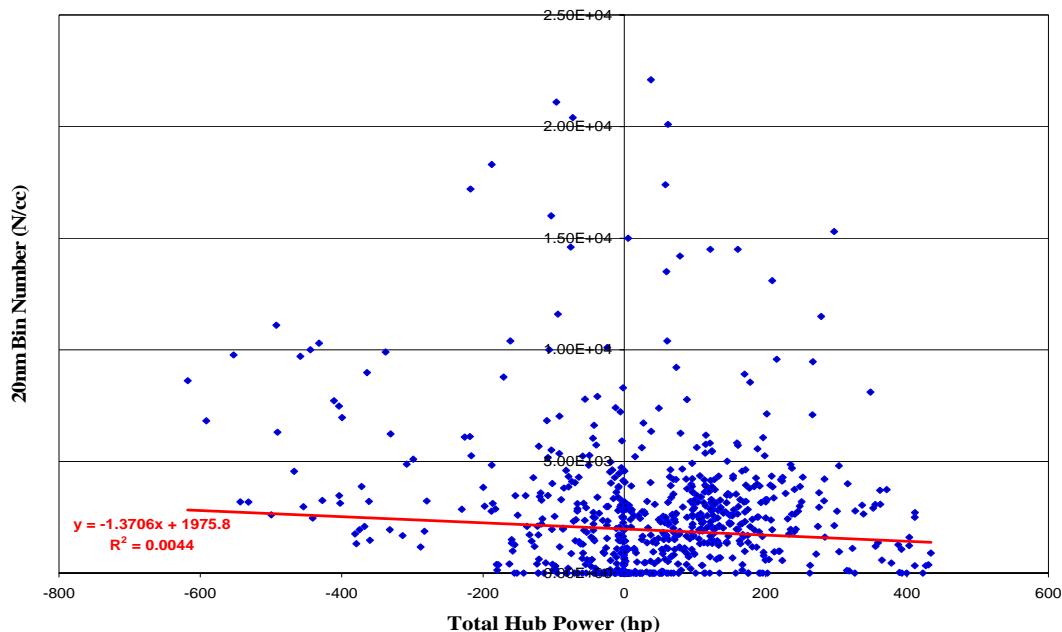
**Figure 51: DMS500 60nm and 20nm Particle Number vs. Time during the UDDS for E55CRC-39 tested at 56,000 lb.**



**Figure 52: DMS500 60nm Particle Number vs. 20nm Particle Number during the UDDS for E55CRC-39 tested at 56,000 lb.**



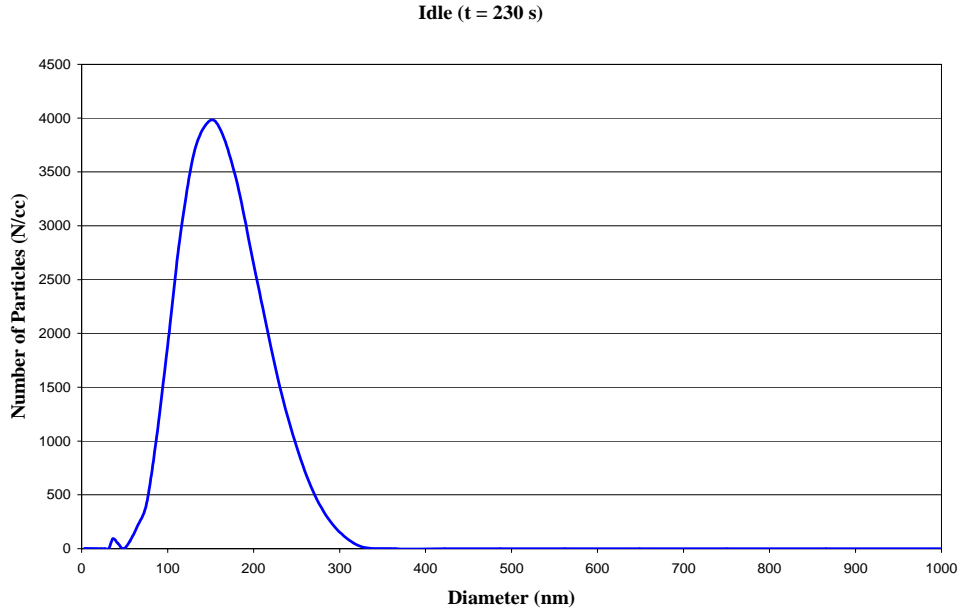
**Figure 53: DMS500 60nm Particle Number vs. Total Hub Power during the UDDS for E55CRC-39 tested at 56,000 lb.**



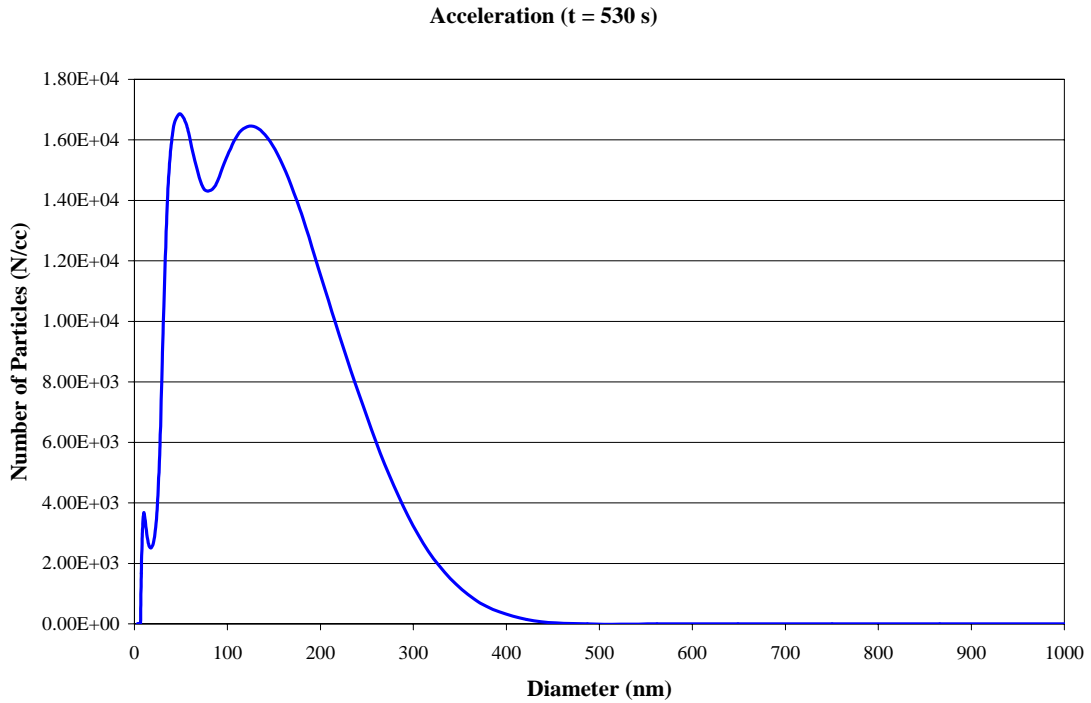
**Figure 54: DMS500 20nm Particle Number vs. Total Hub Power during the UDDS for E55CRC-39 tested at 56,000 lb.**

Figure 53 shows the total number concentration of particles in the 60nm bin versus the total hub power. There is no strong correlation, but the total number shows an upward trend with the positive hub power range. Since 60nm particles are in the accumulation mode, one would expect their count to rise when higher power operation demands lower air to fuel ratio. Figure 54 shows the total number concentration of particles in the 20nm bin versus the total hub power. Again, there is no strong correlation between the two series but in this case as one can observe from the plot, there are more particles in the negative hub power periods, that is during decelerations. This is something we expect since nuclei mode particles are dominant during the deceleration phases.

The following plots show the size distribution of particles during Idle, acceleration and deceleration, respectively for E55CRC-39. As can be observed from Figure 55, particles of around 150nm are mostly observed. This peak size agrees well with the 157nm peak for the SMPS data, shown in Figure 44, but the nuclei mode peak evident in the SMPS plot is absent. One must note that the dilution system used for the two devices differed. During acceleration, as shown in Figure 56, a bimodal distribution is observed where there are two peaks centered at around 58 and 135nm, respectively. This plot shows the transition from the Idle Mode, where particles of diameter 150nm are dominant, to the acceleration mode, where particles of diameter around 60nm are observed, which are the accumulation mode particles. Strong modes in the 50 to 100nm range were observed for the SMPS data shown in Figure 45. Figure 57 shows the distribution during the deceleration region of the UDDS. Again, we see a bimodal distribution. This time, the transition is from deceleration to Idle Mode. The first peak is centered around 15nm, which are mostly nuclei mode particles, and the second peak is centered around 175nm, which is the Idle region distribution.



**Figure 55: DMS500 size distribution of particles during Idle (t = 230 s) of the UDDS for E55CRC-39 tested at 56,000 lb.**



**Figure 56: DMS500 size distribution of particles during acceleration (t = 530 s) of the UDDS for E55CRC-39 tested at 56,000 lb.**

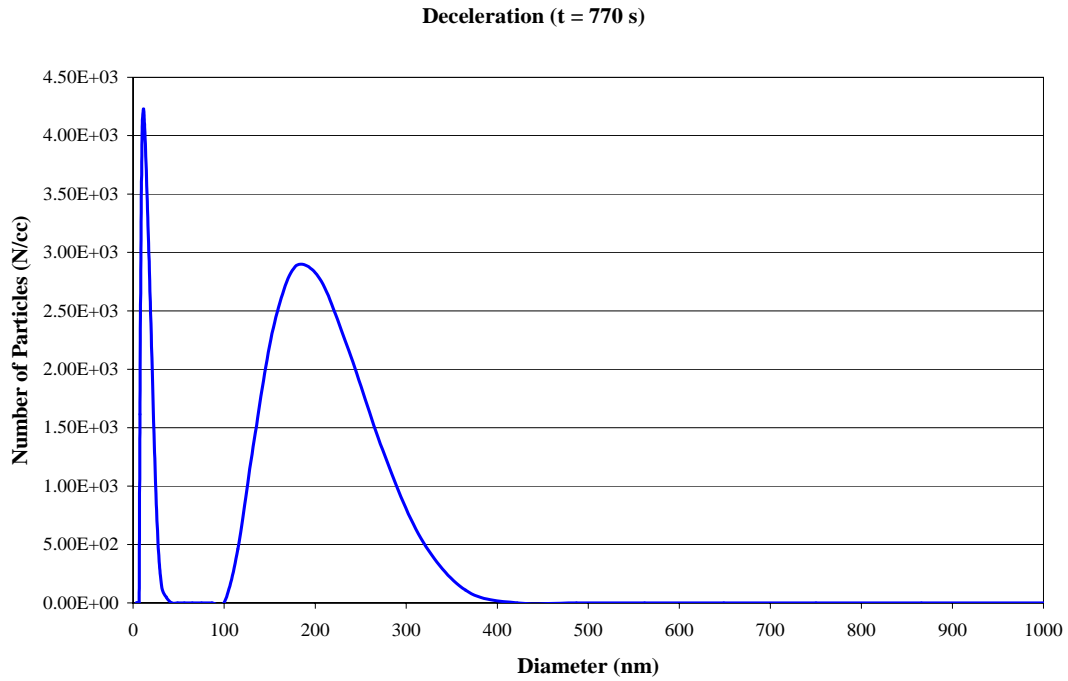


**Figure 57: DMS500 size distribution of particles during deceleration (t = 770 s) of the UDDS for E55CRC-39 tested at 56,000 lb.**

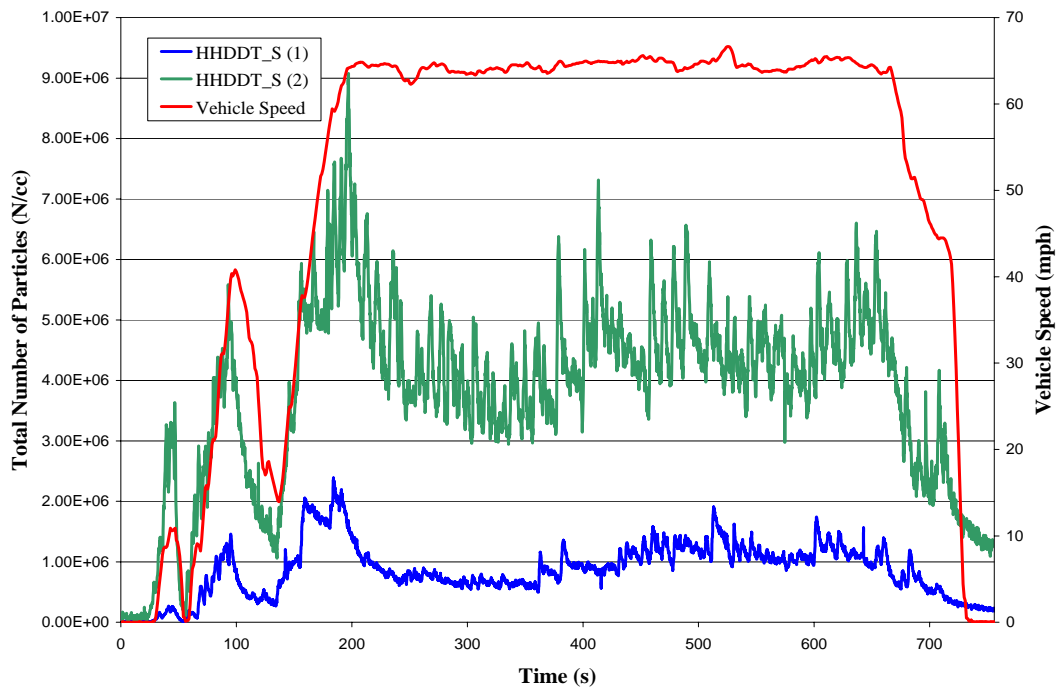


**Figure 58: DMS500 size distribution of particles during HHDDT\_S and Vehicle Speed vs. Time for E55CRC-39 tested at 56,000 lb.**

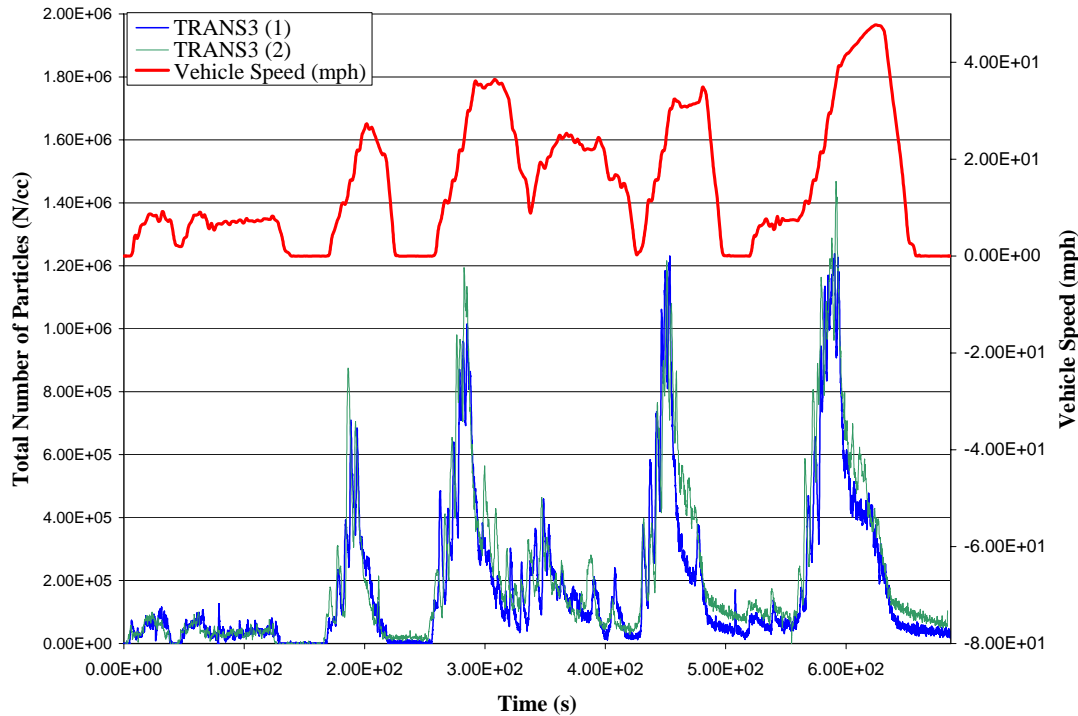


**Figure 59: DMS500 size distribution of particles during Transient and Vehicle Speed vs. Time for E55CRC-39 tested at 56,000 lb.**

Figure 58 shows the total number of particles, determined using the DMS500 and vehicle speed versus time during HHDDT\_S for E55CRC-39. As can be observed, the total number of particles is as high as  $9 \times 10^6$  during step accelerations, and drops to  $9 \times 10^4$  particles/cm<sup>3</sup> during idle regions. Looking at the data profiles for the two tests, the problem may be that the DMS500 inlet probe was not properly mounted on the second HHDDT\_S test, thus sucking in air from the ambient and causing a decrease in the particle number concentration readings."

Figure 59 shows the total number of particles, measured by the DMS500, and vehicle speed versus time for two different Transient runs. Again, as it is observed from previous plots, the total number of particles increases during accelerations and decreases during decelerations. During the High Speed Cruise section, the total number starts to decrease due to the decrease in the total number of accumulation mode particles. Repeatability is good for the two traces in Figure 59.

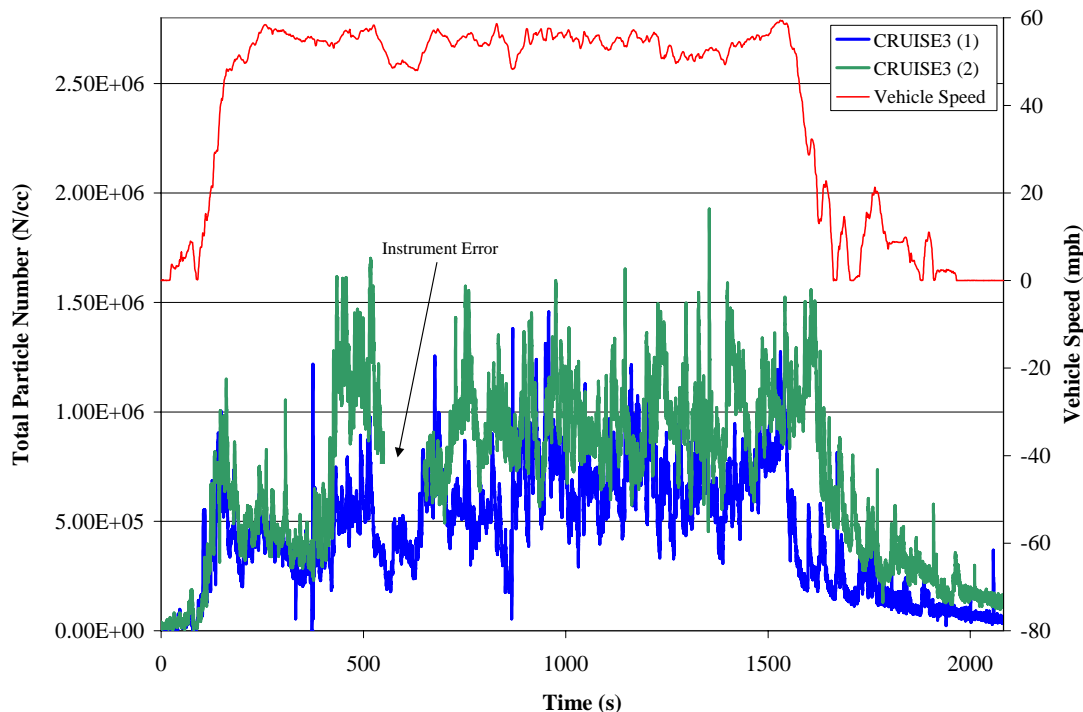


**Figure 60: DMS500 size distribution of particles during Cruise3 and Vehicle Speed vs. Time for E55CRC-39 tested at 56,000 lb.**

Figure 60 shows the total number of particles and vehicle speed versus time for two different Cruise runs. During acceleration, the total number of particles increases and during decelerations, the total number decreases. Repeatability is not as good as illustrated in Figure 59, and the researchers speculate that this may have been due to the accumulation of PM in the instrument. This was the first operation of the instrument in the field by the researchers, and protocols for cleaning the instrument were not well established at time of testing.

### ***E55CRC-40***

E55CRC-40 was a powered by a Detroit Diesel Series 60, model year 2003 engine. Particle sizing and chemical speciation results are presented below for various modes of the HHDDT schedule. Figure 61 and Figure 62 present the SMPS particle size distributions for Idle and steady modes.

A nuclei mode dominated distribution was seen for the Idle Mode with a count median diameter (CMD) of 25.88nm with a concentration of  $8 \times 10^4$  particles/cm<sup>3</sup> and a geometric standard deviation of 1.64. These concentration levels were almost four times lower than those observed for E55CRC-39. This drop in concentration could be attributed to difference in the emissions of volatile organic compounds. The total VOC's emitted for E55CRC-40 at 2.01 g/hour during the Idle Mode was almost eight times lower in magnitude as compared to E55CRC-39 at 15.51 g/hour. The VOC mass emission rates reported here include contributions from unburnt fuel and oil. It should be noted that a

recent study by Sakurai et al. [11] indicated that the volatile component of diesel particles was comprised primarily of unburnt lubricating oil, and that contributions from unburnt fuel, oxidized organic combustion products, and sulfuric acid were small. Sakurai et al. [11] also reported that the organic component of diesel nanoparticles was comprised of compounds with carbon numbers in the C<sub>24</sub> - C<sub>32</sub> range, which are almost entirely derived from unburnt oil.

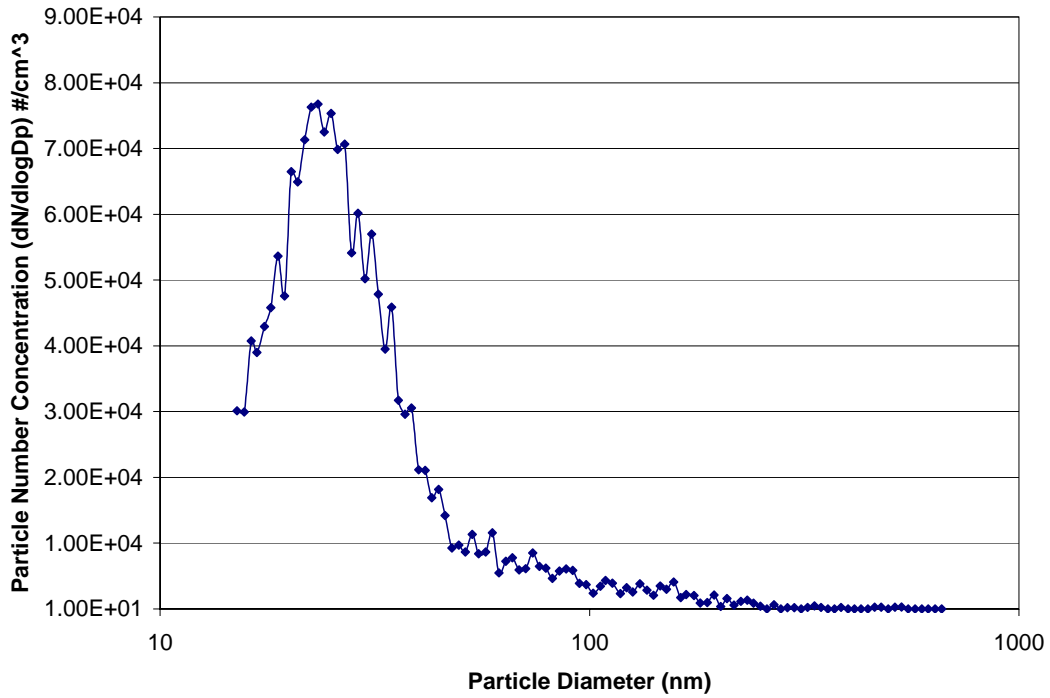


**Figure 61: SMPS Particle Size Distribution for E55CRC-40 Operating on an Idle Mode**

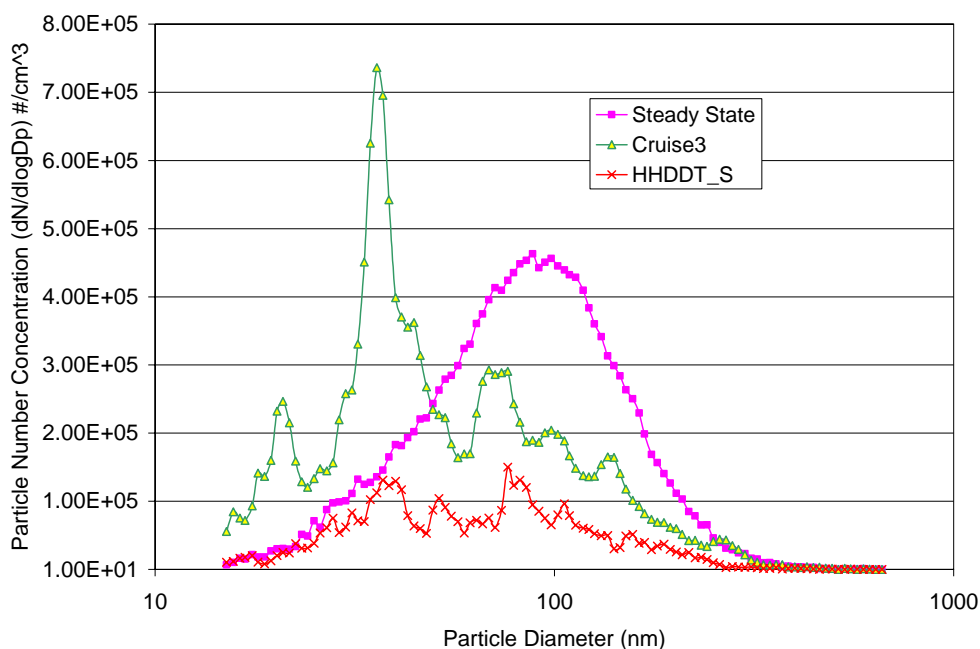


**Figure 62: SMPS Particle Size Distribution for E55CRC-40 Operating on Various Steady Cycles**

VOC results were very similar for E55CRC-40 when Idle and Cruise Mode were compared (Appendix M: Figure M13 to M17). Emissions of n-hexane and 2-methyl-1-pentene were high during the Transient Mode when compared with the Idle and Cruise Modes (Appendix M: Figure M15 and M16). For the steady state mode, the CMD for the particle size distribution was 85nm with a concentration of  $4.5 \times 10^5$  particles/cm<sup>3</sup> and a GSD of 1.75. Particle size distributions were markedly different for the two Cruise Modes with a CMD of 45.1nm for the normal Cruise Mode and 62.24nm for the High Speed Cruise Mode. SMPS size distributions observed in the Cruise Modes were characterized by the accumulation mode particles.

The shift of the size spectrum towards a higher accumulation range during the Cruise Modes when compared to the Idle Mode could be attributed to higher concentrations of carbonaceous agglomerates (EC emissions) and higher sulfate emissions during the Cruise Mode. Sulfate emissions were very high during the Cruise Mode at 0.27 g/hour when compared with the Idle Mode at 0.015g/hour (Figure 65). Sulfate emissions serve as the precursors of particle formation seen in the nuclei mode. Sulfates would undergo a hetero-molecular nucleation with water molecules to form complex clusters. Subsequent adsorption of volatile organics and agglomeration with the elemental carbon results in the distribution seen in Figure 62. Elemental carbon emissions for the Cruise Mode were high at 5.5 g/hour when compared to the Idle Mode at 0.07 g/hour (Figure 65), which also contributed to most of the mass emissions (Figure 64). Semi volatile emissions were similar for Idle and Cruise Modes except for alkanes and hopanes & steranes which were higher during the Cruise Mode (Appendix M: Figure M18 to M22).

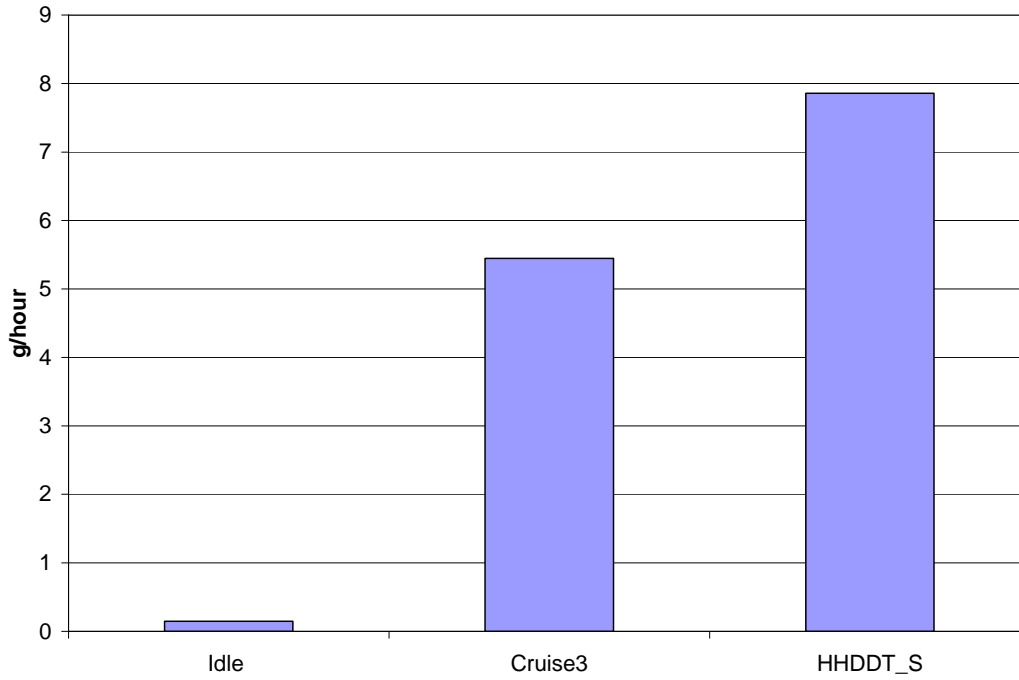


**Figure 63: PM Mass Emissions for E55CRC-40**

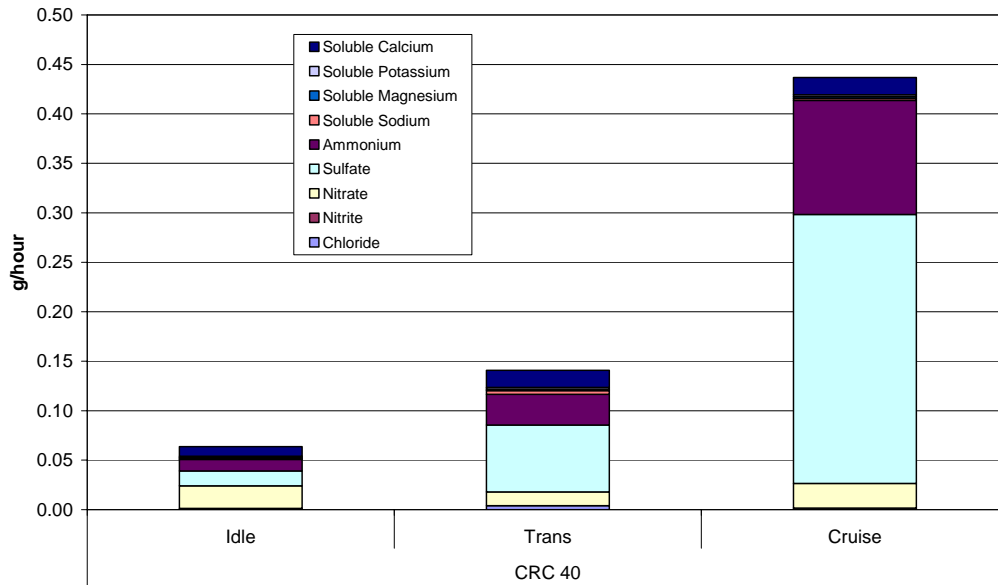


**Figure 64: Ion Composite Results for E55CRC-40**

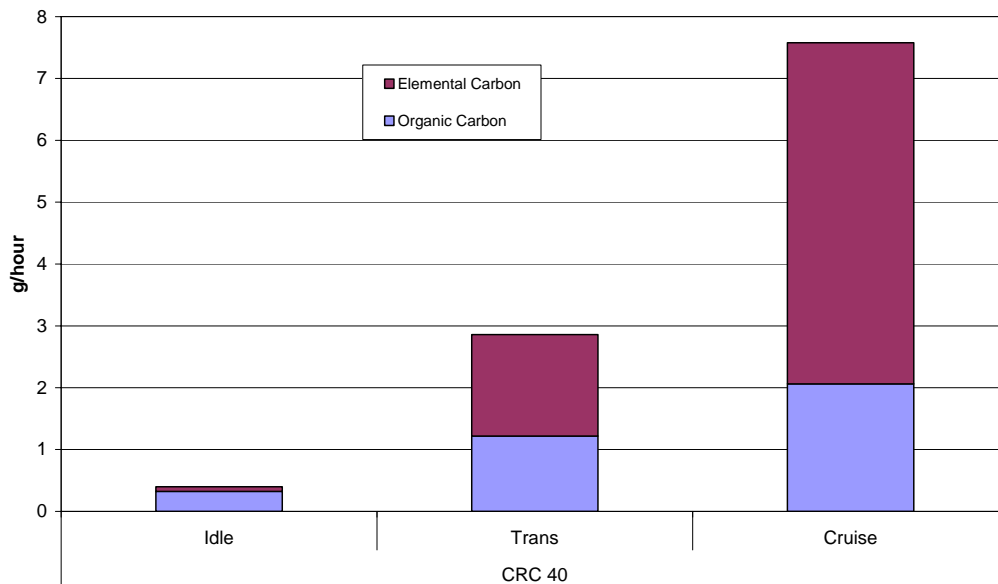


**Figure 65: Elemental Carbon and Organic Carbon PM Analysis for E55CRC-40**

For E55CRC-40, DMS500 data proved unreliable, and were characterized by spikes in the output data that did not represent credible particle counts.

***E55CRC-41***

E55CRC-41 was the only MHDT subjected to speciation.

CRC41 was a Medium Heavy-duty Vehicle (MHDT) powered by a MY1997 Cummins B5.9, 210 hp engine. The vehicle was tested over a lower speed transient, a higher speed transient, and the cruise mode. Additionally, PM concentration and size distribution data was collected over the MHDT schedule that comprised of driving modes mentioned above. Figure 66 shows the PM size distribution over the idle mode.

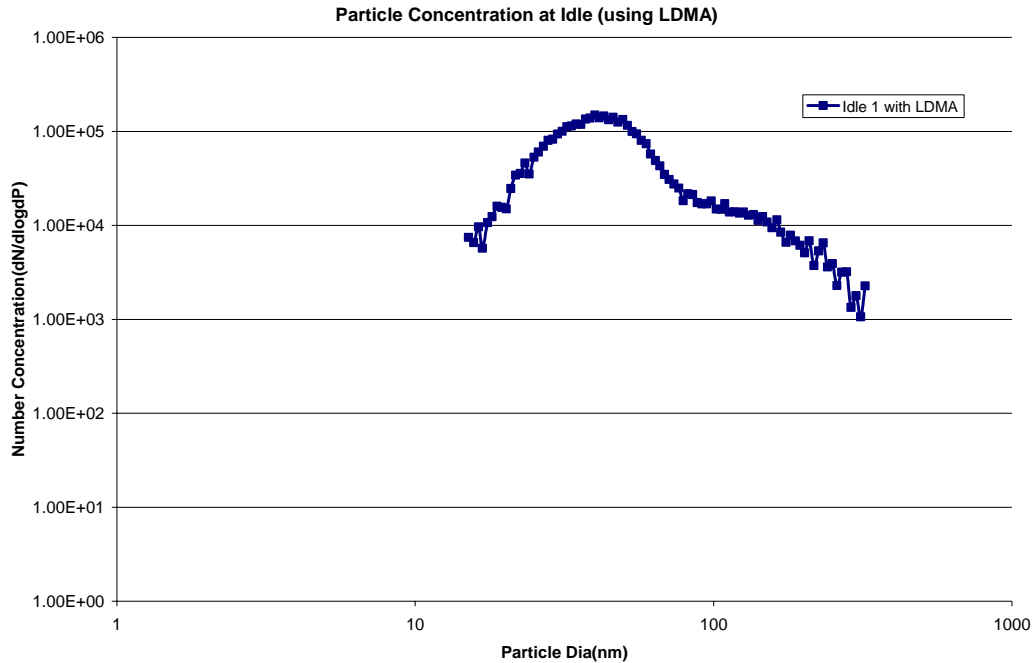
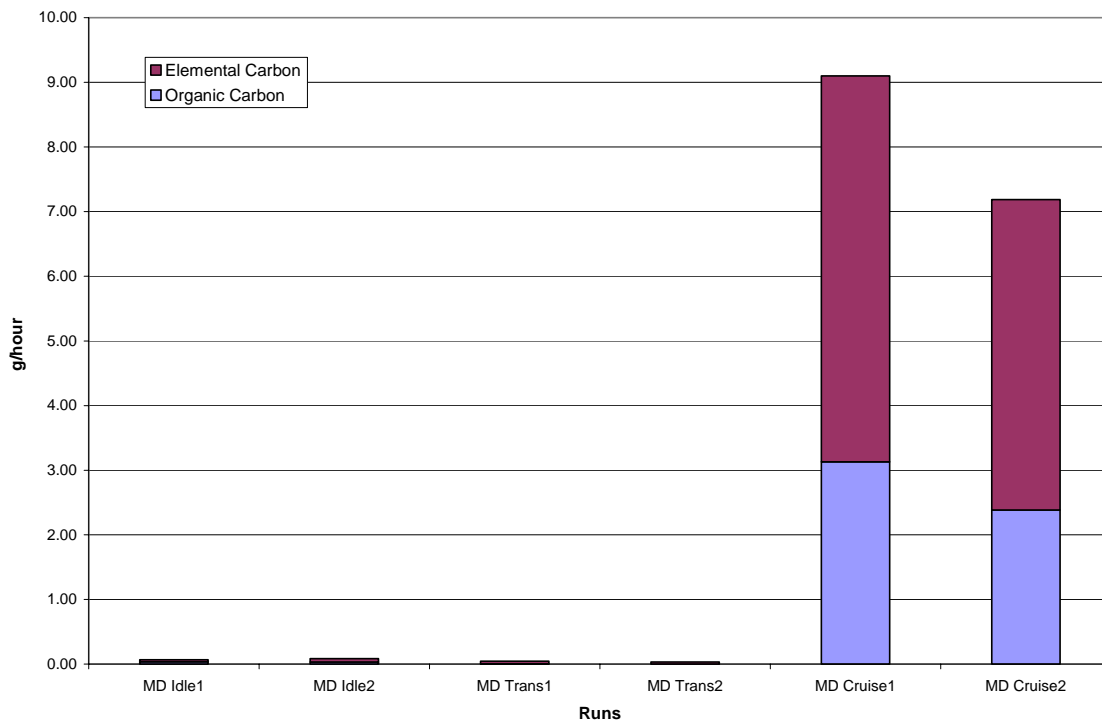


**Figure 66: SMPS Particle Size Distribution for E55CRC-41 Operating on an Idle Mode**

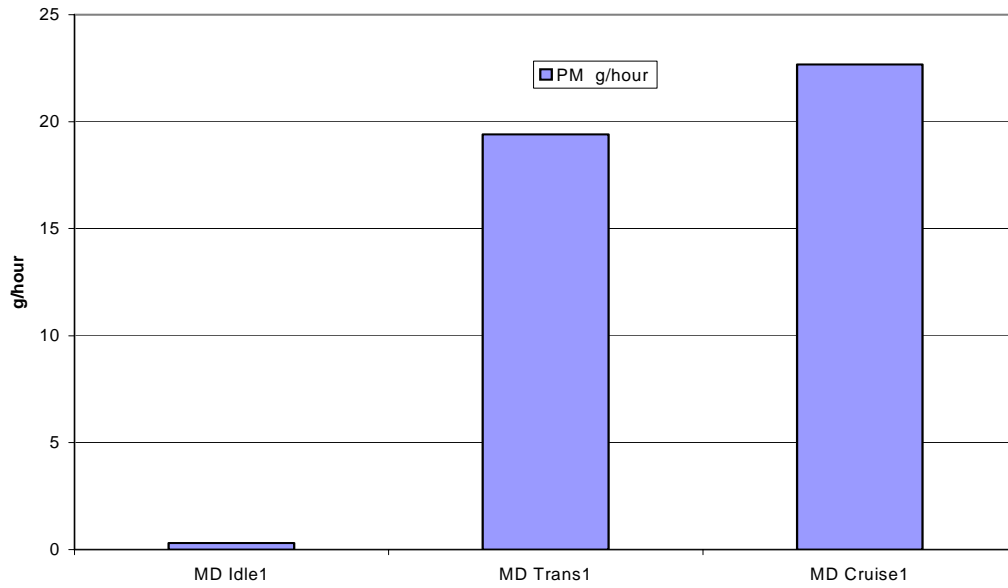
The size distribution during idle operation (Figure 66) showed a nuclei mode centered at 40 nm and an accumulation mode of 136 nm with concentrations in the range of  $1.4 \times 10^5$  and  $1.3 \times 10^5$ , particles/cm<sup>3</sup>, respectively. Again, the lower exhaust temperatures under idling conditions, and the relatively low carbonaceous soot (resulting in higher saturation ratios) leads to formation of higher levels of nuclei mode particles, primarily from the organics compounds originating from the lubricating oil. Recent studies by Gautam et al. [12] on natural gas-fueled heavy-duty vehicles have shown evidence that supports the argument that lubricating oil significantly contributes to nuclei mode particles. When total surface area provided by soot particles is reduced the nucleation process is advanced. Hence, in driving modes where the elemental carbon component of the total PM emissions is lower, the nuclei mode particles are emitted in higher concentrations, provided the exhaust temperatures and relative humidity are conducive to nucleation [13, 14]. The binary nucleation theory of water and sulfuric acid has been shown to underestimate the formation of nucleation mode particles by several orders of magnitude [15]. However, organic compounds have been considered as a key species to control the growth of nucleation mode particles [14].

Chemical speciation of exhaust from CRC41 showed that most volatile organic compounds, except for C<sub>2</sub> to C<sub>5</sub> alkanes, were higher in the transient and cruise modes than in the idle mode of operation (Appendix M: Figure M25 to Figure M36). The polar compound emissions for the transients were the highest (Appendix M: Figure M33). The

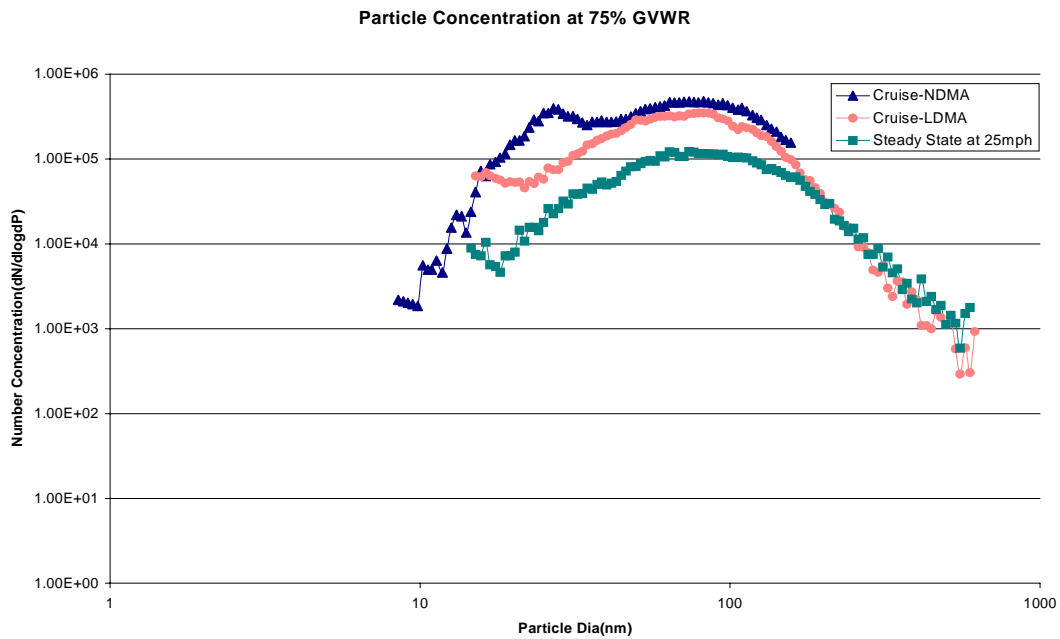
elemental carbon emissions for the cruise mode were nearly seven times higher than the idle emissions (Figure 67). Figure 68 shows that total PM mass emission rates in the cruise mode are dominated by the elemental carbon emissions. However, the organic carbon emissions are also significantly higher under cruise mode than under idle and transient modes. This breakdown is reflected in the PM concentrations and size distributions, as seen in Figure 66, Figure 69 and Figure 70). Cruise operation at a vehicle inertia of 75% GVWR shows a nuclei mode peak at 26.9 nm with a concentration of  $3.9 \times 10^5$  particles/cm<sup>3</sup> when measured with a nano-DMA. The accumulation mode, with a CMD of 76.4 nm is similar for the cruise and steady state (25 mph) operation. Particle concentrations at 50% GVWR at cruising conditions does not produce any significant concentrations of nano-particles. This may be attributed to lower emissions of volatile species. Compared to the idle and transient modes, emissions of sulfate emissions were significantly higher in the cruise mode (Figure 71). As noted earlier, binary nucleation of sulfuric acid and water do contribute to formation of nucleation mode particles, which may or may not survive in the exhaust depending upon levels of carbonaceous soot present in the exhaust stream.



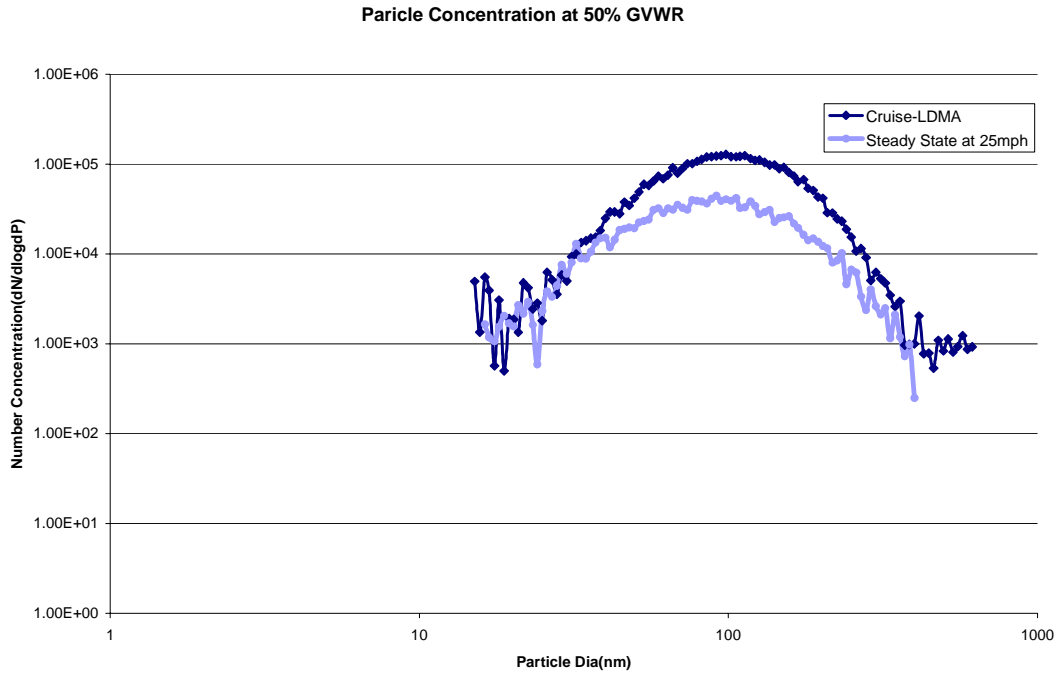
**Figure 67: Elemental Carbon and Organic Carbon PM Analysis for E55CRC-41**



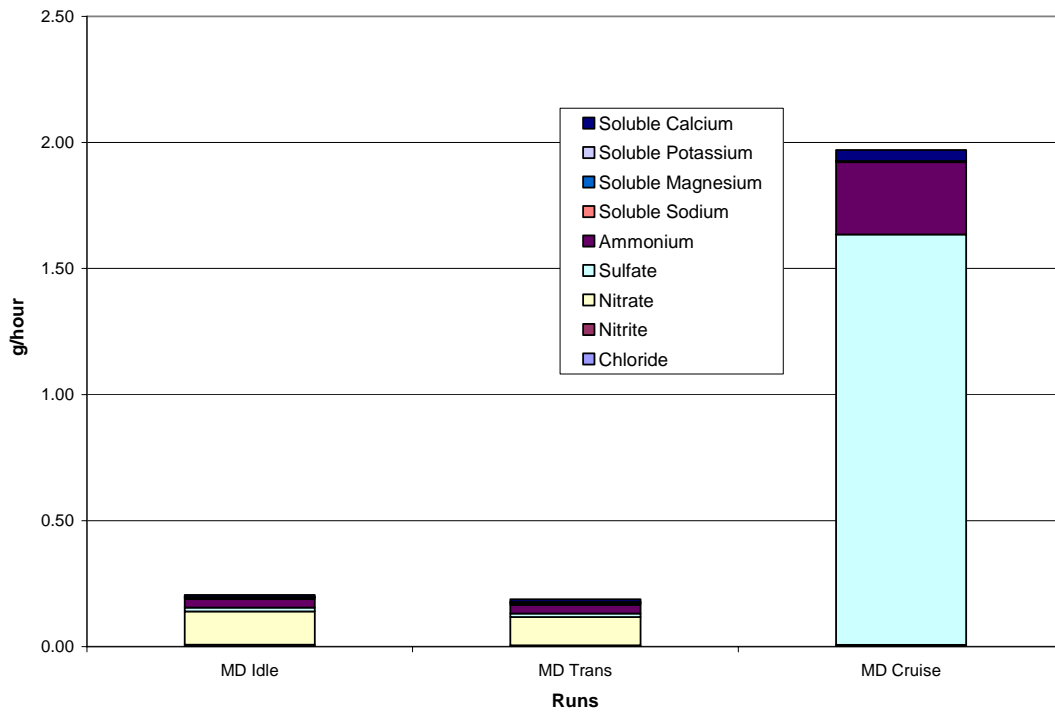
**Figure 68: Total PM Mass Emissions Rate (g/hour) for E55CRC-41**



**Figure 69: SMPS Particle Size Distribution for E55CRC-41 Operating on Cruise and Steady Cycles**

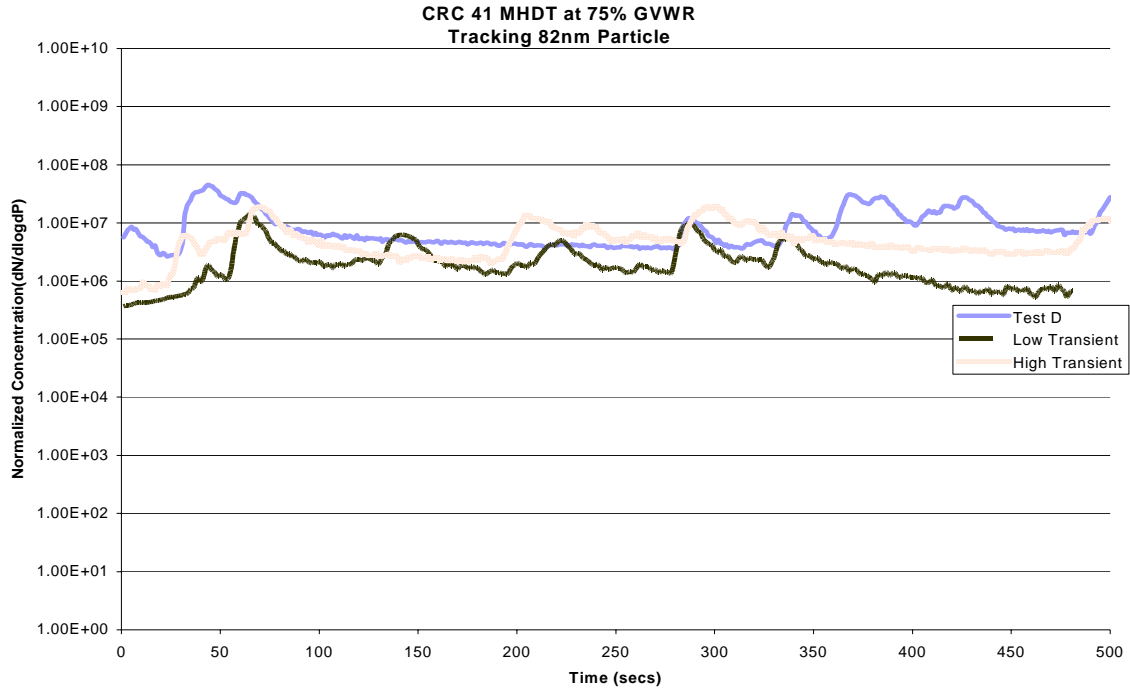


**Figure 70: SMPS Particle Size Distribution for E55CRC-41 Operating on Cruise and Steady Cycles (50% GVWR)**

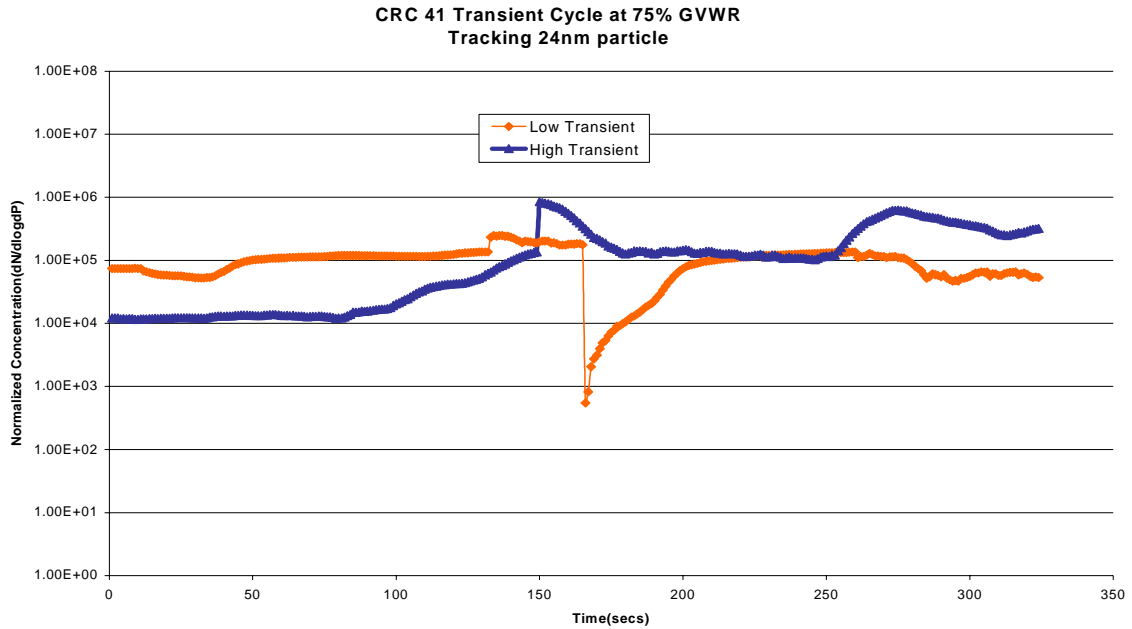


**Figure 71: Ion Composite Results for E55CRC-41**

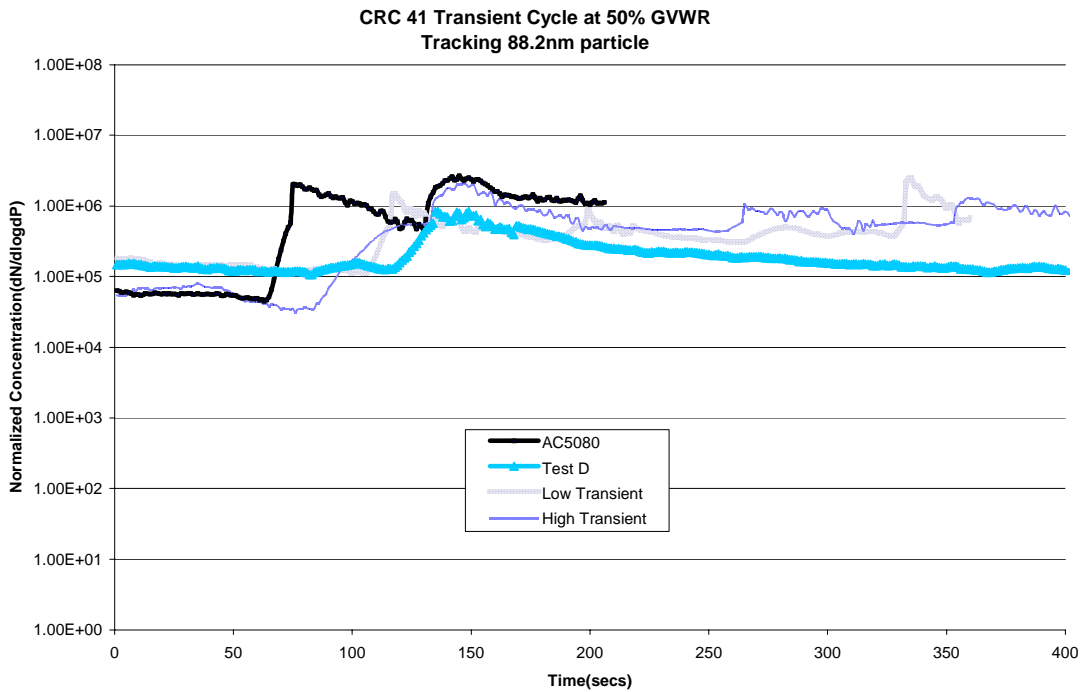
Figure 72 to Figure 74 show traces of single particle tracking (82 nm and 24 nm) under transient operations. At 75% GVWR, the 82 nm particles are emitted at higher concentrations than the 24 nm particles. The concentration of 82 nm particles decreases by an order or magnitude at lower inertia weight (50% GVWR).



**Figure 72: SMPS Single Particle Trace (82 nm) for E55CRC-41 Operating on UDDS, Low Transient and High Transient Cycles (75%GVWR)**

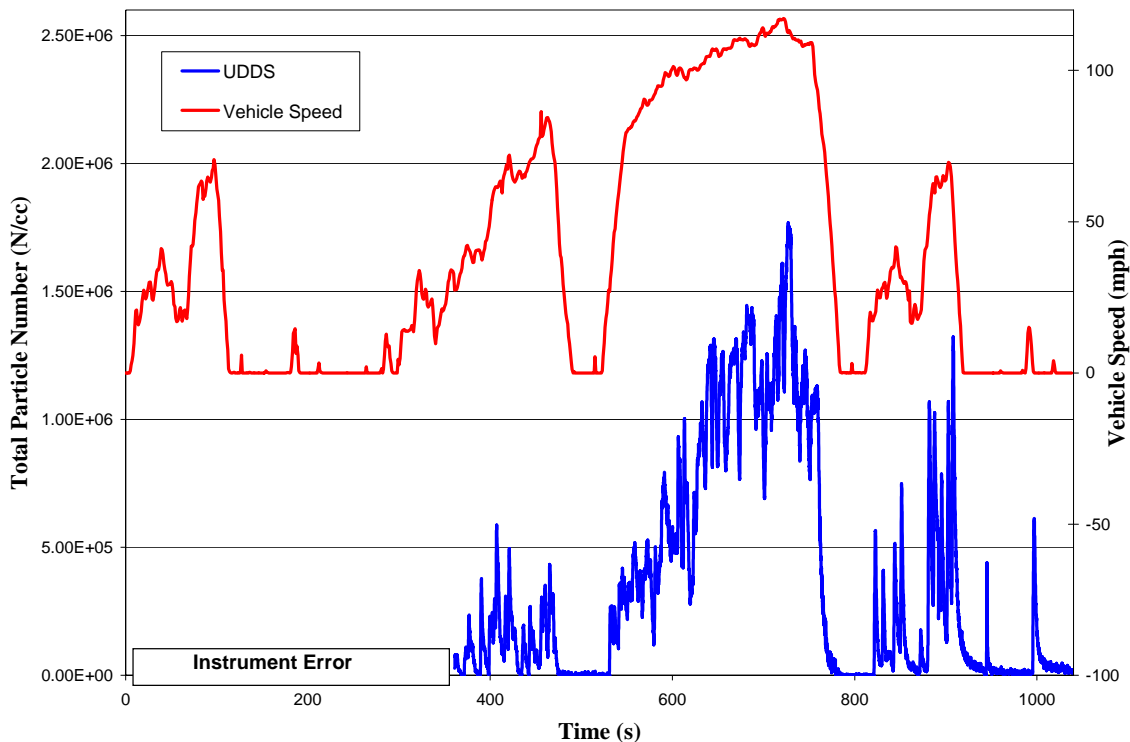


**Figure 73: SMPS Single Particle Trace (24 nm) for E55CRC-41 Operating on Low Transient and High Transient Cycles (75% GVWR)**



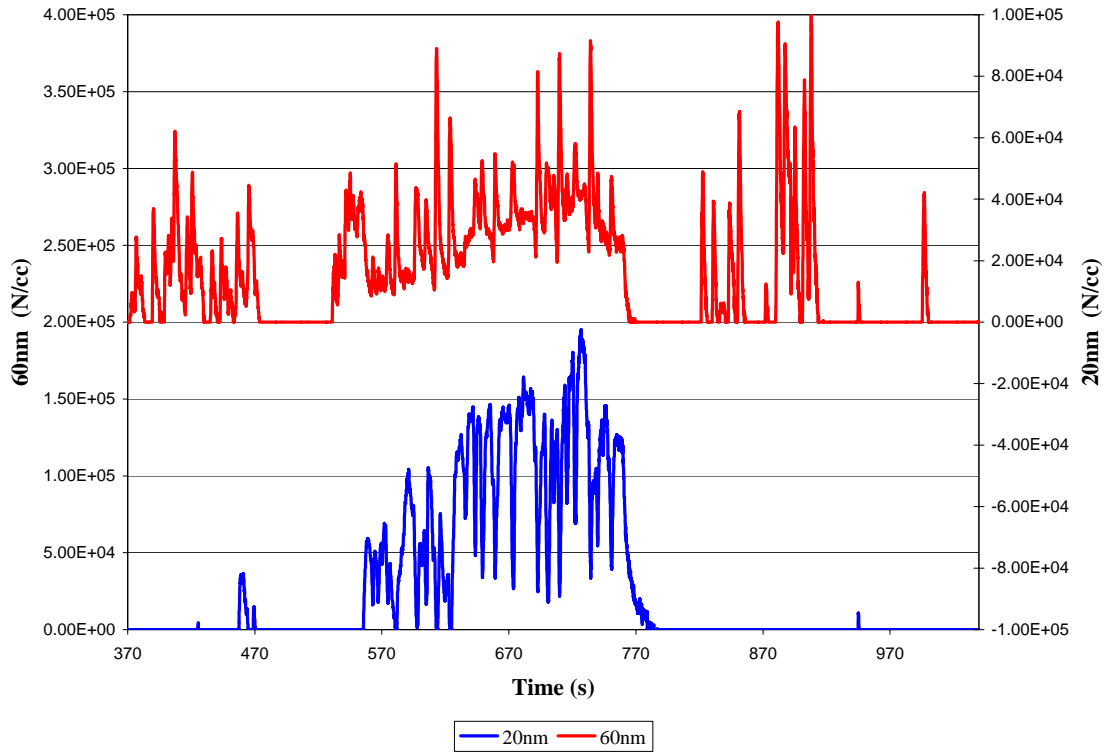
**Figure 74: SMPS Single Particle Trace (88 nm) for E55CRC-41 Operating on Low Transient and High Transient Cycles (50% GVWR)**

Figure 75 shows the DMS500 total number concentration of particles and vehicle speed versus time during the UDDS for E55CRC-41. The total number is as high as  $1.7 \times 10^6$  during steep accelerations and drops to  $1.5 \times 10^4$  during Idle conditions. (There was an error on the readings of the instrument until  $t = 370$ s in Figure 75) In Figure 75 the high count between 620 and 750 seconds is due to a high count of 20nm particles over that time. The overall count versus time differs in behavior between this vehicle and heavy-duty vehicles, such as E55CRC-39 (see Figure 49 for UDDS data) and E55CRC-42 and E55CRC-43 (Figure 87 and Figure 93 for transient behavior). E55CRC-41 did not show a high count associated with acceleration, while the HHDDT showed this behavior clearly. E55CRC-41 had a smaller displacement than the HHDDT, higher engine speed, lower boost, two valves per cylinder (versus four for the HHDDT) and an in-line injection system. However, it should be speculative to associate any of these factors directly with the differing behavior.



**Figure 75: DMS500 Total Number of Particles and Vehicle Speed vs. Time during UDDS for E55CRC-41 tested at 56,000 lb.**

Figure 76 shows the distribution of the total number of particles in the 60 and 20nm bins versus time. The 60nm bin contains particles of diameters between approximately 55 and 65 nm, and the diameters for the 20nm bin range between 17.5 and 22.5nm. There is a sharp increase in the total number of particles in the 20nm bin during decelerations and a sharp increase in the total number of particles in the 60nm bin during accelerations, sharp meaning a greater percentage of decrease/increase.

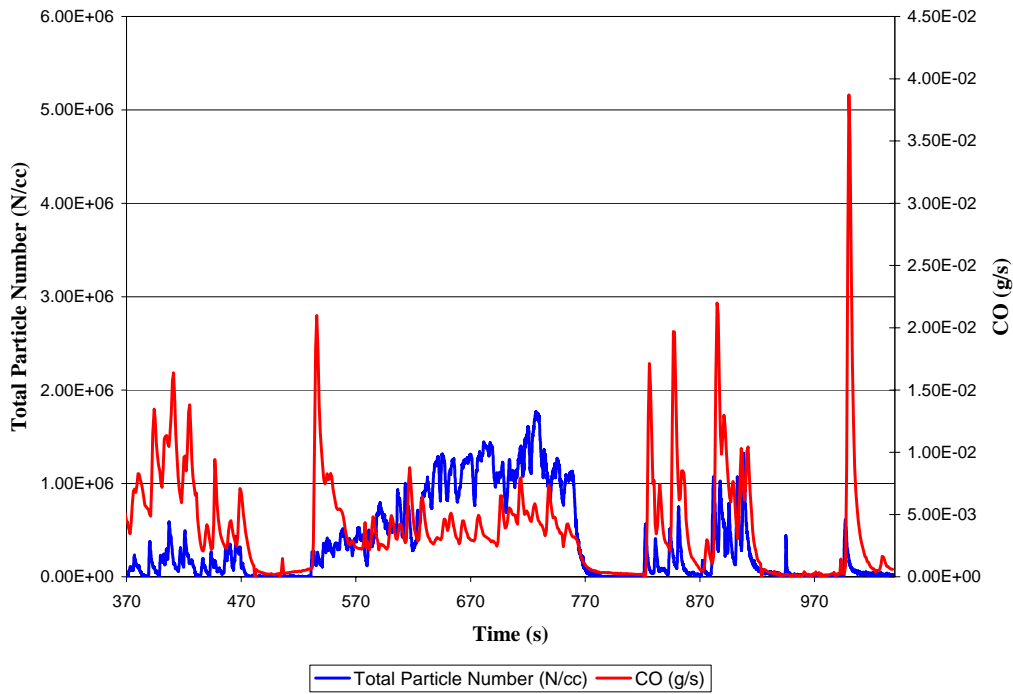


**Figure 76: DMS500 60nm and 20nm Particle Number vs. Time for E55CRC-41 tested at 56,000 lb.**

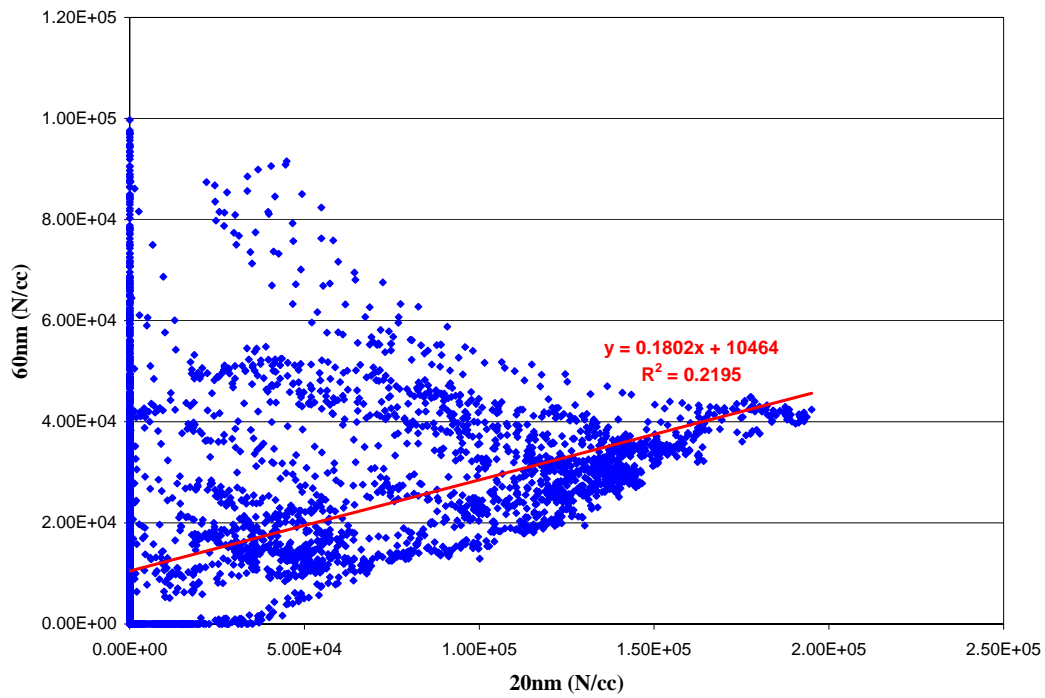
Figure 77 shows the total number of particles and CO versus time. This plot shows the correlation between the two series. This kind of a relation is actually expected due to the fact that a large portion of particulate matter is elemental carbon (EC).

Figure 78 shows the total number of particles in the 60nm bin versus the total number of particles in the 20nm bin. As can be seen, there is no clear correlation between the two size bins, although the envelope of the points is well defined.

Figure 79 shows the total number of particles in the 20nm bin versus the total hub power. There is no strong correlation between the two series. Figure 80 shows the total number of particles in the 60nm bin versus the total hub power. Again, there is no strong correlation, suggesting that the particle formation cannot be attributed to engine load alone.



**Figure 77: DMS500 Total Number of Particles and CO vs. Time for E55CRC-41 tested at 56,000 lb.**



**Figure 78: DMS500 60nm Particle Number vs. 20nm Particle Number for E55CRC-41 tested at 56,000 lb.**

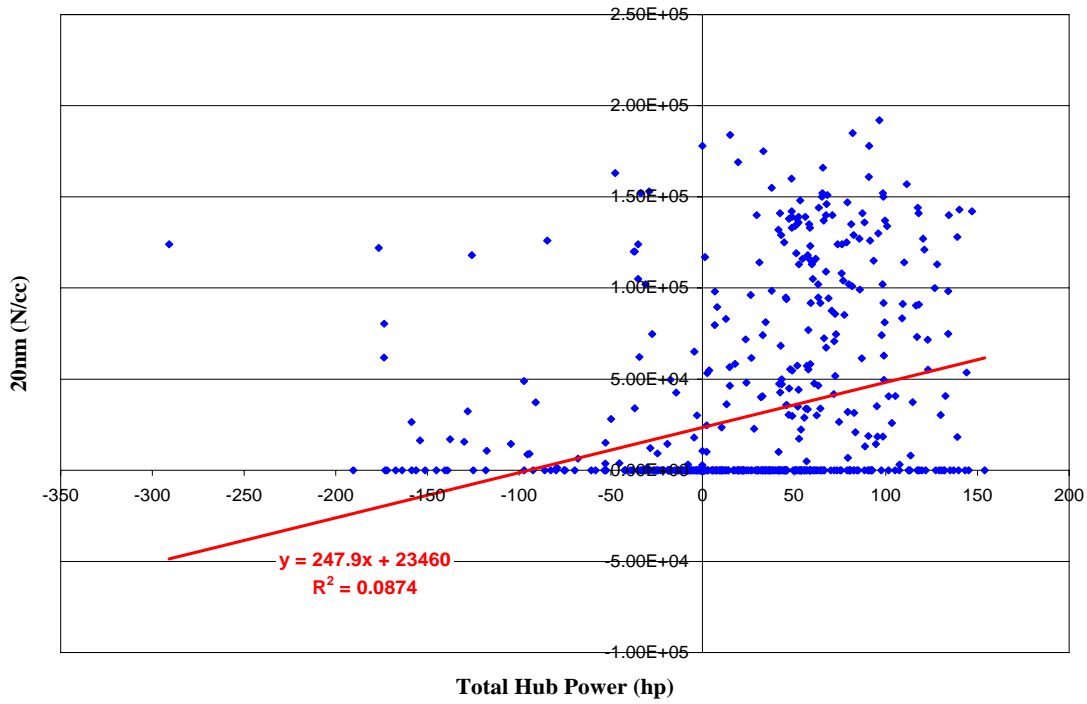


**Figure 79: DMS500 20nm Particle Number vs. Total Hub Power for E55CRC-41 tested at 56,000 lb.**

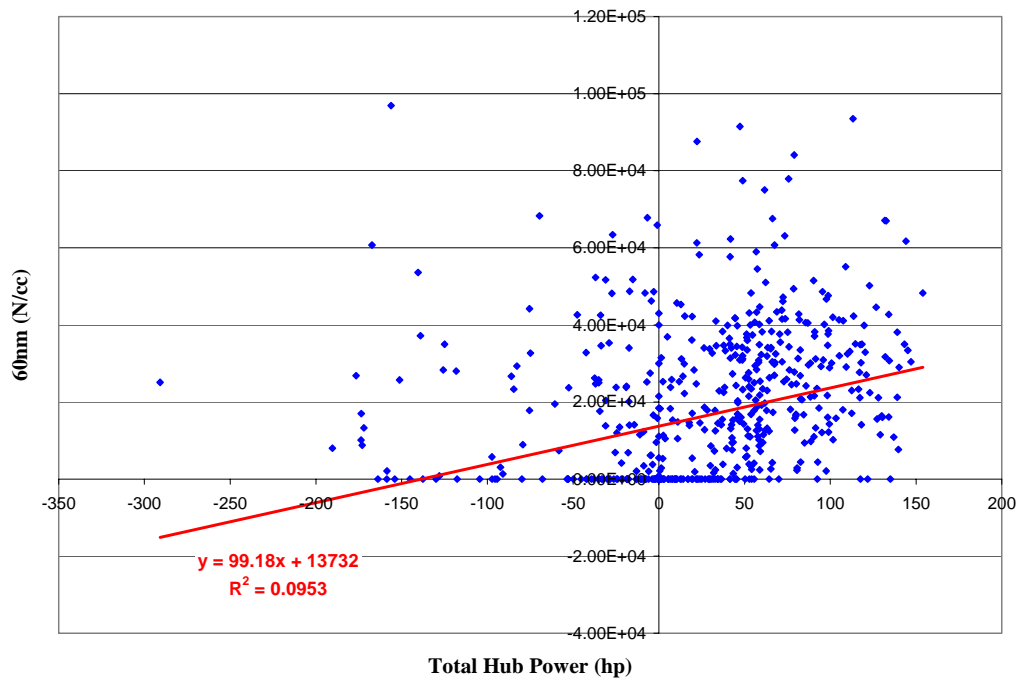


**Figure 80: DMS500 60nm Particle Number vs. Total Hub Power for E55CRC-41 tested at 56,000 lb.**

Figure 81 shows the size distribution of particles during acceleration and deceleration periods. During acceleration, a single mode distribution is observed where the peak is centered at around 100nm. This is expected since during accelerations, accumulation mode particles are formed. For the deceleration region, a single mode distribution is seen. The peak is centered around 20nm, and these are the nuclei mode particles. This mode is observed during deceleration periods, as the plot also shows.

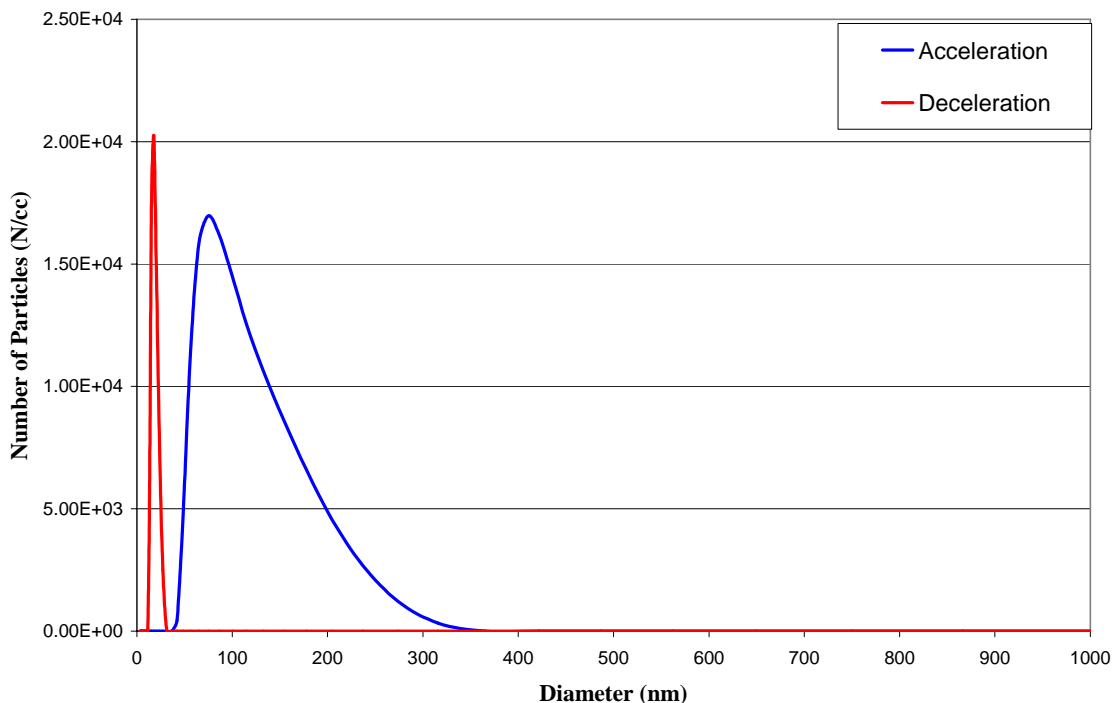


**Figure 81: DMS500 size distribution of particles during acceleration and deceleration for E55CRC-41 tested at 56,000 lb.**

### ***E55CRC-42***

E55CRC-42 was powered by a Caterpillar 3406, model year 1999 engine. Particle sizing and chemical speciation results are presented below for various modes of the HHDDT schedule. Figure 82 and Figure 83 present the particle size distribution for Idle and steady modes.

A typical uni-modal size distribution was noted for the Idle Mode for E55CRC-42 (Figure 83) with a CMD of 40nm and concentration of  $1.3 \times 10^5$  particles/cm<sup>3</sup>. In comparison to E55CRC-39 and E55CRC-40, the size distribution shifted towards a larger particle size for E55CRC-42 during the Idle Mode. In addition to the nuclei mode, the size distribution is also characterized by a mode with a CMD of 100nm.

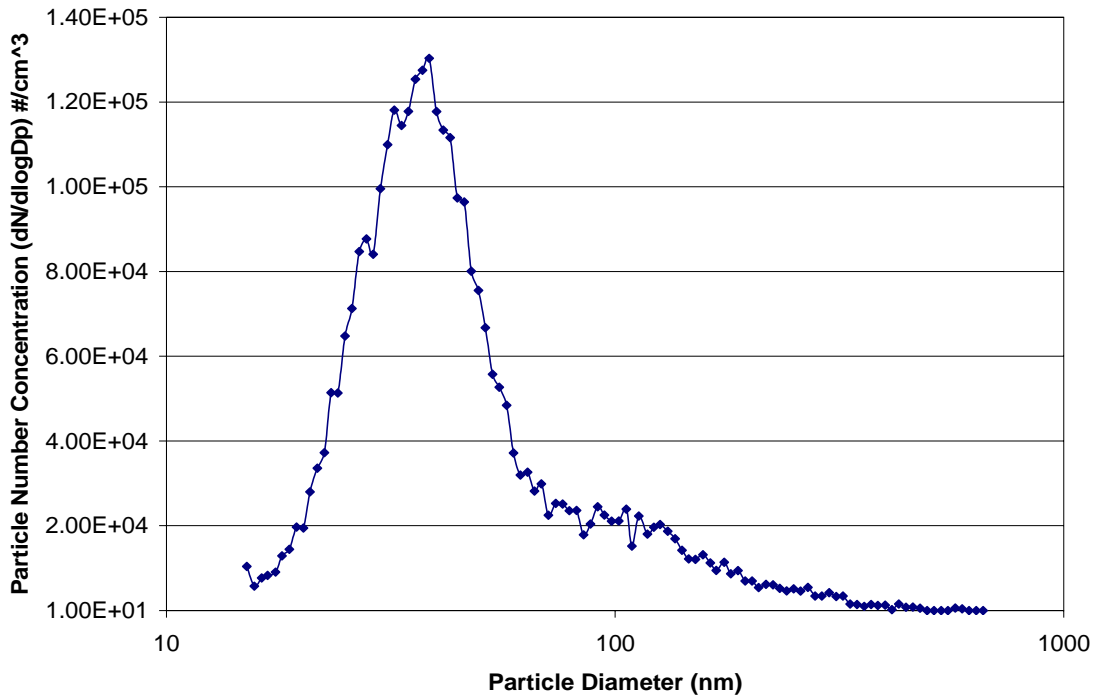


**Figure 82: SMPS Particle Size Distribution for E55CRC-42 Operating on an Idle Mode**

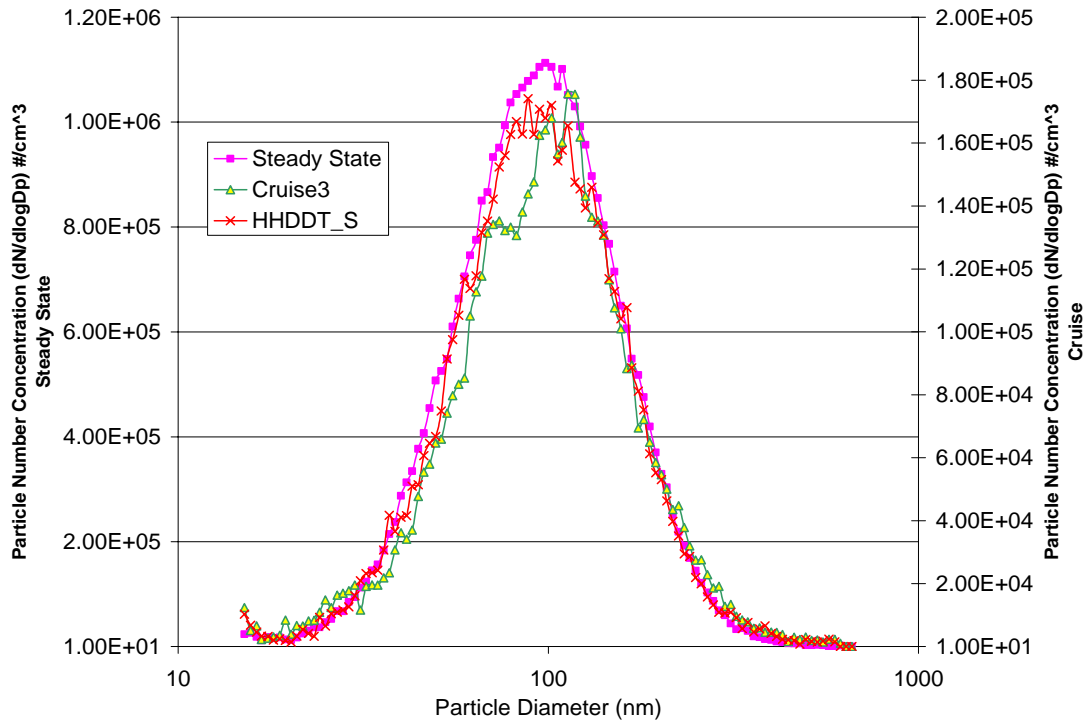


**Figure 83: SMPS Particle Size distribution for E55CRC-42 operating on various steady cycles**

The accumulation mode observed during the Idle could be due to an increase in elemental carbon emission when compared to the previous vehicles tested. During the Idle Mode, the elemental carbon emitted by E55CRC-39 and E55CRC-40 were 0.21 g/hour and 0.07 g/hour, respectively and for E55CRC-42, the values were higher at 0.55 g/hour (Figure 86). This increase in elemental carbon also increased the mass emission for the Idle Mode at 1.34 g/hour (Figure 84). Mass emissions during Idle for E55CRC-39 and 40 were 0.35 g/hour and 0.14 g/hour, respectively. Total volatile organic compounds emitted by E55CRC-42 during the Idle Mode at 2.99 g/hour were much lower when compared with the Cruise Mode at 6.04 g/hour (Appendix M: Figure M25 to M29).

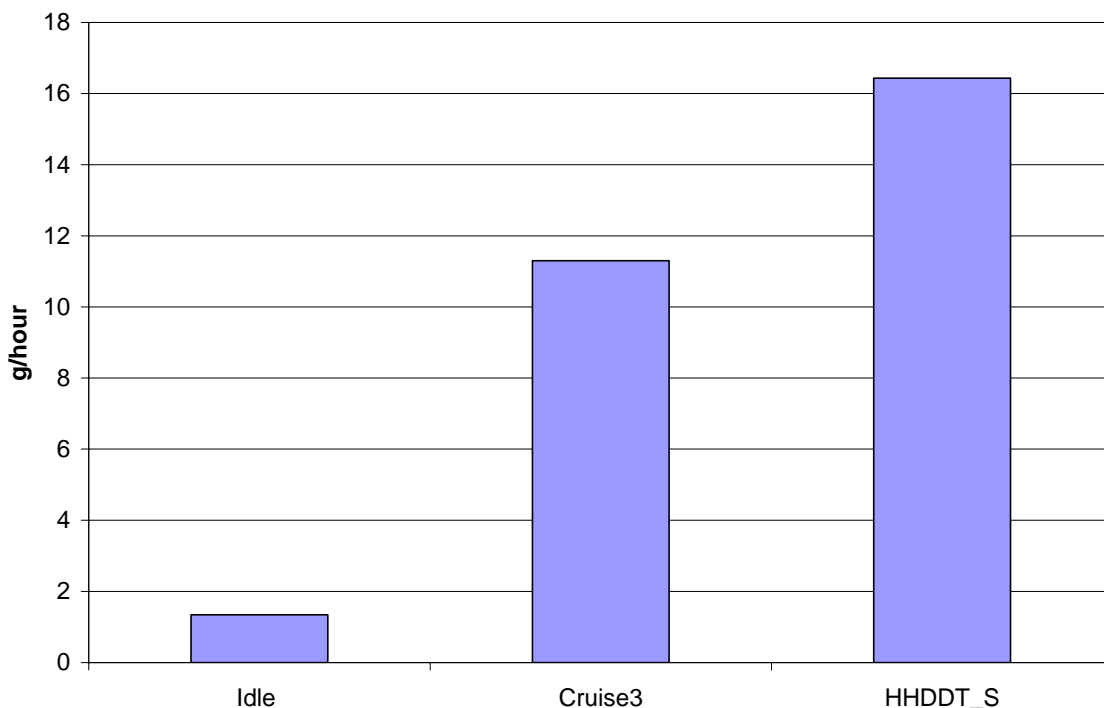


**Figure 84: PM Mass Emissions for E55CRC-42**

Particle sizes measured during the steady state and Cruise Mode were similar with a CMD of 93.6nm, 98.39nm and 93.71nm for the steady state, normal Cruise and High Speed Cruise Modes, respectively. Concentrations for the steady state mode were 6 times higher in magnitude as compared with both the Cruise Modes. Concentration drop for the Cruise Mode could be due to a higher exhaust temperature. Sulfate emissions were higher during the Cruise Mode at 0.54 g/hour when compared to Idle Mode at 0.06 g/hour (Figure 86). Carbonaceous particles along with sulfates, and adsorbed of volatile and semi-volatile particles mostly constitute the nature of the particles emitted during the steady cycles. The total carbon in the idle mode PM is approximately evenly split between organic and elemental carbon. While the idle mode emissions are characterized by a distinct nuclei mode, the contribution of this fraction to the total PM mass emission rate is very small.

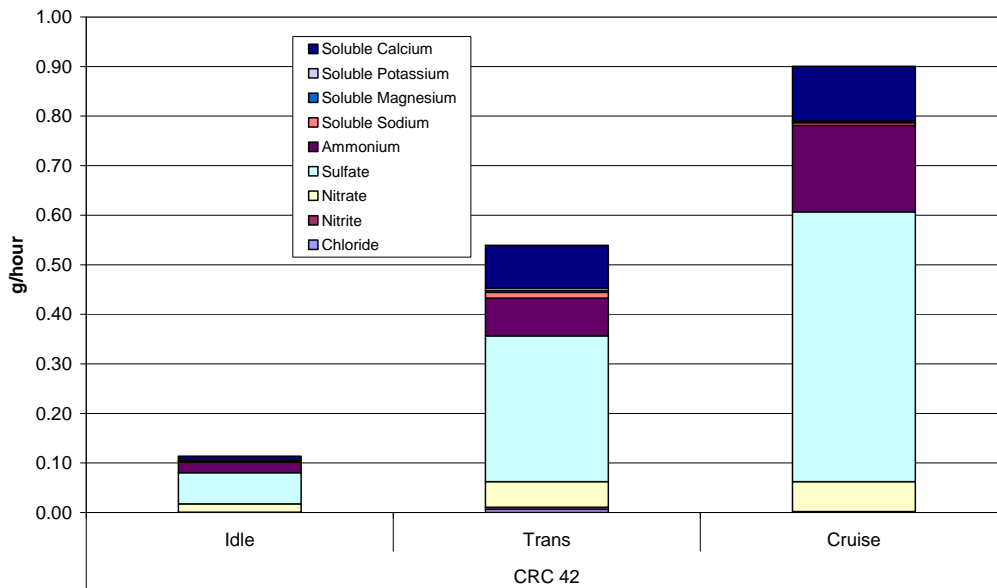


**Figure 85: Ion Composite Results for E55CRC-42**

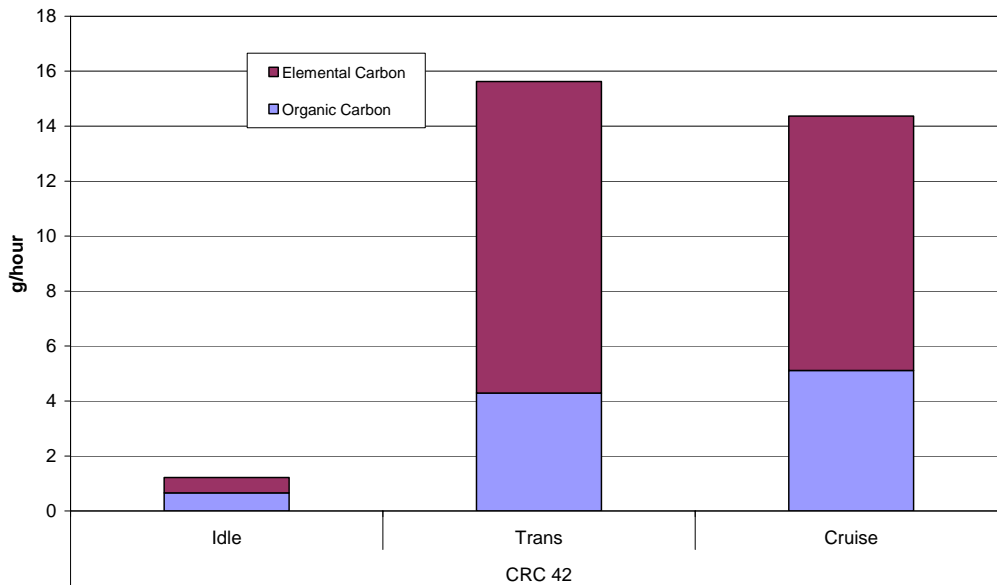


**Figure 86: Elemental Carbon and Organic Carbon PM Analysis for E55CRC-42**

For E55CRC-42, DMS500 data on the UDDS, Cruise Mode and HHDDT\_S showed anomalous behavior (output spikes) but two repeat runs on the Transient Mode agreed acceptably well, as shown in Figure 87.

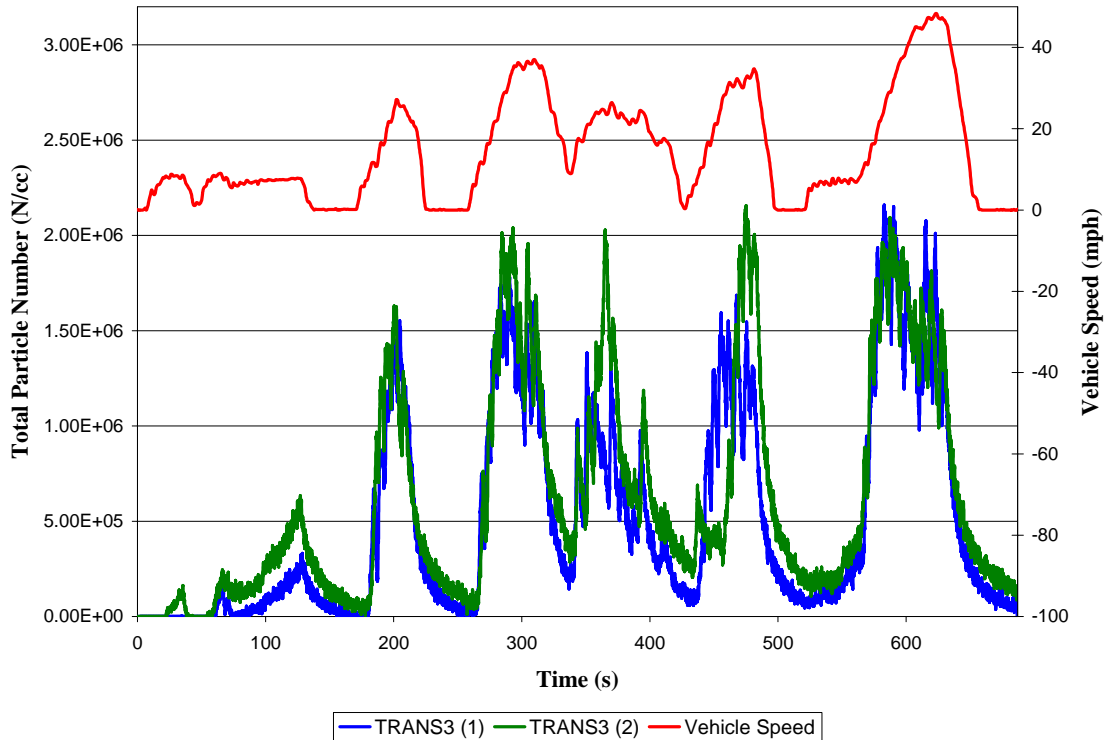


**Figure 87: DMS500 Total Number of Particles and Vehicle Speed vs. Time on Transient Mode for E55CRC-42 tested at 56,000 lb.**

### ***E55CRC-43***

E55CRC-43 was a powered by a Detroit Diesel Series 60, model year 1994 engine. Particle sizing and chemical speciation results are presented below for various modes of the HHDDT schedule. Figure 88 and Figure 89 present the particle size distribution for Idle and steady modes.

Particle size distribution for Idle Mode was unimodal with a CMD of 51.43nm and a GSD of 1.44 which indicates a good distribution about the mean. Maximum concentration level was around  $2.25 \times 10^5$  particles/cm<sup>3</sup>. These particles are mostly accumulation mode particles as observed for E55CRC-42. Reasons for this accumulation mode are similar to those presented above for E55CRC-42.

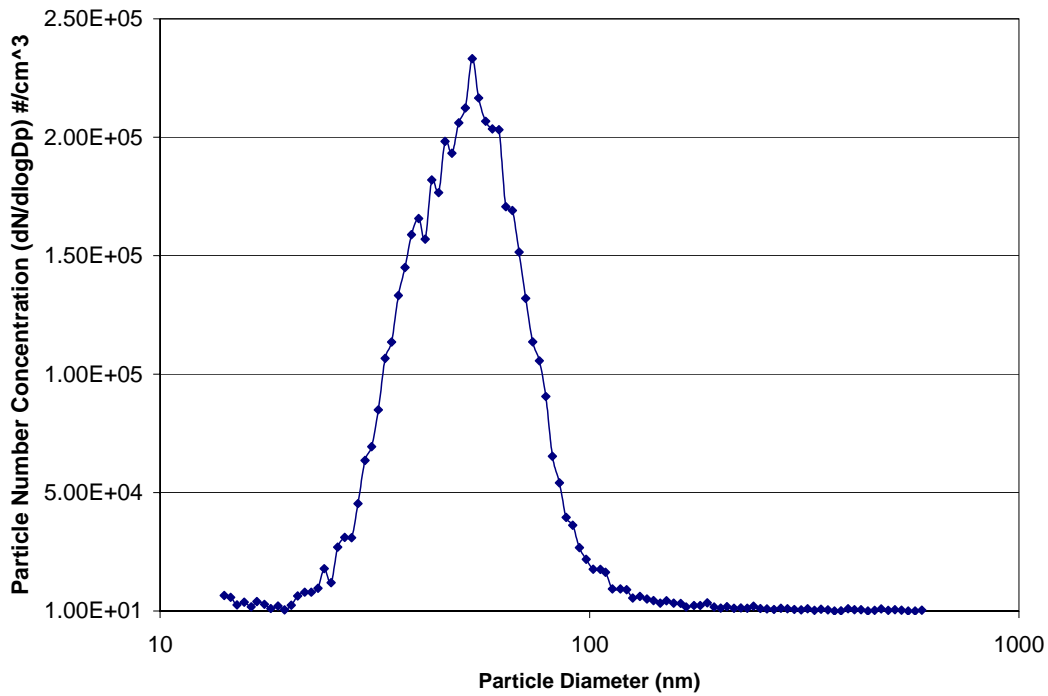


**Figure 88: SMPS Particle Size Distribution for E55CRC-43 Operating on an Idle Mode**

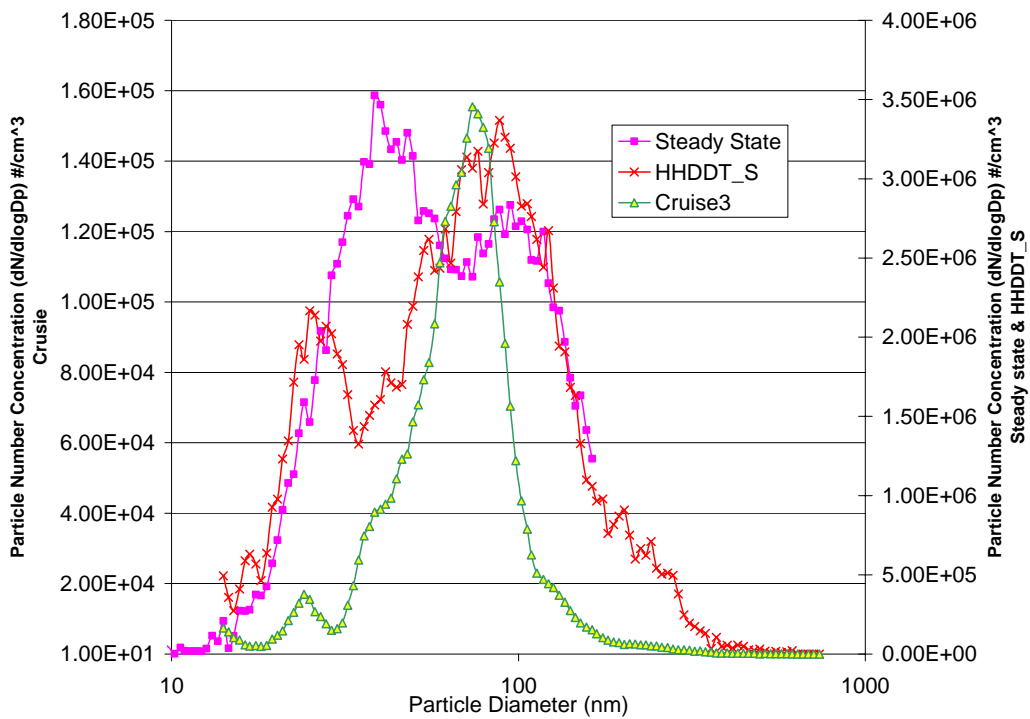


**Figure 89: SMPS Particle Size Distribution for E55CRC-43 Operating on Various Steady Cycles**

The total volatile organic compounds emitted by this particular vehicle were 2.28 g/hour for Idle and 3.39 g/hour for Cruise. Volatile compound emissions at idle were 20% lower than E55CRC-42. A shift in the particle size was noted for the steady cycles. For the steady state and High Speed Cruise Modes, the GSD were 1.88 and 2.6, respectively, which is higher than the normal GSD which denotes a random distribution about the mean which can be clearly observed from Figure 89. The CMD noted for the steady state, normal Cruise and High Speed Cruise Modes were 54.32, 68.5 and 69.56nm, respectively. It should be noted that in the case of a HHDDT\_S or Cruise Mode scan, there is no assurance that the driver might not move the pedal and disturb the steady operation during SMPS scan. Elemental carbon emissions were very high during the Cruise Mode at 3.17 g/hour when compared to Idle Mode emissions at 0.25 g/hour. Organic carbon emissions were also higher during the Cruise Mode at 6.15 g/hour when compared to Idle Mode emissions at 1.03 g/hour.

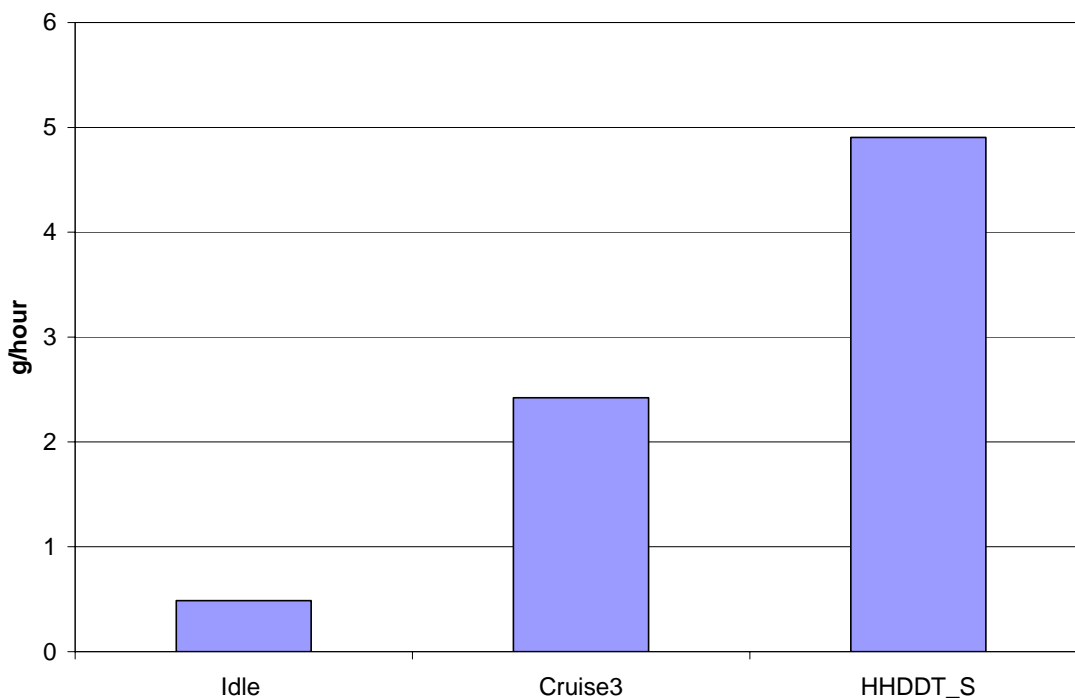


**Figure 90: PM Mass Emissions for E55CRC-43**

The increase in the particle size and concentration in the Cruise Modes is attributed to the very high increase in the elemental carbon emissions. A slight increase by 12% in the VOC emission was noted for the Cruise Mode (Appendix M: Figure M37 to M41). An 85% increase in the sulfate emission was noted for the Cruise Mode (Figure 91). Calcium was also a major contributor to the inorganic species with an increase of 91% for the Cruise Mode. Calcium emissions are attributed to lubrication oil, since calcium is a major constituent in lube oil. Particles measured during the Cruise Mode of this particular

vehicle were primarily carbonaceous soot with heavy hydrocarbons adsorbed onto the surface.

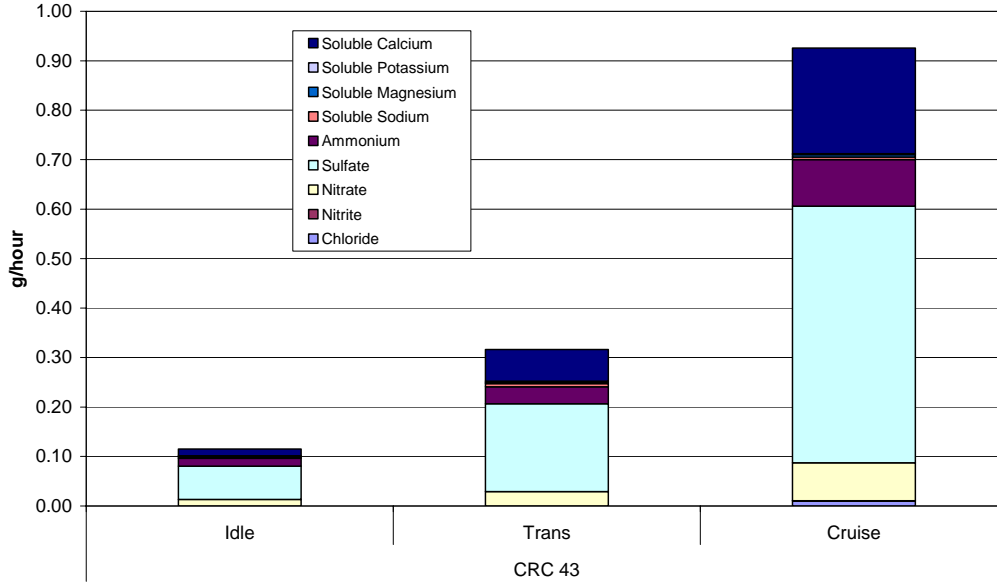


**Figure 91: Ion Composite Results for E55CRC-43**

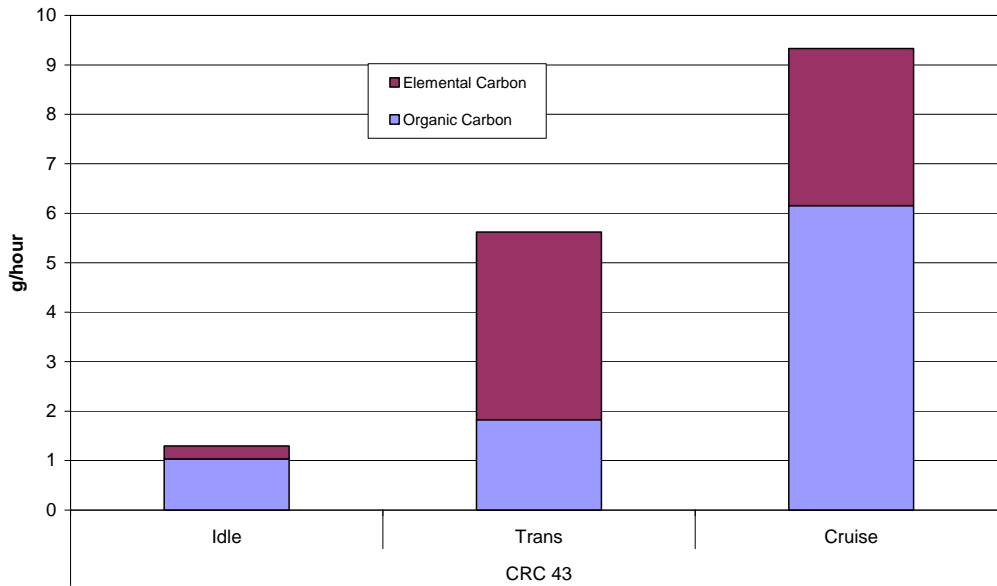


**Figure 92: Elemental Carbon and Organic Carbon PM Analysis for E55CRC-43**

DMS500 data were acquired for the Transient Mode, and are shown in Figure 93.

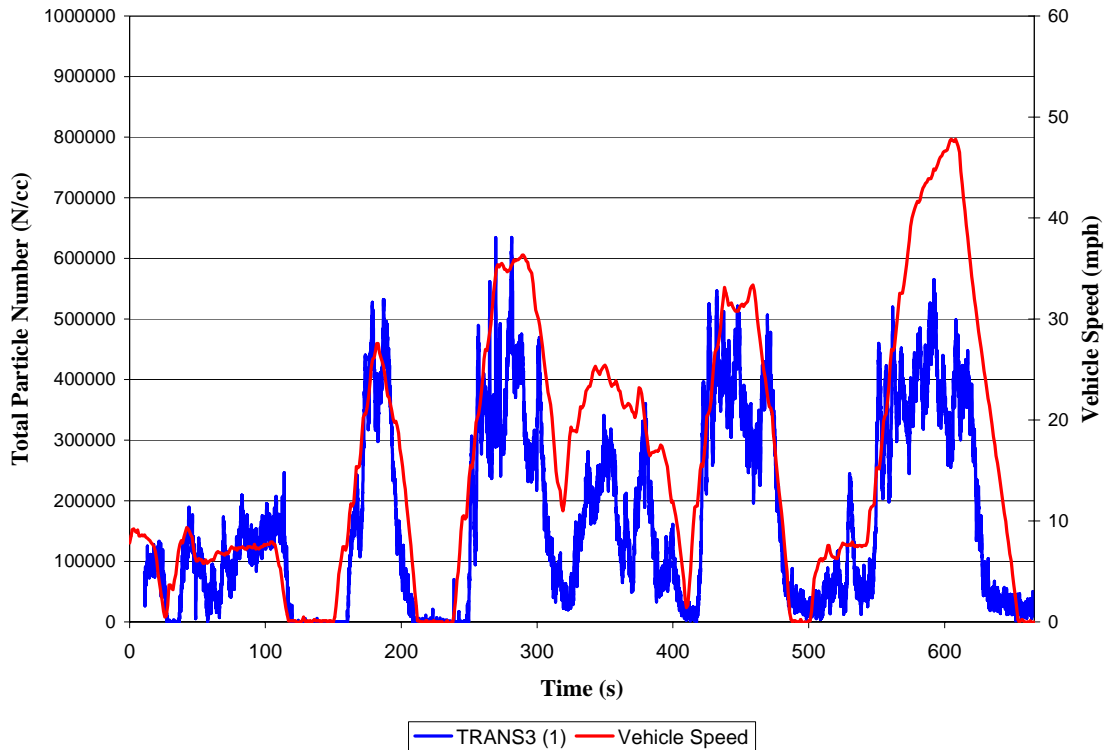


**Figure 93: DMS500 Total Number concentration of Particles and Vehicle Speed vs. Time for E55CRC-43 tested at 56,000 lb.**

#### ***E55CRC-44***

E55CRC-44 was a powered by a Caterpillar 3406, model year 1989 engine. Particle sizing and chemical speciation results are presented below for various modes of the HHDDT schedule. Figure 94 and Figure 95 present the particle size distribution for Idle and steady modes.

A bimodal distribution was noted for this particular vehicle during the Idle Mode, with one nano-particle peak at 26.9 nm and another accumulation mode peak at 122nm. It should be noted that the idle mode is characterized by relatively lower PM number concentrations. The only other vehicle where a bimodal distribution was observed was E55CRC-39 which was a 2004 year model engine. The reason for the bimodal distribution for E55CRC-39 was due to high levels of volatile compounds and elemental carbon during the Idle Mode. The elemental carbon contributed to the accumulation mode.

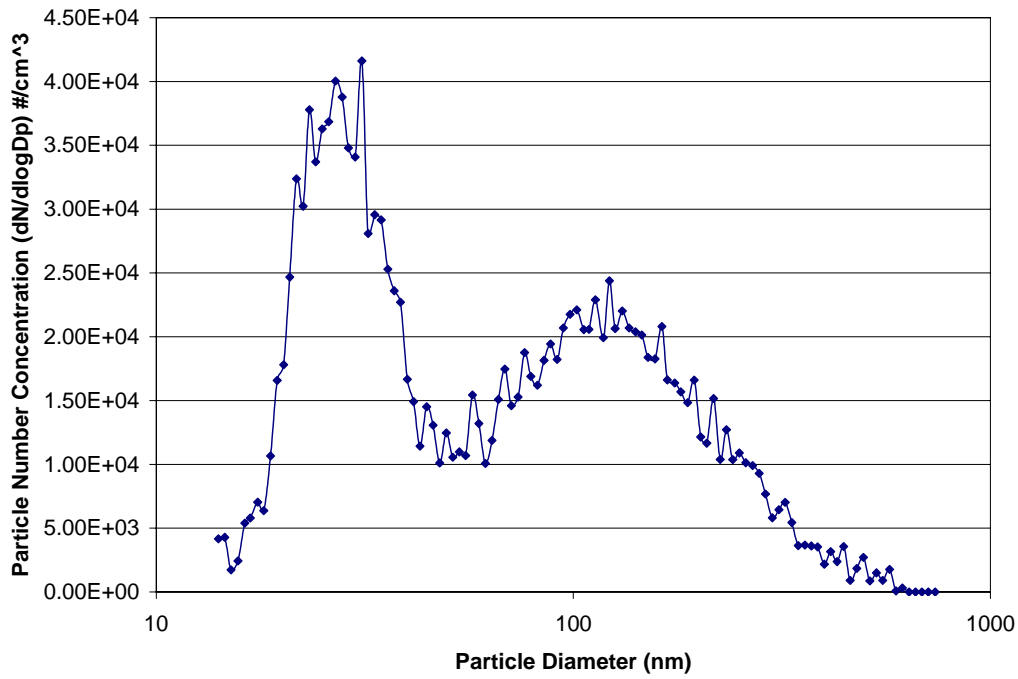


**Figure 94: SMPS Particle Size Distribution for E55CRC-44 Operating on an Idle Mode**

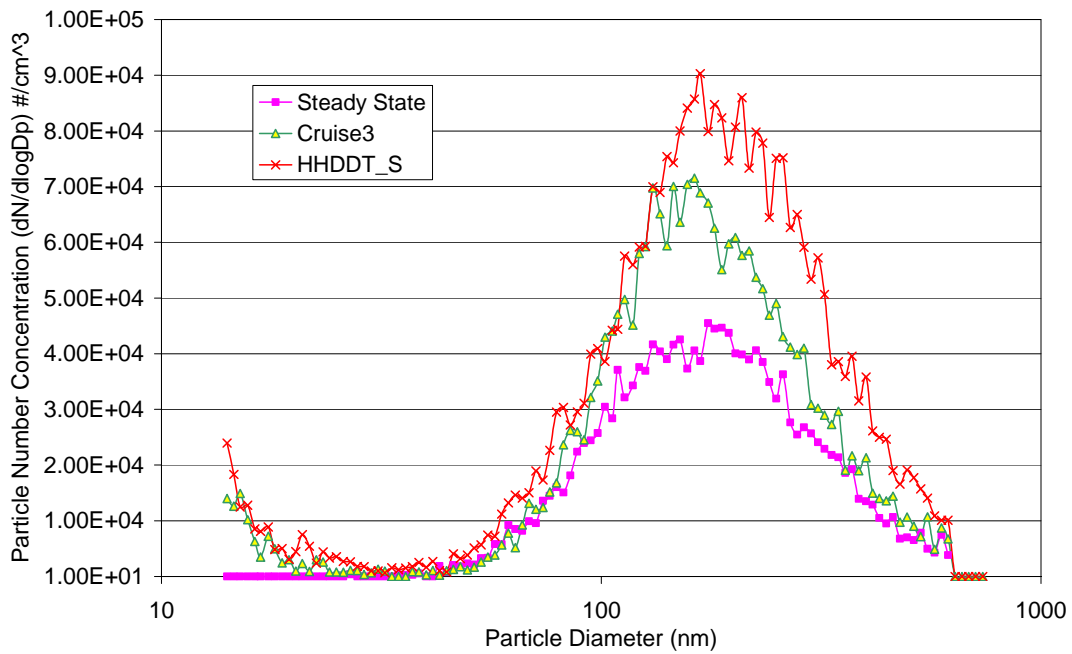


**Figure 95: SMPS Particle Size Distribution for E55CRC-44 Operating on Various Steady Cycles**

The precursors of the nano-particle emissions could be traced back to lube oil based volatile hydro-carbons, and the lower exhaust temperature during exhaust mode. Again, nano-particle peak could be due to high emissions of semi-volatile compounds (Appendix M: Figure M54 and M55). The total volatile compound emissions for this vehicle were 25% higher than E55CRC-43 and 35% higher than E55CRC-40. Further analysis yields that aromatic emissions during the Idle Mode, especially benzene were prominent for E55CRC-39 and E55CRC-44 when compared with the rest of the vehicles in the study (Appendix M: Figure M53). The accumulation mode in the Idle was attributed to the presence of carbonaceous agglomerates, with elemental carbon emission during the Idle Mode being the highest among all the vehicles at 1.22 g/hour.

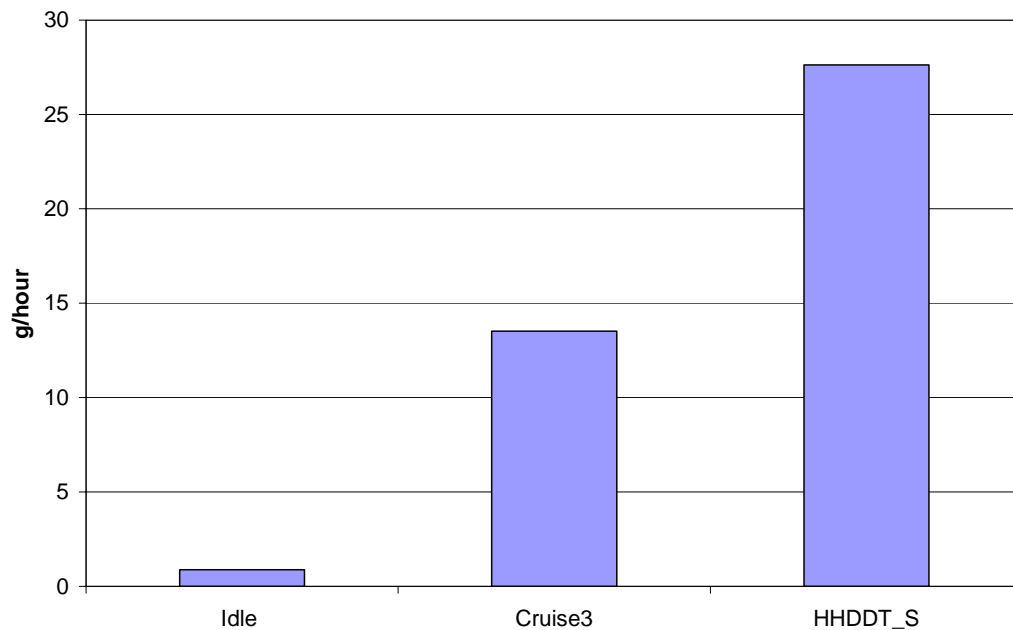


**Figure 96: PM Mass Emissions for E55CRC-44**

The steady state particle size distributions were compatible with vehicle speed. Particle concentrations were increasing, though minimally, with increasing speed without much variation in the particle size. The count median diameter for the steady state, normal Cruise and High Speed Cruise were 173, 166 and 178nm, respectively. Mass emissions were highest during the Cruise and High Speed Cruise Modes when compared to other vehicles (Figure 96). Elemental carbon which is basically soot was noted to be the highest among all the vehicles during the Cruise Mode (Figure 98) was also a major contributor to the mass emission. This would also contribute to low saturation ratios; hence, the absence of nano-particles. Sulfate emissions were among the lowest when compared with all other vehicles (Figure 97). Results from these data suggest that the fine particles measured during the Cruise Mode were mostly solid carbonaceous particles.

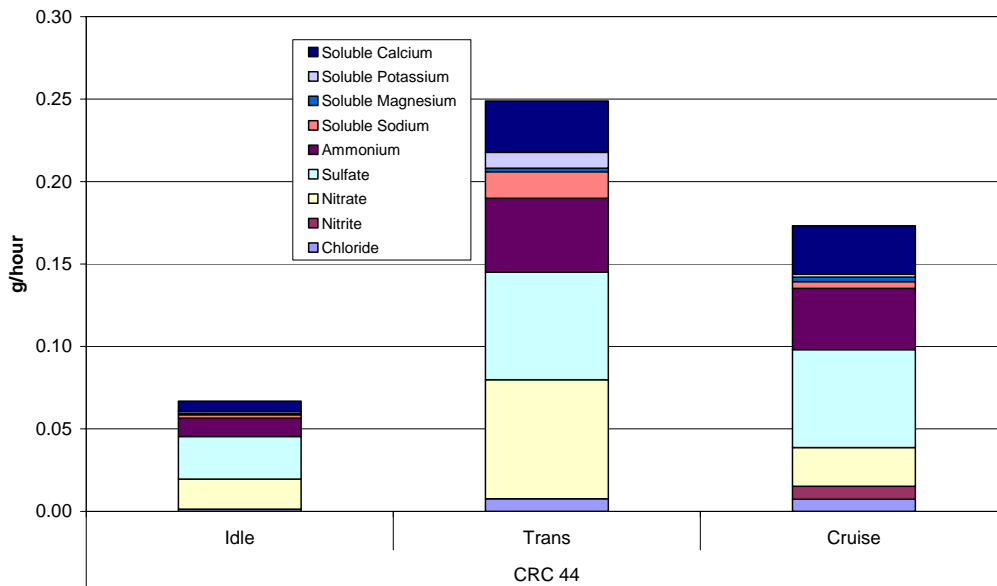


**Figure 97: Ion Composite Results for E55CRC-44**

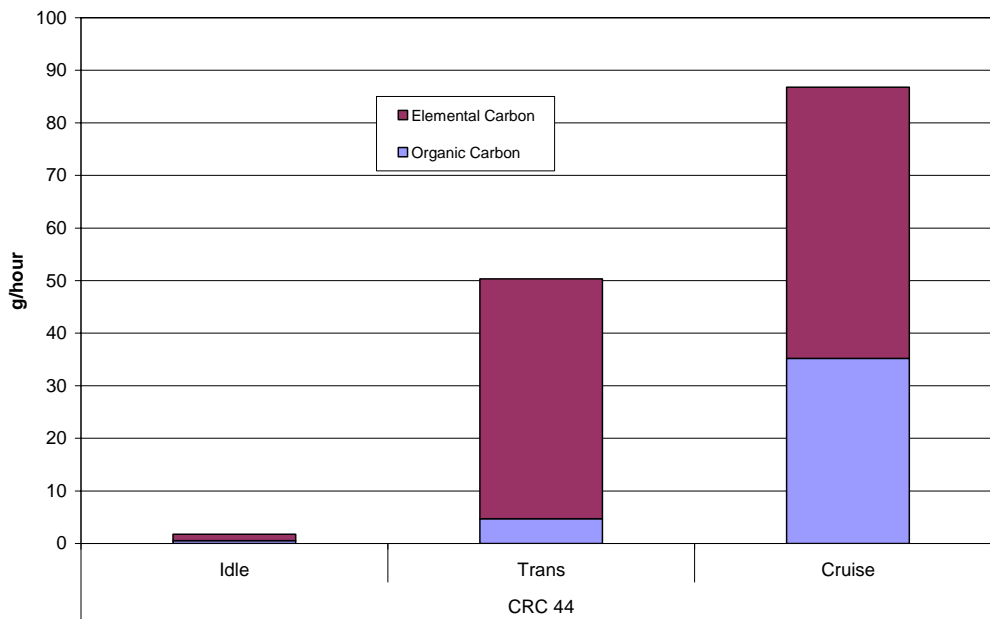


**Figure 98: Elemental Carbon and Organic Carbon PM Analysis for E55CRC-44**

No DMS500 data are available for E55CRC-44.

## Conclusions

Twenty heavy-duty trucks (HHDT and MHDT) were characterized for emissions in Phase 2 of the E-55/59 program. The HHDDT emissions were characterized using a test weight of 56,000lb. The MHDT were tested at unladen (50% of GVW) and laden (75% of GVW) weights, and the GVW varied over the MHDT fleet. The Urban Dynamometer Driving Schedule (UDDS) and five modes of the HHDDT Schedule were used for the HHDDT. The MHDT were all tested using a Lower Speed Transient Mode, a Higher Speed Transient Mode and a Cruise Mode, and three were tested using the High Speed HHDDT\_S mode as well.

Oxides of nitrogen (NO<sub>x</sub>) were high (32.1 g/mile) on the Transient Mode for a 1998 model year truck, but all other trucks had NO<sub>x</sub> emissions below 19 g/mile on that mode. The average HHDDT Transient Mode NO<sub>x</sub> emissions were 18.46 g/mile and the average HHDDT\_S Mode NO<sub>x</sub> emissions were 14.56 g/mile. On the HHDDT\_S mode, the 1994 truck (21.8 g/mile) and the 1998 truck (22.2 g/mile) were the highest emitters. Two of the HHDDT were 2004 MY trucks, with EGR engines. The two 2003 trucks emitted NO<sub>x</sub> at a similar level on the Transient Mode at 56,000lb test weight, but one vehicle emitted 10.9 g/mile on the HHDDT\_S whereas the other emitted only 8.1 g/mile. PM emissions were below 3.4 g/mile for the Transient Mode, except for one high emitter (E55CRC-45) discussed below. The two 2004 model year trucks emitted 0.42 and 0.26 g/mile of PM on the Transient Mode, and 0.28 and 0.14 g/mile of PM on the HHDDT\_S.

One MHDT (E55CRC-57) was unable to follow a high speed target trace due to a sensor malfunction. Except for this truck, NO<sub>x</sub> was lower at unladen weight than laden weight on the Lower Speed Transient Mode. Test weight did not cause a large change in NO<sub>x</sub>, and had virtually no effect on the Cruise Mode for MHDT for all trucks of MY earlier than 1998. For the UDDS, the average of the diesel-fueled MHDT fleet changed from 10.49 g/mile (unladen) to only 11.03 g/mile when laden. In contrast, test weight had a stronger influence on distance-specific PM for the MHDT. Two gasoline MHDT were tested. The 2001 MY gasoline vehicle showed low NO<sub>x</sub> (7.42 and 3.81 g/mile on laden Lower and Higher Speed Transient Modes), but the older 1993 gasoline truck emitted NO<sub>x</sub> at levels similar to the diesel vehicles. PM was very low for both gasoline MHDT.

One HHDDT (E55CRC-45: 1993 model year) was found to have very high PM emissions (16.59 g/mile on the Transient Mode) a defective solenoid for the fuel pump. This vehicle was repaired and re-tested, but the PM emissions rose substantially on the HHDDT\_S and fell only slightly on the Transient Mode.

PM data were acquired using both conventional filters and a Tapered Element Oscillating Microbalance. The TEOM correlated very well with the filters ( $R^2 = 0.9893$ ) and provided distance specific emissions that were 7% lower than the filter.

Regulated emissions data for the HHDDT were compared with data from Phase 1 of the E-55/59 and Phase 1.5 of the E-55 study. Variability of NO<sub>x</sub> and PM between phases suggested that the fleet within each phase was too small to draw conclusions, but the

constancy of fuel economy across phases supported the repeatability of vehicle load and dilution tunnel operation.

Size distributions of PM from the six trucks were selected for non-regulated emissions measurement. These were acquired using a Scanning Mobility Particle Sizer (SMPS), as well as a Differential Mobility Spectrometer, Model 500 (DMS500), which was a newly released instrument. The SMPS was fed dilute exhaust from a mini-dilution tunnel, using a dilution ratio of thirty, while the DMS used the main dilution tunnel of the TransLab. The SMPS detected a bimodal distribution with a nuclei mode for Idle operation of one 2004 MY truck (E55CRC-40), and the DMS 500 detected both the nuclei mode and accumulation mode during deceleration on this truck. The nuclei mode was not evident under load for E55CRC-40. The other 2004 MY truck had only one mode, with a very low particle count on Idle. A 1989 MY truck had a bimodal Idle distribution, but the remaining HHDDT were unimodal. Comprehensive data were acquired for steady operation using the SMPS on all trucks, and the DMS500 acquired transient distributions for four of the trucks.

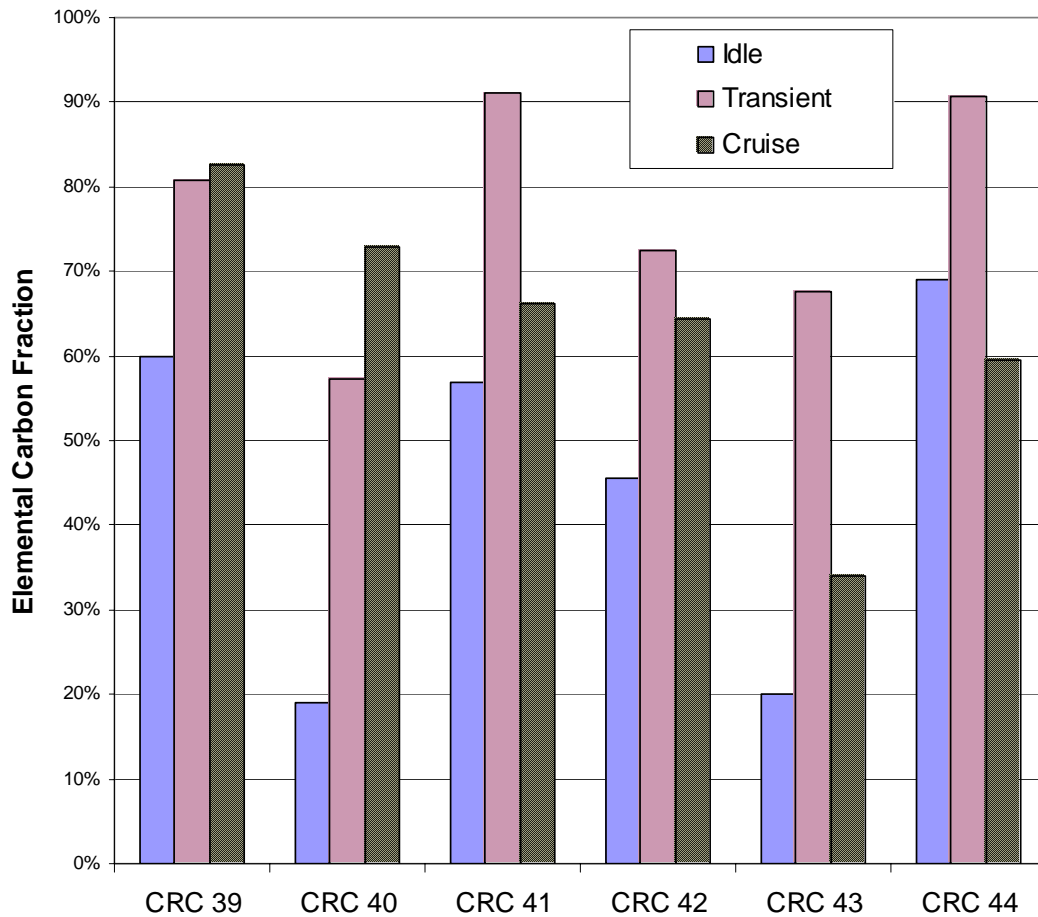
Chemical speciation was performed on the six trucks, with exhaust from the TransLab tunnel fed to a residence time chamber of the Desert Research Institute (DRI). Data were acquired for methane and volatile organic compounds using a canister and a field gas chromatograph. Semi-volatile organic compounds were captured in PUF/XAD media and PM soluble fraction was captured on TIGF filters, and these were extracted and analyzed at the DRI laboratory. Carbonyls were captured using DNPH cartridges, nitrosamines in Thermosorb cartridges. Ions and Elemental/Organic carbon (EC/OC) split were determined from quartz filters. Results from the speciation data are legion, and examples include the fact that the EC/OC split differed substantially on Idle between the two 2004 MY trucks equipped with EGR, and that the ion and metal analyses varied widely between trucks.

Summarized below in a graphical form are the emissions of elemental carbon (as a percentage of total), inorganic ionic species, lubrication oil-based elemental emissions, and engine wear emissions in Figure 99 through Figure 102, respectively. Figure 99 shows that except for idle operation, the elemental carbon constitutes a significant portion of total carbon emissions. Transient operation, in particular, yields in excess of 60% of total carbon as elemental carbon. Total PM mass emissions, as discussed in the text, are the highest for the transient mode, followed by cruise, and then idle. Total PM mass emissions under idle are significantly lower than the transient and cruise mode. However, in terms of total carbon mass emission rates, the cruise mode emits the highest levels, followed by the transient mode of operation. The idle mode is characterized by significantly lower rates of total carbon mass emissions.

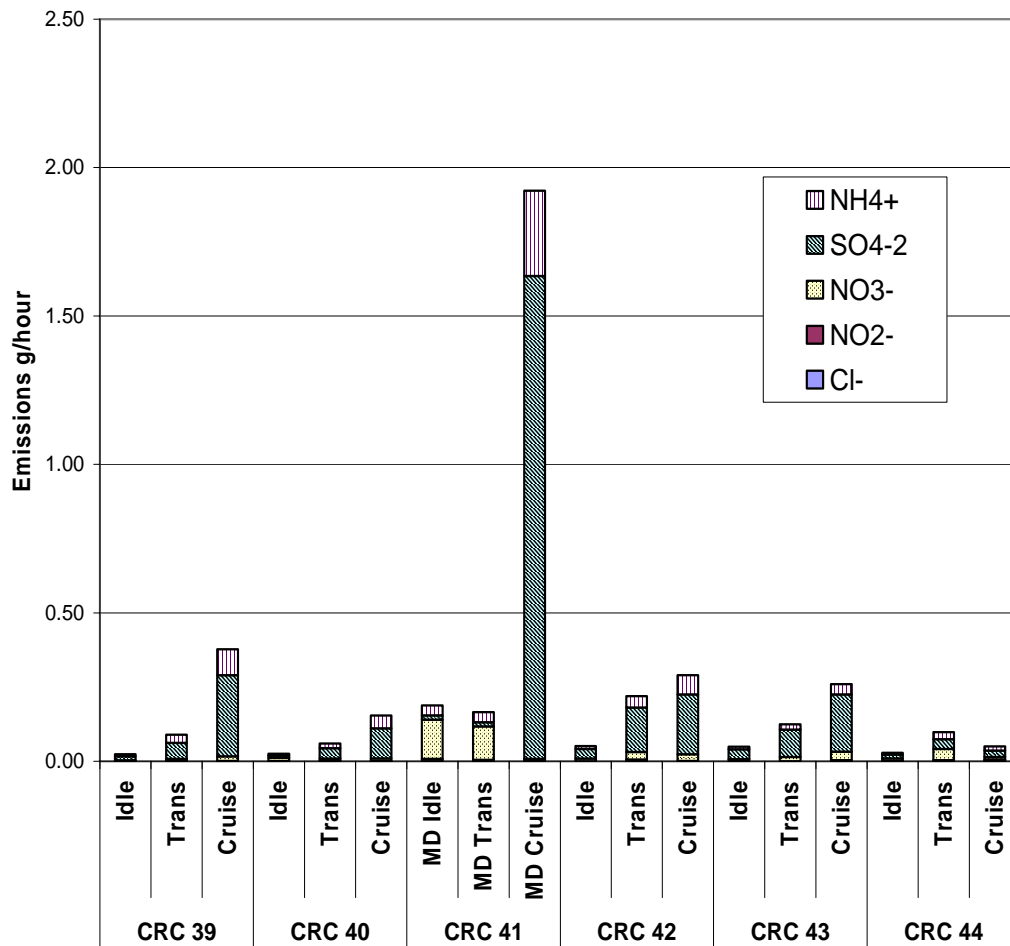
The mass emissions rates of sulfates dominate the ionic species in the cruise and transient modes. The only other species of significance were nitrates and ammonium.

Total particulate matter comprises of elemental carbons, organic carbon, engine wear elements, lube oil based ash components, water, and ionic species. Most of these emissions are a result of un-burnt fuel and lubricating oil. Apart from severe engine wear

(abrasive wear) on boundary lubricated surfaces (cam lobe wear, tappet polishing, rocker/crosshead wear, ring wear at top and bottom reversal locations, etc.), oil control is extremely critical from an emissions point of view. Based upon prior studies by Lapin et al. [16] and Gautam et al. [12], it may be hypothesized that products of lubricating oil combustion (partial) result in higher potential mutagenicity of exhaust emissions, and that lubricating oil contributes to high concentrations of nanoparticles in exhaust emissions [12]. Lubricating oil enters the combustion chamber through the following routes: as blow-by gas, leakage past valve stem seals, piston rings and vaporization from the cylinder liner walls and combustion space [17].



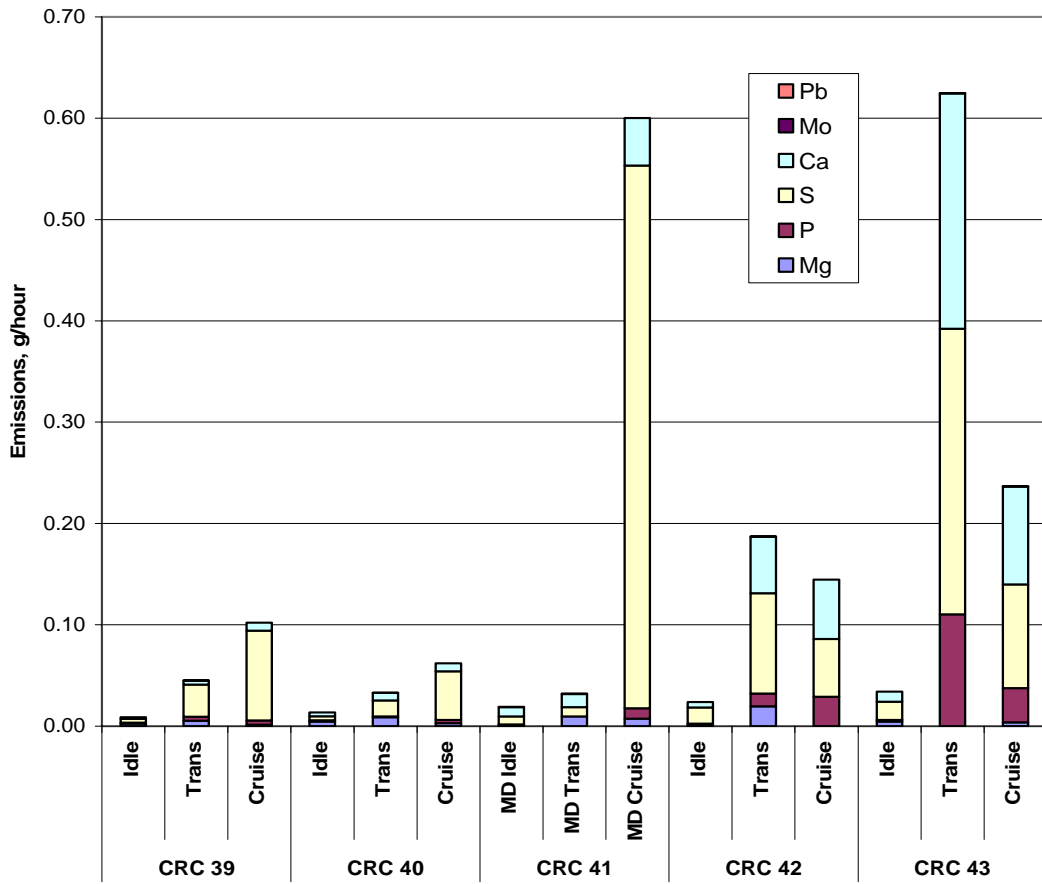
**Figure 99: Elemental Carbon Emissions (Percentage of Total Carbon)**



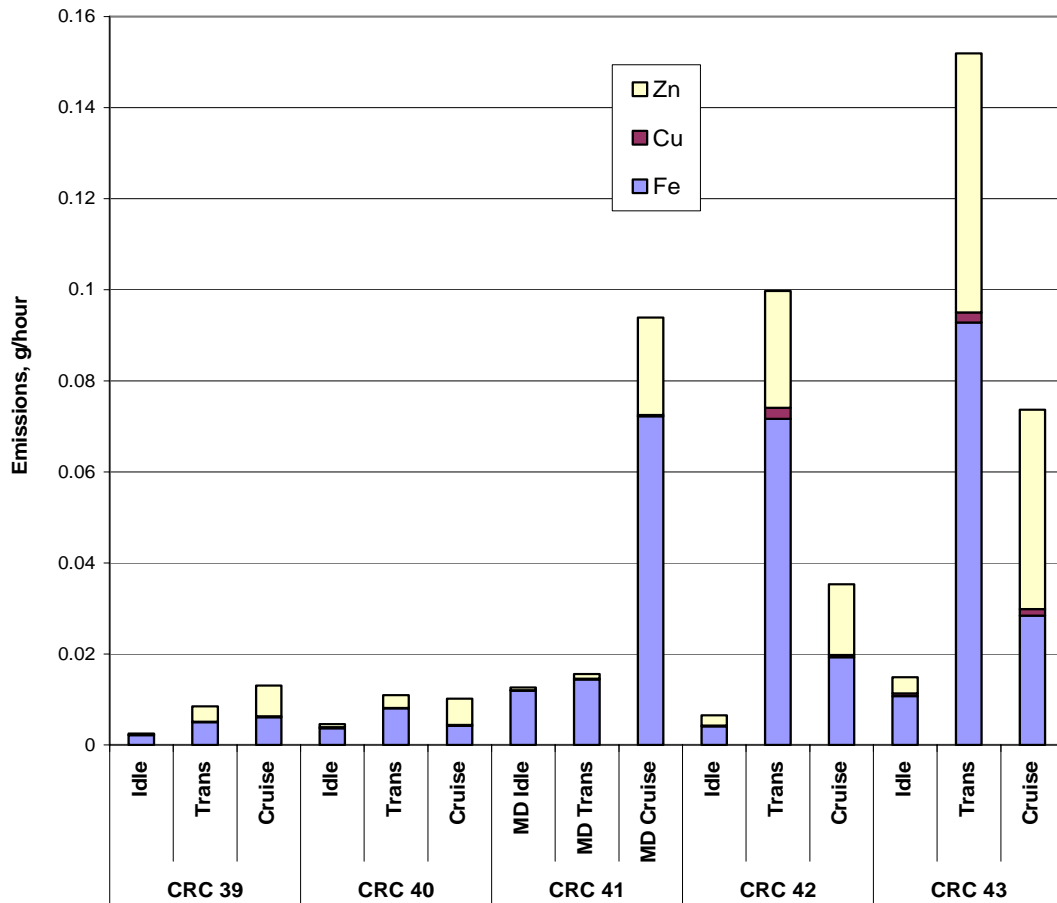
**Figure 100: Inorganic Ionic Species Emissions**

Figure 101 shows the mass emission rates of lubricating oil based elements from the test engines. These elements contribute to the total PM mass. Again, sulfur and calcium are the principal pollutants that can be traced back to the lubricating oil. In the older engines (CRC 42 and CRC 43) phosphorus emissions were significantly higher than those from other newer engines.

Figure 102 shows a summary of mass emissions rates of engine wear elements. Among these elements, iron contributed the most to the total PM emissions under all modes of operation. Of course, in terms of mass emission rates, iron emissions were the higher in the transient and cruise modes of operation.



**Figure 101: Lubrication Oil Emissions**



**Figure 102: Engine Wear Emissions**

## Acknowledgements

The WVU researchers are grateful to the sponsors listed below, for support of this program.

- Coordinating Research Council, Inc.
- California Air Resources Board
- U.S. Environmental Protection Agency
- U.S. Department of Energy Office of FreedomCAR & Vehicle Technologies through the National Renewable Energy Laboratory
- South Coast Air Quality Management District
- Engine Manufacturers Association

The dedication of the WVU field research team is gratefully acknowledged.

Ralph's Grocery was kind to provide a location for the WVU laboratory during part of this research program.

The contributions of Thomas R. Long, Jr., Sairam Thiagarajan and Shuhong (Susan) Xu in preparing and editing sections of this report are acknowledged.

## References

1. Traver, M.L., Tennant, C.J, McDaniel, T.I., McConnell, S.S, Bailey, B.K. and Maldonado, H., "Interlaboratory Cross-Check of Heavy-Duty Vehicle Chassis Dynamometer," SAE Paper 2002-01-2879.
2. Gautam, M., Clark, N.N., Riddle, W., Nine, R., Wayne, W.S., Maldonado, H., Agrawal, A. and Carlock, M., "Development and Initial Use of a Heavy-Duty Diesel Truck Test Schedule for Emissions Characterization," 2002 SAE Transactions: Journal of Fuels & Lubricants Vol. 111, pp. 812-825.
3. Clark, N.N., Gautam, M., Wayne, W.S., Nine, R.D., Thompson, G.J., Lyons, D.W., Maldonado, H., Carlock, M. & Agrawal, A., "Creation and Evaluation of a Medium Heavy-Duty Truck Test Cycle," SAE Powertrain Conf., Pittsburgh, Oct. 2003, SAE Paper 2003-01-3284.
4. Gilbert, M.S. and Clark, N.N., "Measurement of Particulate Matter from Diesel Engine Exhaust using a Tapered Element Oscillating Microbalance," International Journal of Engine Research, Vol. 2, No. 4, pp. 277-287, 2001.
5. "Code of Federal Regulations 40, Part 86, Subpart N," Environment Protection Agency (2001).
6. Hildemann, L. M., Cass, G. R., and Markowski, G. R., "A dilution stack sampler for collection of organic aerosol emissions: design, characterization and field tests," Journal of Aerosol Science and Technology , Vol. 10, pp 193-204, 1989.
7. TSI model 3936 SMPS Instruction Manual, 1999.
8. Collings, N., Reavell, K., Hands, T., Tate, J., "Roadside Aerosol Measurements with a Fast Particulate Spectrometer," JSAE Paper 20035407, 2003.
9. Reavell, K., Hands T., Collings, N., "A Fast Response Particulate Spectrometer for Combustion Aerosols," SAE Paper 2002-01-2714, 2002.
10. Reavell, K.S., Hands, T., Collings, N., "Determination of Real Time Particulate Size Spectra and Emission Parameters with a Differential Mobility Spectrometer," 6<sup>th</sup> International ETH-Conference on Nanoparticle Measurement, August 2002.
11. Sakurai, H., Tobias, H.J., Park K., Zarling, D., Docherty, K.S., Kittelson, D.B., McMurry, P.H., and Ziemann, P.J., "On-line Measurements of Diesel Nanoparticle Composition and Volatility," Atmospheric Environment, Vol. 37, pp. 1199-1210, 2004.

12. Gautam, M, Thiagarajan, S., Burlingame, T., Wayne, W.S., Clark, N., Carder, D., "Characterization of Exhaust Emissions from a Catalyzed Trap Equipped Natural Gas Fueled Transit Bus," 14<sup>th</sup> CRC On-Road Vehicle Emissions Workshop, March 29-31, 2004, San Diego.
13. Kim, D., Gautam, M., and Gera, D., "Parametric Studies on the Formation of Diesel Particulate Matter via Nucleation and Coagulation Modes," *Journal of Aerosol Science*, Vol. 33, pp. 1609-1621, 2002.
14. Mathis, U., Mohr, M., and Zenobi, R., "Effect of Organic Compounds on Nanoparticle Formation in Diluted Diesel Exhaust," *Atmospheric Chemistry and Physics*, 4, pp. 609-620, 2004.
15. Mohr, M., Jaeger, L. W., Boulouchos, K., "The Influence of Engine Parameters on Particulate Emissions," *MTZ Worldwide*, 62, pp. 686-692, 2001.
16. Lapin, C.A., Gautam, M., Zielinska, B., Wagner, V.O., McClellan, R.O., "Mutagenicity of Emissions from a Natural Gas Fueled Truck," *Mutation Research*, Vol. 519, pp. 205-209, 2002.
17. Matz, G., "Massenspektrometrische Bestimmung der Ölemission im Abgas von Otto- und Dieselmotoren," Technische Universität Hamburg-Harburg, Zwischenbericht über das Vorhaben Nr. 758 (FVV-Nr. 67580).